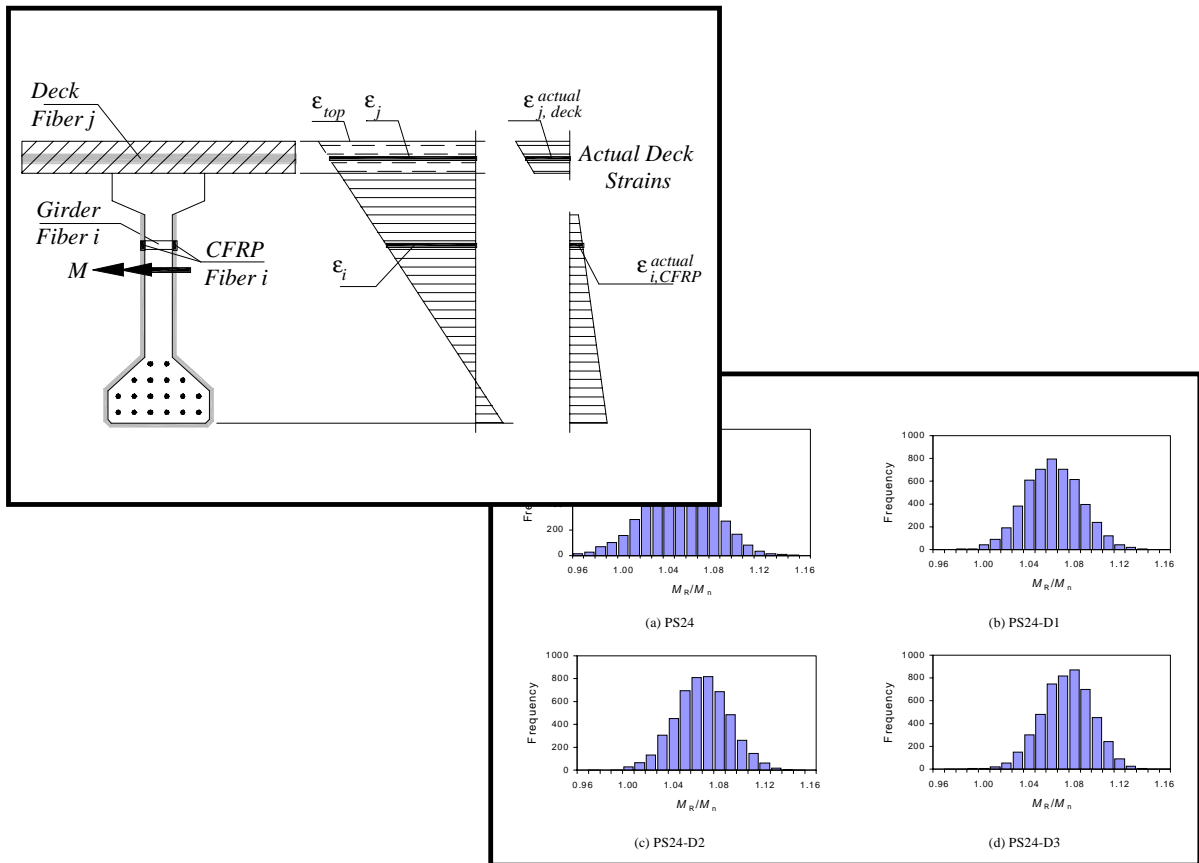


# DESIGN OF CONCRETE BRIDGE GIRDERS STRENGTHENED WITH CFRP LAMINATES

STATIC STRENGTH, FATIGUE BEHAVIOR AND RELIABILITY



UNIVERSITY OF CENTRAL FLORIDA

FDOT CONTRACT BC-190

# **DESIGN OF CONCRETE BRIDGE GIRDERS STRENGTHENED WITH CFRP LAMINATES**

STATIC STRENGTH, FATIGUE BEHAVIOR AND RELIABILITY

## ***FINAL REPORT***

- July 1<sup>st</sup> 2001 -

**Sherif El-Tawil, PhD, PE and Ayman Okeil, PhD**

Department of Civil and Environmental Engineering  
University of Central Florida, Orlando, FL 32816-2450

*This report was prepared in cooperation with the State of Florida Department of Transportation and the U.S. Department of Transportation. The report does not constitute a design standard, specification, or regulation. The opinions, findings, and conclusions expressed in this publication are those of the authors in the course and scope of employment by the University of Central Florida and not necessarily those of the Florida Department of Transportation or the U.S. Department of Transportation.*

## **ACKNOWLEDGEMENT**

This project was funded in part by the Florida Department of Transportation (contract BC-190) and the Department of Civil and Environmental Engineering at the University of Central Florida. The authors would like to express their appreciation to Dr. Mohsen Shahawy of SDR Engineering and Mr. Tom Beitelman of the FDOT Research Office for their substantial contributions to this project. Their valuable suggestions and timely cooperation helped ensure the success of the research reported herein. Special thanks are due to UCF graduate student assistant Cahit Ogunc. Parts of this report correspond to his MS thesis.

# TABLE OF CONTENTS

<b>1</b>	<b>INTRODUCTION.....</b>	<b>3</b>
1.1	BACKGROUND .....	3
1.2	MOTIVATION AND RESEARCH OBJECTIVES.....	3
1.3	REPORT OUTLINE .....	4
<b>2</b>	<b>CROSS-SECTION FIBER ANALYSIS .....</b>	<b>5</b>
2.1	INTRODUCTION.....	5
2.2	FIBER SECTION ANALYSIS - GENERAL ANALYSIS PROCESS .....	5
2.3	FIBER SECTION ANALYSIS OF PRESTRESSED CONCRETE GIRDERS.....	7
2.3.1	<i>At Transfer</i> .....	7
2.3.2	<i>Moment-Curvature relationship after Transfer</i> .....	11
2.3.3	<i>Accounting for the Construction Sequence</i> .....	13
2.3.4	<i>General Moment-Curvature Response</i> .....	15
2.4	CONSTITUTIVE PROPERTIES OF COMPONENT MATERIALS.....	15
2.4.1	<i>Concrete in Compression</i> .....	16
2.4.2	<i>Concrete Cracking</i> .....	16
2.5	TIME-DEPENDENT BEHAVIOR OF COMPONENT MATERIALS.....	17
2.5.1	<i>Fatigue Response of Concrete</i> .....	18
2.5.2	<i>Additional Model Assumptions</i> .....	21
2.5.3	<i>Fatigue Response of Steel, CFRP, and Epoxy</i> .....	21
2.6	FATIGUE CALCULATIONS .....	22
2.7	BEAM DEFLECTION CALCULATION .....	23
2.8	COMPUTER IMPLEMENTATION - T-DACS PROGRAM .....	25
2.9	COMPUTER IMPLEMENTATION - MACS PROGRAM .....	25
<b>3</b>	<b>SHORT-TERM CFRP LAMINATE STRENGTH .....</b>	<b>32</b>
3.1	INTRODUCTION .....	32
3.2	WEIBULL THEORY FOR COMPOSITE MATERIALS .....	33
3.3	APPLICATION OF WEIBULL'S THEORY TO CFRP LAMINATES USED TO STRENGTHEN RC AND PC BEAMS.....	35
3.3.1	<i>Size Effect</i> .....	36
3.3.2	<i>Stress Gradient Effect</i> .....	37
3.3.3	<i>Constant Moment Case</i> .....	38
3.3.4	<i>Concentrated Load at Mid-Span (Fig. 3.5)</i> .....	41
3.3.5	<i>Four Point Loading (Fig. 3.5)</i> .....	41
3.3.6	<i>Uniformly Distributed Load (Fig. 3.5)</i> .....	41
3.4	VERIFICATION OF THEORY .....	42
3.4.1	<i>Short-term Tensile Stress</i> .....	43
3.4.2	<i>Comparison of Flexural Capacities</i> .....	45
3.5	DESIGN IMPLICATIONS .....	45
3.6	SUMMARY AND CONCLUSIONS.....	47
<b>4</b>	<b>STATIC AND FATIGUE BEHAVIOR.....</b>	<b>48</b>
4.1	INTRODUCTION .....	48
4.2	SHAHAWY AND BEITELMAN'S (1999, 2000) TESTS.....	48
4.2.1	<i>Monotonic Analyses of Shahawy and Beitleman's (1999, 2000) Specimens</i> .....	49

4.2.2	<i>Cyclic Analyses of Shahawy and Beitleman's (1999, 2000) Specimens</i>	54
4.2.3	<i>Fatigue Life of Shahawy and Beitleman's (1999, 2000) Specimens</i>	59
4.3	ANALYSIS OF BARNES AND MAYS' (1999) SPECIMENS	61
4.4	DESIGN CONSIDERATIONS	62
4.5	SUMMARY AND CONCLUSIONS	64
<b>5</b>	<b>RELIABILITY OF REHABILITATED BRIDGE GIRDERS</b>	<b>65</b>
5.1	INTRODUCTION	65
5.2	RELIABILITY INDEX	66
5.3	FIRST ORDER RELIABILITY METHOD (FORM)	66
5.4	MONTE CARLO SIMULATIONS	68
5.5	RELIABILITY OF REINFORCED CONCRETE BRIDGE GIRDERS	68
5.5.1	<i>Design of RC Bridges</i>	71
5.5.2	<i>Bridge Geometry, Material Properties, and Loading</i>	71
5.5.3	<i>Design of RC Cross Sections</i>	72
5.5.4	<i>Monte Carlo Simulations for RC Bridges</i>	75
5.5.5	<i>Results for RC Bridges</i>	78
5.5.6	<i>Target <math>\beta</math> for RC Bridges</i>	79
5.5.7	<i>Effect of <math>\phi = 0.85</math> on RC Bridges</i>	80
5.5.8	<i>Design Implications for RC Bridges</i>	82
5.6	RELIABILITY OF PRESTRESSED CONCRETE BRIDGE GIRDERS	82
5.6.1	<i>Design of PSC Bridges</i>	82
5.6.2	<i>Resistance Models</i>	88
5.6.3	<i>LRFD Calibration - <math>\beta</math> based on current AASHTO provisions (LRFD - 1998)</i>	90
5.6.4	<i>LRFD Calibration of the design procedure</i>	91
5.6.5	<i>Proposed Resistance Factor, <math>\phi</math></i>	92
5.6.6	<i>Design Implications for PSC Bridges</i>	94
<b>6</b>	<b>SUMMARY AND CONCLUSIONS</b>	<b>95</b>
6.1	SUMMARY OF WORK	95
6.2	MAIN CONCLUSIONS	96
6.2.1	<i>Tensile Strength of CFRP Laminates</i>	96
6.2.2	<i>Static Response of CFRP Strengthened Girders</i>	96
6.2.3	<i>Fatigue Response of CFRP Strengthened Girders</i>	96
6.2.4	<i>Flexural Reliability of Prestressed Concrete Girders</i>	97
6.2.5	<i>Flexural Reliability of Prestressed Concrete Girders</i>	97
6.3	FUTURE WORK	98
<b>7</b>	<b>REFERENCES</b>	<b>99</b>
<b>8</b>	<b>APPENDIX A - IMPLEMENTATION OF FORM ALGORITHM IN MATLAB</b>	<b>104</b>
8.1	FIRST ORDER RELIABILITY METHOD (FORM)	104
8.1.1	<i>FORM Algorithm</i>	105
<b>9</b>	<b>APPENDIX B - USER'S MANUAL FOR MACS<sup>®</sup></b>	<b>111</b>
9.1	PROGRAM INSTALLATION	111
9.2	USING MACS <sup>®</sup>	112
9.3	STARTING A NEW ANALYSIS	112
9.3.1	<i>Span Length</i>	112

9.3.2	<i>Span Loads</i> .....	113
9.3.3	<i>Section Details</i> .....	113
9.3.4	<i>Problem Execution</i> .....	115
9.3.5	<i>Viewing Results</i> .....	116
<b>10</b>	<b>APPENDIX C - REHABILITATION EXAMPLE</b> .....	<b>119</b>
10.1	CROSS SECTION GEOMETRY .....	119
10.2	DESIGN OF DAMAGED CROSS SECTION .....	119
<b>11</b>	<b>APPENDIX D - RESEARCH DISSEMINATION</b> .....	<b>124</b>
11.1	PAPERS ACCEPTED FOR PUBLICATION .....	124
11.2	PAPERS SUBMITTED FOR PUBLICATION .....	124
11.3	THESES .....	124

## LIST OF TABLES

<b>Table 3.1:</b> Properties of CFRP Laminates (Provided by manufacturer)	43
<b>Table 3.2:</b> Comparison of Failure Moments	44
<b>Table 4.1:</b> Properties of sections (calculated from cracked section analysis)	59
<b>Table 5.1:</b> Statistical properties of variables involved in the study	69
<b>Table 5.2:</b> Usable tensile stress used in design of RC Bridges	72
<b>Table 5.3:</b> Design summary of bridge cross sections	74
<b>Table 5.4:</b> Results of Monte Carlo simulation (moment units in kNm)	77
<b>Table 5.5:</b> Optimum $\phi$ to achieve $\beta_{RC-CFRP}^{target}$	80
<b>Table 5.6:</b> Design moments for interior girder of reinforced concrete bridges	82
<b>Table 5.7:</b> Summary of design stresses and capacities	83
<b>Table 5.8:</b> Usable tensile stress used in design of PS Bridges	84
<b>Table 5.9:</b> Design summary of bridge cross sections	85
<b>Table 5.10:</b> Results of Monte Carlo simulation (moment units in kN.m)	87
<b>Table 5.11:</b> Optimum $\phi$ to achieve $\beta_{PS-CFRP}^{target}$	89
<b>Table A.1:</b> Progress of FORM algorithm	107
<b>Table C.1:</b> Design trials for damaged cross section	120

## LIST OF FIGURES

<b>Figure 2.1:</b> Fiber section discretization of a reinforced concrete section strengthened with CFRP laminates.	6
<b>Figure 2.2:</b> Cross section of single T-girder used for illustration.	8
<b>Figure 2.3:</b> Strain and stress distributions at the end of each stage (a- 1 <sup>st</sup> iteration, b- $n^{th}$ iteration).	9
<b>Figure 2.4:</b> Convergence of girder top strain, $\epsilon_{top}$ , and curvature, $\theta$ during two-stage equilibrium process at transfer (analysis step number 1).	10
<b>Figure 2.5:</b> Observed force error, $\epsilon_F$ , and moment error, $\epsilon_M$ , after each iteration.	11
<b>Figure 2.6:</b> Concrete stress distribution for T-beam example at transfer.	11
<b>Figure 2.7:</b> Experimental vs. analytical $M - \theta$ relationship for verification.	13
<b>Figure 2.8:</b> Sequence of analysis for girders with CFRP-strengthened girders with composite decks.	14
<b>Figure 2.9:</b> Idealized moment-curvature relationships for PSC girders strengthened with CFRP laminates.	15
<b>Figure 2.10:</b> Monotonic constitutive models for component material.	17
<b>Figure 2.11:</b> Compressive behavior of concrete subjected to repeated loading.	18
<b>Figure 2.12:</b> Proposed constitutive model for concrete subjected to fatigue loading.	19
<b>Figure 2.13:</b> Principle of superposition for cyclic creep strain calculations.	23
<b>Figure 2.14:</b> Degrees of freedom of beam elements used in this research.	24
<b>Figure 2.15:</b> Calculation of flexural stiffness from moment-curvature relationship.	24
<b>Figure 2.16:</b> Main window that controls input data and analysis results.	26
<b>Figure 2.17:</b> Reinforcement types, geometric and material properties window.	27
<b>Figure 2.18:</b> Input window for beam name and length.	27
<b>Figure 2.19:</b> Input window for definition of loading.	28
<b>Figure 2.20:</b> Status window that runs during the analysis.	28
<b>Figure 2.21:</b> Mid-span load-deflection results window.	29
<b>Figure 2.22:</b> Positive and negative moment-curvature relationship of the cross-section.	30
<b>Figure 2.23:</b> Displacement, bending moment and shear force diagrams.	31
<b>Figure 3.1:</b> Effect of fiber length on failure stress (Weibull size effect).	34



<b>Figure 3.2:</b> Effect of composite size on damage sequence based on approximate method. ( $n_k=8$ , $\lambda_k=0.1$ mm, $c_k=1+0.5k$ ).	37
<b>Figure 3.3:</b> Normal stress distribution in CFRP sheets due to flexure (a-wrap-around detail, b-normal stress distribution on bottom and web parts).	39
<b>Figure 3.4:</b> Coordinate system for integration purposes (Case of constant moment).	40
<b>Figure 3.5:</b> Common loading configurations: (a) concentrated load, (b) four-point loading, (c) uniform load.	42
<b>Figure 3.6:</b> Loading setup for FDOT girders (dimensions in inches).	43
<b>Figure 3.7:</b> Cross-section details (dimensions in inches).	44
<b>Figure 3.8:</b> Cross-section details (dimensions in inches).	46
<b>Figure 4.1:</b> Experimental vs. analytical moment curvature. Specimen C-L0-5.	50
<b>Figure 4.2:</b> Experimental vs. analytical moment curvature. Specimen W-L1-5.	51
<b>Figure 4.3:</b> Experimental vs. analytical moment curvature. Specimen W-L2-5.	51
<b>Figure 4.4:</b> Experimental vs. analytical moment curvature. Specimen W-L3-5.	52
<b>Figure 4.5:</b> Experimental vs. analytical moment curvature. Specimen W-L4-5.	52
<b>Figure 4.6:</b> Moment curvature relationships for beam with different number of CFRP layers.	53
<b>Figure 4.7:</b> Analytical and experimental ultimate moment increase vs. number of CFRP layers.	53
<b>Figure 4.8:</b> Analytical and experimental yield moment increase vs. number of CFRP layers.	54
<b>Figure 4.9:</b> Calculated versus experimental mid-span deflection for (a) beams with 2 CFRP layers (Shahawy and Beitelman 2000) and (b) beams with 3 CFRP layers (Shahawy and Beitelman 1999).	55
<b>Figure 4.10:</b> Calculated stresses in (a) top concrete fiber and (b) bottom steel layer versus number of cycles for beam with 2 CFRP layers.	56
<b>Figure 4.11:</b> Time-dependent analysis for Specimen C-L0-5.	57
<b>Figure 4.12:</b> Stress in bottom steel layer as a function of number of cycles. Specimen C-L0-5.	57
<b>Figure 4.13:</b> Time-dependent analysis for Specimen W-L1-5.	58
<b>Figure 4.14:</b> Stress in bottom steel layer as a function of number of cycles. Specimen W-L1-5.	58
<b>Figure 4.15:</b> Different views of the failure surfaces of steel reinforcement.	60
<b>Figure 4.16:</b> Typical fatigue fracture of reinforcing bar.	61
<b>Figure 4.17:</b> $S_r$ -N Curve for Shahawy and Beitelman's (1999, 2000) fatigue tests.	61

<b>Figure 4.18:</b> Calculated versus experimental mid-span deflection for Beam 2 (Barnes and Mays 1999).	62
<b>Figure 4.19:</b> Calculated versus experimental mid-span deflection for Beam 4 (Barnes and Mays 1999).	63
<b>Figure 5.1:</b> A simple reduced design space showing the design point, reliability index, $\beta$ , and limit state function, $Z$ .	67
<b>Figure 5.2:</b> Cross section of 5-girder bridge.	72
<b>Figure 5.3:</b> Loading cases considered in design of bridges.	73
<b>Figure 5.4:</b> Cross sections of undamaged interior bridge girders.	74
<b>Figure 5.5:</b> Moment-curvature relationship obtained from Monte Carlo simulation (50 cases shown).	76
<b>Figure 5.6:</b> Idealized moment-curvature relationship.	76
<b>Figure 5.7:</b> Histograms of flexural resistance for Bridges RC60, RC60-D1, RC60-D2, and RC60-D3.	77
<b>Figure 5.8:</b> Determining reduction factor, $\phi$ . (Bridges RC60-D1, RC60-D2, and RC60-D3).	80
<b>Figure 5.9:</b> Effect of $M_L/M_D$ on Reliability Index, $\beta$ . (Bridge RC45, $\phi=0.85$ ).	81
<b>Figure 5.10:</b> Cross section of 6-girder bridge.	83
<b>Figure 5.11:</b> Cross sections of undamaged interior bridge girders.	84
<b>Figure 5.12:</b> Moment - curvature relationships for interior girder (PS100).	87
<b>Figure 5.13:</b> Histograms of flexural resistance for Bridges PS80, PS80-D1, PS80-D2, and PS80-D3.	89
<b>Figure 5.14:</b> (a) effect of changing $\phi$ on the $\beta$ , (b) determining the optimum reduction factor, $\phi$ . (Bridges PS80-D1, PS80-D2, and PS80-D3).	92
<b>Figure 5.15:</b> Proposed reduction factor, $\phi$ .	93
<b>Figure 5.16:</b> Effect of $M_L/M_D$ on Reliability Index, $\beta$ . (Bridge PS60, proposed $\phi$ ).	94
<b>Figure 6.1:</b> Delamination due to shear and flexural actions.	98
<b>Figure A.1:</b> Statistical distribution (PDF) of resistance ( $R$ ), loads ( $Q$ ), and performance function ( $Z$ ).	108
<b>Figure A.2:</b> A simple reduced design space showing the design point, reliability index.	109
<b>Figure A.3:</b> Flow chart for MATLAB implementation of FORM.	110
<b>Figure B.1:</b> Main window of the MACS <sup>®</sup> program.	112
<b>Figure B.2:</b> MACS <sup>®</sup> Span data window.	113

<b>Figure B.3:</b> MACS <sup>®</sup> Span Loading window.	114
<b>Figure B.4:</b> MACS <sup>®</sup> cross section interface for Florida DOT tested T-girders.	115
<b>Figure B.5:</b> Status window of the MACS <sup>®</sup> .	116
<b>Figure B.6:</b> Main Interface of MACS <sup>®</sup> showing Moment-Curvature for Specimen W-3L5.	117
<b>Figure B.7:</b> Main Interface of MACS <sup>®</sup> showing Load-Deflection relationship for Specimen W-3L5.	118
<b>Figure C.1:</b> Cross sections of undamaged interior bridge girders.	121
<b>Figure C.2:</b> Main Interface of the MACS program.	122
<b>Figure C.3:</b> MACS cross section interface for 3 <sup>rd</sup> design trial. [All fields in US customary units (i.e. inch and pound)]	123

# EXECUTIVE SUMMARY

## Problem Statement

Externally bonded carbon fiber reinforced polymer (CFRP) laminates are a feasible and economical alternative to traditional methods for strengthening and stiffening deficient reinforced concrete and prestressed concrete girders. Although extensive research has already been undertaken to investigate both short term and long term behavior of CFRP strengthened bridge girders, the majority of work conducted to date has been experimental in nature. Furthermore, while some studies have proposed design models and methodologies to identify the necessary number of laminates to achieve a target strength or stiffness, many important design issues still remain unresolved.

## Objectives

The overall objective of the research reported herein is to use state-of-the-art numerical techniques to resolve some of the open questions. The intent of this work is to provide information that complements existing data and that will be useful for formulating comprehensive design guidelines for CFRP rehabilitation. Specific objectives include:

- Develop analytical models for simulating the static response and accelerated fatigue behavior of concrete beams strengthened with CFRP laminates. Use the developed models to investigate the static and fatigue behavior of CFRP strengthened beams.
- Investigate the short-term tensile strength of CFRP laminates and establish a relationship between the fiber tensile strength and the tensile strength of CFRP laminates attached to a concrete girder. Such a relationship facilitates the design process and enables structural engineers to estimate laminate strength from fiber properties published by the manufacturer.
- Develop resistance models for reinforced and prestressed concrete bridge girders flexurally strengthened with externally bonded CFRP laminates. Use the developed models to calculate the probability of failure, reliability index, and flexural resistance factor of CFRP strengthened cross-sections.

## Summary of Work

Models for simulating the static and accelerated fatigue behavior of reinforced and prestressed concrete beams strengthened with CFRP were developed. The models are based on the fiber section technique and account for the nonlinear time-dependent behavior of concrete, steel yielding, and rupture of CFRP laminates. The effect of size on the tensile strength of CFRP laminates is accounted for in the calculations.

The models were implemented in a MatLab computer program, T-DACS (Time-Dependent Analysis of Composite Sections), and were verified and exercised by comparing analytical results to data from several experimental investigations. A second computer program MACS (Monotonic Analysis of Composite Sections) was developed to run only the static portion of the developed models within a Visual Basic environment. MACS is user-friendly and features an easy to use graphical user interface.

The developed computer programs were used to investigate the static and fatigue response of RC and PSC concrete girders strengthened with CFRP laminates. Additional Monte-Carlo simulations (120,000 runs) were conducted using MACS to develop resistance models for both reinforced and prestressed concrete bridge girders flexurally strengthened with CFRP laminates. The resistance models were used to calculate the probability of flexural failure and flexural reliability index of CFRP strengthened cross-sections. The first order reliability method was employed to calibrate the proposed flexural resistance factors for a broad range of design variables.

## Main Findings and Conclusions

Following are the most important findings and conclusions from this work:

- The use of coupons to obtain the in-situ strength of CFRP laminates can lead to unconservative estimates of strength if the size effect is not properly considered.
- The short-term tensile strength of CFRP laminates can be calculated by applying the Weibull Theory. Two steps are needed to compute the short-term tensile strength. The first step accounts for the size effect and predicts the tensile strength of a uniformly stressed volume that shares the size of the CFRP used in the real structure. The second step accounts for the effect of stress gradients.
- Cyclic fatigue leads to an internal redistribution of stresses similar to that obtained under static creep. To account for the increase in steel stresses due to cyclic fatigue as well as shrinkage, creep under dead loads and the variability in reinforcing steel strength, it is recommended that the service steel stress be limited such that  $\sigma_s < 0.85f_y$ .
- The reliability index of CFRP strengthened RC cross-sections is greater than that of unstrengthened sections and increases with increasing CFRP ratio. Although the reliability index improves with addition of CFRP, the flexural resistance factor is recommended as  $\phi=0.85$ , which is lower than that recommended by AASHTO-LRFD for RC sections under flexure. The reduced  $\phi$  value results in a larger target reliability index than is normally specified in recognition of the brittle nature of CFRP behavior.
- The strength reduction factor,  $\phi$ , for CFRP strengthened PSC bridge girders is recommended to vary linearly from 0.85 to 1.0 depending on the ratio between the resistance provided by the CFRP and prestressing steel. This is shown to result in acceptable reliability for a wide range of dead load to live load ratios.

# 1 INTRODUCTION

## 1.1 Background

Concrete bridge girders become structurally deficient for many reasons including corrosion of reinforcing bars or prestressing strands, change in load requirements, vandalism, collision between vehicles and bridge components, etc. National concern about the increasing cost of bridge rehabilitation has prompted extensive research efforts to find effective and economical rehabilitation means. One of the emerging technologies that has proven particularly suited for strengthening and stiffening reinforced and prestressed concrete bridge girders is the use of externally bonded carbon fiber reinforced plastic (CFRP) laminates. This rehabilitation technique has gained popularity in recent years as bridge engineers have become more familiar with the appealing attributes of CFRP which include light weight, high strength and stiffness, resistance to corrosion, and good fatigue characteristics.

Carbon fiber reinforced plastic laminates are attached using epoxy adhesives to the bottom surface of beams or are wrapped around the girder stems to provide additional tensile reinforcement. The Florida Department of Transportation (FDOT) has been a pioneer of this technology and has been extensively involved in its development for the past decade. Extensive testing at FDOT and elsewhere has focused on the effect of CFRP rehabilitation on the stiffness, strength, fatigue, ductility, mode of failure, and reliability of reinforced concrete girders strengthened with CFRP laminates.

Research in this field has matured to the extent that code committees are starting to crystallize available knowledge into code provisions. ACI committee 440 is currently developing design guidelines for external strengthening of concrete structures using fiber reinforced polymer systems, and a synthesis of the provisions of the Canadian Highway Bridge Design Code for fiber-reinforced structures has been recently published (Bakht et al 2000). Prominent examples of the use of this technology in bridge rehabilitation can be found in a report published by ACI (1996).

## 1.2 Motivation and Research Objectives

The majority of research conducted to date for investigating both short term and long term behavior of CFRP strengthened bridge girders has been experimental in nature. Furthermore, while some studies have proposed design models and methodologies to identify the necessary number of laminates to achieve a target strength or stiffness, many important design issues still remain unresolved. The overall objective of the research reported herein is to use state-of-the-art numerical techniques to resolve some of these questions. The intent of this work is to provide information that will be useful for the development of comprehensive design guidelines for rehabilitation schemes employing CFRP technology. Specific objectives include:

- Develop an analytical model for simulating the static response and accelerated fatigue behavior of concrete beams strengthened with CFRP laminates. Use the developed model to investigate the static and fatigue behavior of CFRP strengthened beams.
- Investigate the short-term tensile strength of CFRP laminates and establish a relationship between the fiber tensile strength and the tensile strength of CFRP laminates attached to a concrete girder. Such a relationship facilitates the design process and enables structural engineers to estimate laminate strength from fiber properties published by the manufacturer.
- Develop resistance models for reinforced and prestressed concrete bridge girders flexurally strengthened with externally bonded CFRP laminates. Use the developed models to calculate the probability of failure, reliability index, and flexural resistance factor of CFRP strengthened cross-sections.

### **1.3 Report Outline**

This report is comprised of 6 chapters and an appendix. Chapter 1 provides background and motivation for this work. Specific objectives are also listed in this chapter. Chapter 2 describes the fiber section method used to characterize the static and fatigue behavior of composite cross-sections. Constitutive models and the solution method are described and discussed. In Chapter 3, the Weibull theory is used to establish a relationship between the strength of a CFRP laminate and the fiber strength reported by the manufacturer. A chart for quickly determining laminate strength is provided for design convenience. The fiber section program developed in Chapter 2 is exercised and the results reported in Chapter 4. Both static and fatigue analyses are conducted using the program and compared to experimental results for verification purposes. Chapter 5 provides details of the reliability study used to develop flexural strength reduction factors for both reinforced and prestressed concrete girders. The work is summarized and the most important conclusions are drawn in Chapter 6. Finally Appendix A lists the details of the First Order Reliability Method (FORM) employed for the reliability study reported in Chapter 5.

## 2 CROSS-SECTION FIBER ANALYSIS

### 2.1 Introduction

The static and fatigue analyses presented in this report are based on the fiber section technique. The fiber section method is an accurate and practical technique for computing the moment-curvature response of a reinforced or prestressed concrete section strengthened with CFRP. This chapter presents a detailed description of the method.

### 2.2 Fiber Section Analysis - General Analysis Process

As shown in Fig. 2.1, fiber section analysis of a composite cross section entails discretization of the section into many small layers (fibers) for which the constitutive models are based on uniaxial stress-strain relationships. Each region represents a fiber of material running longitudinally along the member and can be assigned one of several constitutive models representing concrete, CFRP, reinforcing steel, or prestressing steel. The main assumptions employed in the fiber section method are:

- Plane sections are considered to remain plane after bending. It is generally accepted that this assumption is reasonable even well into the inelastic range. Measurements of strains along the height show that this assumption is good for beams with either partial or full wrapping (Shahawy and Beitelman 2000 and Inoue et. al 1995)
- Perfect bond is assumed between concrete and other materials (steel reinforcement and CFRP laminates).
- Shear stresses are not accounted for. The fiber section method, as presented in this report, is therefore limited to long thin members whose behavior is dominated by flexure.

In their general discretized form, the cross-sectional forces are determined as stress resultants according to the following general equations:

$$F = \sum_{i=1}^n \sigma_i A_i \quad (2.1)$$

$$M = \sum_{i=1}^n \sigma_i A_i d_i \quad (2.2)$$



where:

- $i$  concrete, steel, or CFRP fiber
- $F$  axial load
- $M$  major bending moment
- $\sigma_i$  longitudinal stress at centroid of fiber  $i$
- $A_i$  area of fiber  $i$
- $d_i$  distance between centroid of fiber  $i$  and top of section.
- $n$  total number of section fibers

The general solution procedure is organized around calculating the moment-curvature response for a fixed value of axial load,  $F$ , where,  $F=0$  for the case of pure flexure. The moment-curvature response is obtained by incrementally increasing the curvature and solving for the corresponding value of moment. The location of the neutral axis and the fiber strains are a function of the curvature,  $\theta$ , and strain at the extreme top fiber,  $\epsilon_{top}$ . Based on the “plane sections remain plane” assumption, the fiber strains are equal to  $\epsilon_{top}$  minus the product of the curvature times the orthogonal distance from the centroid of each fiber to the neutral axis (see Fig. 2.1). The fiber stresses in Eqs. 2.1 and 2.2 above are calculated from the fiber strains using appropriate constitutive relationships (described later on). For given values of curvature, the top fiber strain is solved for by iteration until the specified value of  $F$  is reached. Resulting from this process is a set of unique values of moment and curvature. The moment-curvature calculations are stopped when a prespecified number of curvature increments are applied.

The solution process for prestressed girders is described in the following section. While the solution method for reinforced concrete girders is conceptually identical to that for prestressed concrete, it is actually simpler because the effects of the prestressing force do not have to be dealt with.

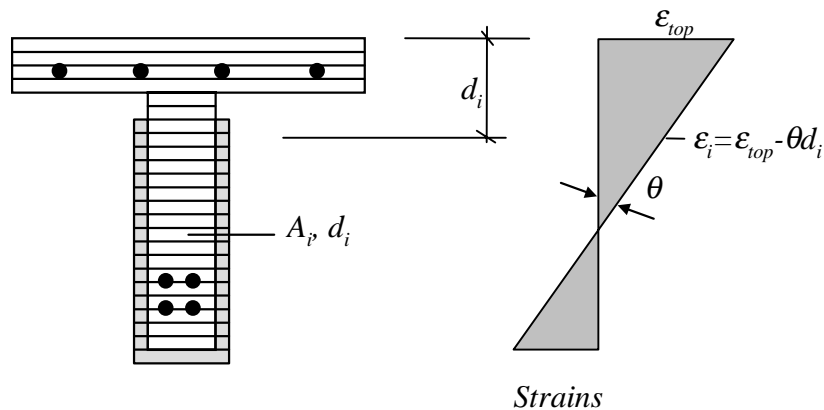


**Figure 2.1:** Fiber section discretization of a reinforced concrete section strengthened with CFRP laminates.

## 2.3 Fiber Section Analysis of Prestressed Concrete Girders

This section describes the solution process of the fiber section method and outlines how the effects of prestressing are handled.

### 2.3.1 At Transfer

At the beginning of the life of a prestressed girder, the prestressing force is activated either by releasing fixation to the bulkheads for a pre-tensioned girder, or by jacking a post-tensioned girder. In both cases, the induced stresses due to the prestressing force cause the girder to camber (deflect upward for a simply supported configuration). Handling this initial stage of loading in the fiber section method is achieved through an equilibrium step to calculate the initial camber-causing curvature at the time of transfer. The algorithm involves a two-stage iterative process that satisfies force then moment equilibrium within each iteration.

The analysis progress is explained using the cross section shown in Fig. 2.2. The algorithm proceeds as follows:

1. The entire prestressing force, without losses, is first applied on the cross-section. The corresponding initial prestressing strains,  $\varepsilon_{PS,o}$ , are then calculated.
2. The first-stage of the iterative procedure finds a strain distribution that results in an internal force that satisfies force equilibrium according to the following equation:

$$\sum F = \sum_{i=1}^m \sigma_{PS,i} A_{PS,i} + \sum_{j=1}^n \sigma_{c,j} A_{c,j} + \sum_{k=1}^p \sigma_{CFRP,k} A_{CFRP,k} + \sum_{l=1}^q \sigma_{s,l} A_{s,l} + \varepsilon_F = 0.0 \quad (2.3)$$

where  $\sigma_{PS,i}$  and  $A_{PS,i}$  are the stress and area of prestressed strand layer  $i$ ,  $\sigma_{c,j}$  and  $A_{c,j}$  are the stress and area of concrete fiber  $j$ ,  $\sigma_{CFRP,k}$  and  $A_{CFRP,k}$  are the stress and area of CFRP fiber  $k$  (in case CFRP exists at this stage),  $\sigma_{s,l}$  and  $A_{s,l}$  are the stress and area of steel fiber  $l$ , and  $\varepsilon_F$  is the force error. Note that Eq. 2.3 is a generalized version of Eq. 2.1. Force equilibrium is achieved if  $\varepsilon_F$  is less than an acceptable tolerance as set by the user (taken as  $10^{-4}$  of the total force in concrete fibers in this study). First stage iterations are executed in search for a top strain value that satisfies Eq. 2.1. The initial iteration of the procedure starts by assuming that the strain in the top concrete fiber is positive. A bisection algorithm is used while decreasing top strain value (compression = negative strain), and hence strains in all fibers, until the error is within the acceptable tolerance. The result of this iterative process is a value for the top strain denoted by  $\varepsilon_{top,1}$  where the subscript 1 corresponds to the iteration number, in this case, the first iteration.

In the preceding calculations, the strains in the prestressing strand fibers are adjusted like any other fiber. The only difference in determining strand fiber stresses is that the strain value,  $\varepsilon_{PS,i}$ , used in calculating the stress  $\sigma_{PS,i}$  is taken as the sum of the strain value from the distribution in Fig. 2.3,  $\varepsilon_{PS,i}^*$ , and the initial prestressing strain,  $\varepsilon_{PS,o}$ .

At the end of this first stage, the resulting strain distribution is uniform which obviously does not satisfy moment equilibrium (unless the effective depth of the prestressing strands lies on the centroid of the cross section). Therefore, the second stage of the procedure is necessary to achieve moment equilibrium.

3. In the second-stage, moment equilibrium is calculated according to the following equation:

$$\sum M = \sum_{i=1}^m (\sigma_{PS,i} A_{PS,i}) (d_{PS,i}) + \sum_{j=1}^n (\sigma_{c,j} A_{c,j}) (d_{c,j}) + \Lambda \quad (2.4)$$

$$\sum_{k=1}^p (\sigma_{CFRP,k} A_{CFRP,k}) (d_{CFRP,k}) + \sum_{l=1}^q (\sigma_{s,l} A_{s,l}) (d_{s,l}) + \epsilon_F = 0.0$$

where  $d_{PS,i}$ ,  $d_{c,j}$ ,  $d_{CFRP,k}$ , and  $d_{s,l}$  are the distances from the girder top to the centroid of prestressed strand layer  $i$ , concrete fiber  $j$ , CFRP fiber  $k$ , and steel bar layer  $l$ , respectively.  $\epsilon_M$  is the moment error which must fall within an acceptable tolerance as set by the user for convergence (also taken in this study as  $10^{-4}$  of the total moment caused by forces in concrete fibers). Note once again that Eq. 2.4 is a more detailed version of Eq. 2.2. To achieve moment equilibrium, the top strain obtained in the previous step,  $\epsilon_{top,1}$ , is maintained and iterations are executed in search for the correct curvature,  $\theta_1$  as can be seen in Fig. 2.3(a).

At the end of this second stage (end of first full iteration), the resulting non-uniform strain distribution satisfies moment equilibrium, however, force equilibrium is clearly violated. The force in concrete fibers has obviously increased due to the increase in strain levels, especially in lower fibers.

4. Steps 2 and 3 are repeated until both  $\epsilon_F$  and  $\epsilon_M$  from 2 subsequent iterations fall within the acceptable tolerance. This implies that convergence has been reached and that an acceptable solution for the problem is achieved.

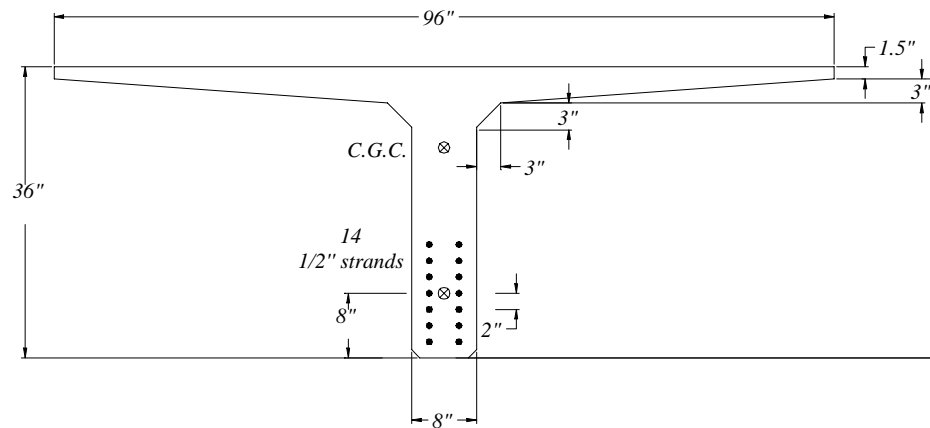
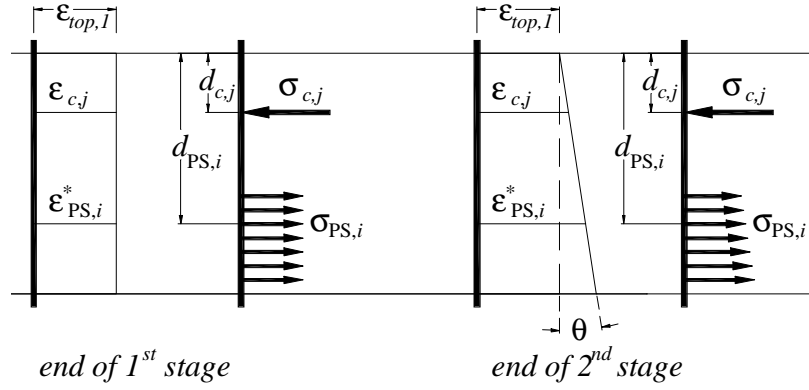
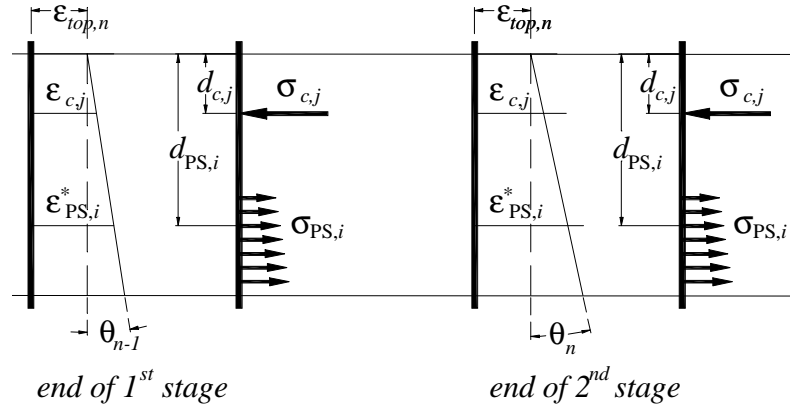


**Figure 2.2:** Cross section of single T-girder used for illustration.



(a)



(b)

**Figure 2.3:** Strain and stress distributions at the end of each stage (a- 1<sup>st</sup> iteration, b-  $n^{\text{th}}$  iteration).

Figure 2.4 shows the progress of the algorithm from the initial step until convergence for the cross-section in Fig. 2.2. Figure 2.4 shows a plot of the top strain,  $\epsilon_{top}$ , and curvature,  $\theta$ , at the end of each iteration. In Fig. 2.5, the error values,  $\epsilon_F$  and  $\epsilon_M$ , are shown at the end of each iteration. Both figures show that the solution has reached convergence in 10 iterations. Experience with the algorithm suggests that it usually converges in less than 30 iterations.

The stress and strain distributions at the end of the transfer stage is given in Fig. 2.6. Also plotted in the figure are the values obtained using hand calculations using the well-known equations:

$$f_{top} = -\frac{P}{A} + \frac{Pe}{I} y_{top} - \frac{M_G}{I} y_{top} \quad (2.5a)$$

$$f_{bot} = -\frac{P}{A} - \frac{Pe}{I} y_{bot} + \frac{M_G}{I} y_{bot} \quad (2.5b)$$

In Eq. 2.5,  $e$  (positive upwards) is the eccentricity of prestressing strands from the concrete section center of gravity (CGC),  $A$  and  $I$  are area and moment of inertia of the cross section,  $y_{top}$  and  $y_{bot}$  are the distances from top and bottom concrete fibers to CGC, and  $M_G$  is the moment due to girder self-weight. Equation 2.5 was used to obtain two strain distributions; the first is based on gross concrete cross section properties,  $A_g$  and  $I_g$ , and the second is based on the transformed cross section properties,  $A_t$  and  $I_t$ , taking into account the contribution of prestressing strands to these properties. As can be seen in Fig. 2.6, the more accurate representation (using  $A_t$  and  $I_t$ ) is in better agreement with the results obtained from the fiber section analysis. The plots in Fig. 2.6 are calculated using  $M_G = 0$ .

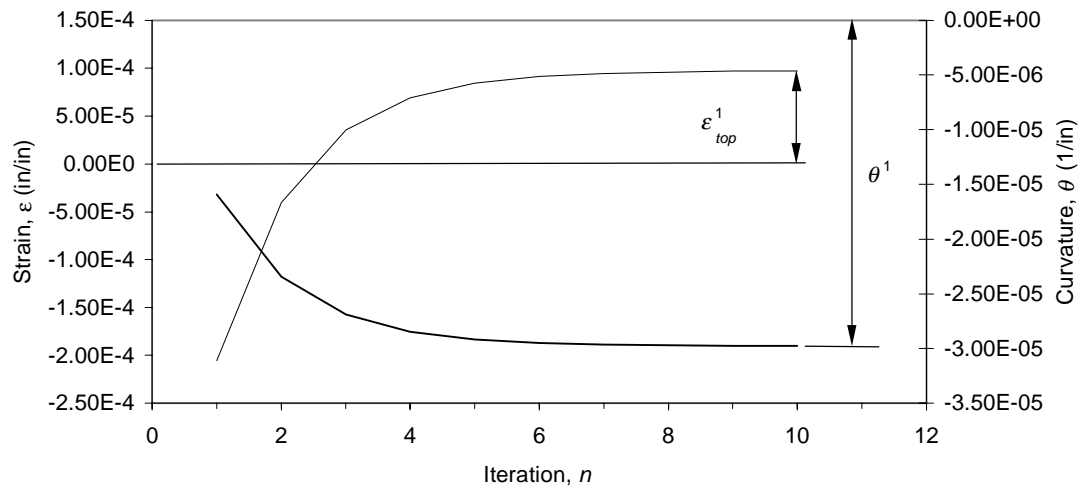


**Figure 2.4:** Convergence of girder top strain,  $\epsilon_{top}$ , and curvature,  $\theta$  during two-stage equilibrium process at transfer (analysis step number 1).

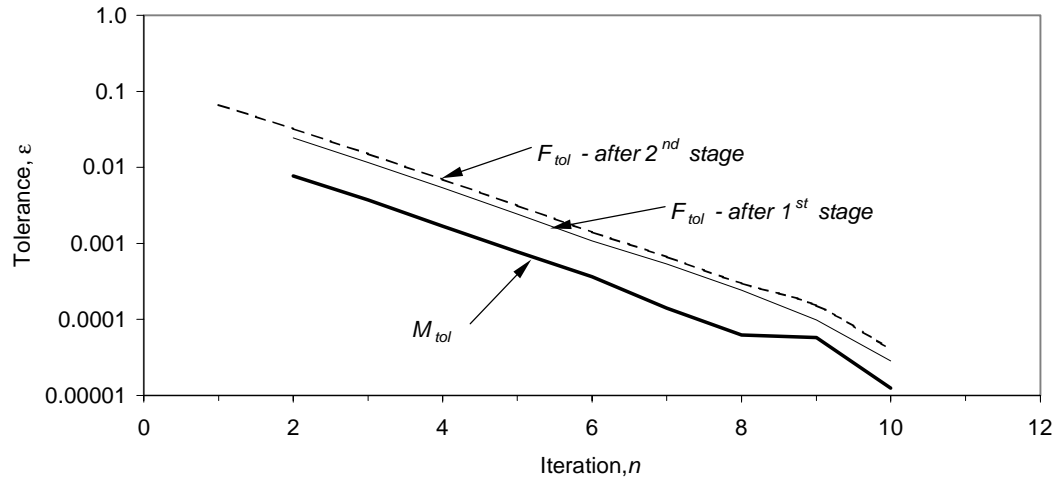


**Figure 2.5:** Observed force error,  $\epsilon_F$ , and moment error,  $\epsilon_M$ , after each iteration.

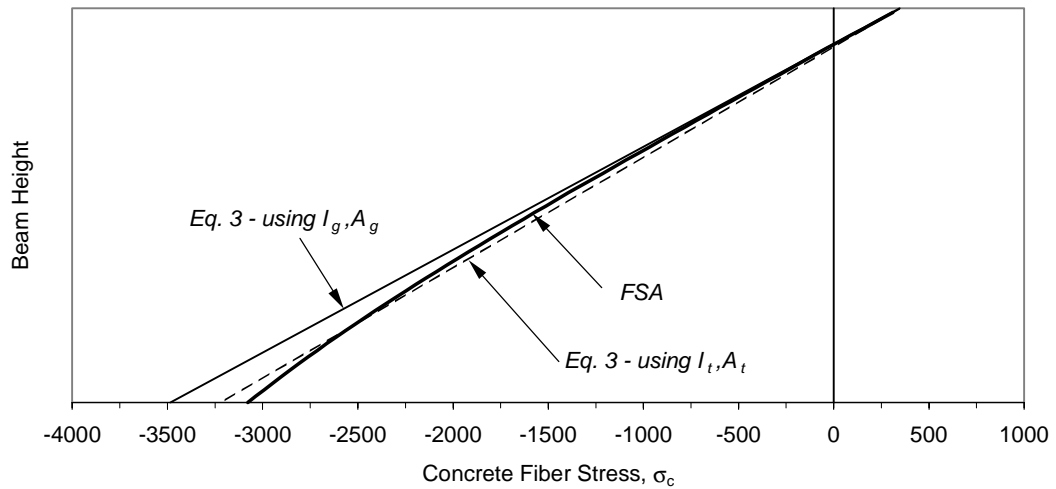


**Figure 2.6:** Concrete stress distribution for T-beam example at transfer.

### 2.3.2 Moment-Curvature relationship after Transfer

At the end of the two-stage process described in the previous section, the analysis algorithm proceeds in steps to find points on the cross-section  $M - \theta$  relationship. The procedure for developing the  $M - \theta$  curve is as follows:

1. After transfer calculations, the applied prestress force is adjusted for prestress loss due to elastic shortening and all other sources of loss. The cross-section response is then calculated in a manner similar to that used in transfer. Although approximate, the assumption that all prestress losses occur immediately after transfer simplifies the analysis algorithm considerably. In reality, prestress losses occur in a nonlinear manner over time, which would necessitate a time-dependent analysis, the accuracy and scope of which are not warranted for the type of research reported herein.
2. The calculated strains (after transfer and losses) are stored for all fibers of all component materials in the cross section including prestressing strands. These strains are designated  $\epsilon_{PS,i}^*$ ,  $\epsilon_{c,i}^*$ ,  $\epsilon_{CFRP,i}^*$ , and  $\epsilon_{s,i}^*$  for prestressing strand layers, concrete fibers, CFRP fibers, and steel bar layers, respectively.
3. The post-transfer/loss curvature is then calculated. For example, the curvature,  $\theta$ , for the first step is equal to the curvature increment,  $\Delta\theta$ , i.e.  $\theta = \Delta\theta$ . The total curvature at this level is

$$\theta^1 = \theta + \theta^* \quad (2.6)$$

where  $\theta^*$  is the curvature of the section just after transfer and loss calculations. The superscripts indicate the step number in the solution process. For example, a superscript of 1 corresponds to the first step in the post transfer/loss calculations.

4. Strains in all component fibers are adjusted to account for the initial prestressing stage according to the following equations:

$$\epsilon_{PS,i} = \epsilon_{top} + \theta d_{PS,i} + \epsilon_{PS,i}^* \quad (2.7a)$$

$$\epsilon_{c,i} = \epsilon_{top} + \theta d_{c,i} + \epsilon_{c,i}^* \quad (2.7b)$$

$$\epsilon_{CFRP,i} = \epsilon_{top} + \theta d_{CFRP,i} + \epsilon_{CFRP,i}^* \quad (2.7c)$$

$$\epsilon_{s,i} = \epsilon_{top} + \theta d_{s,i} + \epsilon_{s,i}^* \quad (2.7d)$$

In the previous equations,  $i$  denotes a fiber or a reinforcement layer. Strains in the CFRP and the concrete deck are adjusted once again to account for the construction sequence as described in the following section.

5. An iterative procedure is carried out to reach force equilibrium by performing a bisection algorithm in search of the girder top strain corresponding to the applied curvature. The top strain is denoted  $\epsilon_{top}^1$  for it represents the top strain at the 1<sup>st</sup> step.

6. Once equilibrium is achieved, the corresponding moment,  $M^1$ , is calculated from the contribution of individual components (i.e. fibers and reinforcement layers). This moment value and the corresponding curvature,  $\theta^1$ , represent a point on the  $M - \theta$  relationship.
7. Subsequent steps are conducted the same way by repeating 3 through 6. This yields a number of points on the  $M - \theta$  relationship for the analyzed girder.

Figure 2.7 shows the final  $M - \theta$  relationship for the single T-girder in Fig. 2.2. It is clear that the developed algorithm accurately captures all aspects of the flexural behavior of the beam. The results compare well with experimental values reported in Mitchell and Collins (1991). Additional verification studies for reinforced concrete cross-sections strengthened with CFRP are presented in Chapter 4.

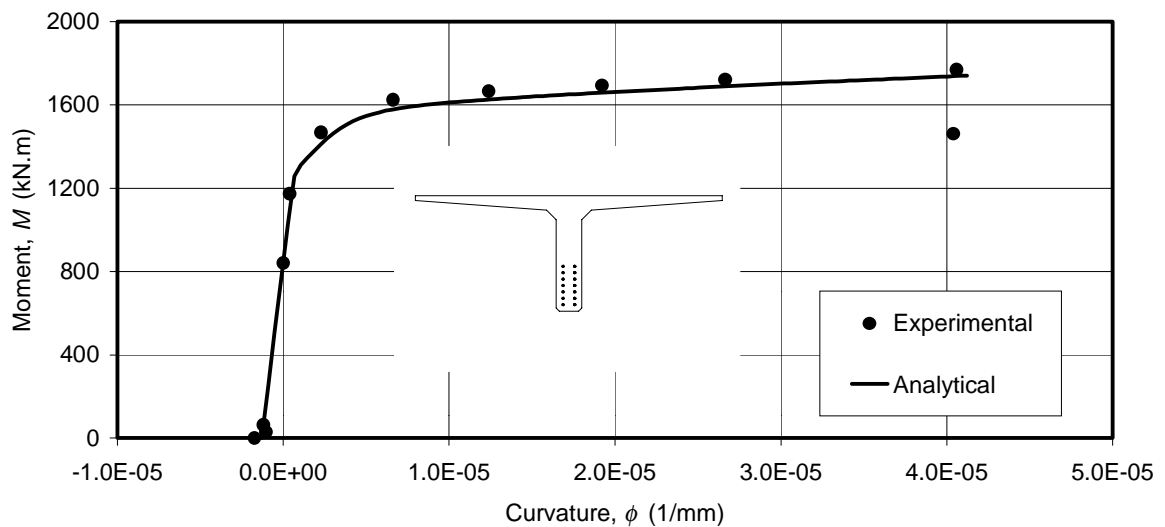


**Figure 2.7:** Experimental vs. analytical  $M - \theta$  relationship for verification.

### 2.3.3 Accounting for the Construction Sequence

As discussed in the previous sub-section, equilibrium steps are carried out at the time of transfer/loss to calculate the initial camber-causing curvature using a two-stage iterative process that satisfies moment then force equilibrium within each increment. After transfer/loss calculations, the loading sequence associated with placement of non-monolithic decks is taken into account during the moment-curvature calculations using a process similar to that described below for CFRP laminates (Fig 2.8).



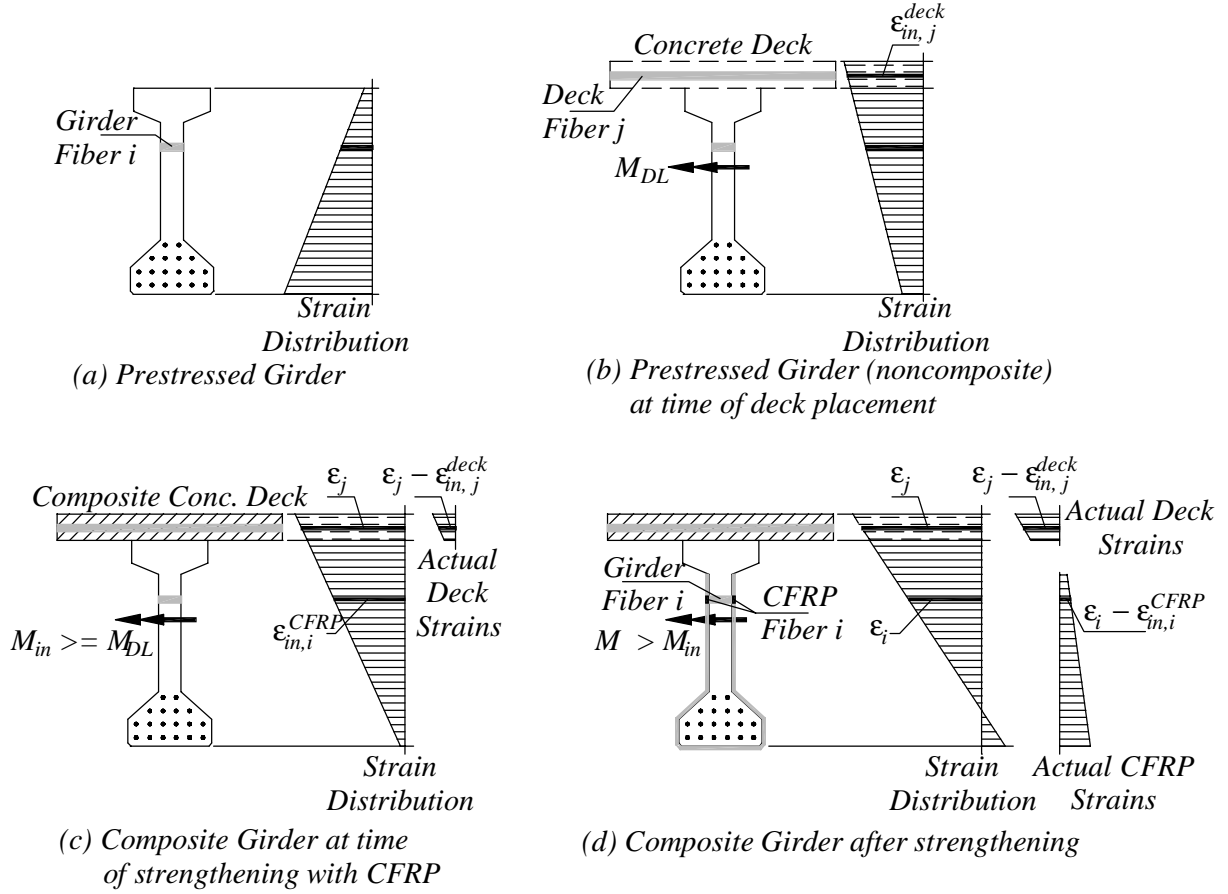


**Figure 2.8:** Sequence of analysis for girders with CFRP-strengthened girders with composite decks.

Rehabilitation of concrete structures using CFRP laminates usually takes place while the structure is subjected to a certain level of loading (taken equal to the full dead load in this study). Therefore, CFRP laminates are not strained while concrete and steel are both strained at the time of strengthening. The analysis method takes into account this situation as shown in Fig. 2.8. Just prior to strengthening the cross section with CFRP laminates, the cross section is subjected to a threshold moment  $M_{in}$  resulting in the corresponding strain gradient shown in Fig. 2.8(c). Knowing that CFRP strains must be zero at this stage, and that subsequently applied moments (beyond  $M_{in}$ ) will not result in identical strains in adjacent CFRP and concrete fibers, strains in CFRP fiber  $i$  are adjusted using the following equation:

$$\epsilon_{CFRP,i}^{adjusted} = \epsilon_{CFRP,i} - \epsilon_{CFRP,i}^{in} \quad (2.8)$$

As shown in Figure 2.8(d),  $\epsilon_{CFRP,i}$  is the strain in the CFRP fibers corresponding to a moment higher than  $M_{in}$  and calculated assuming that the strain in adjacent concrete and CFRP fibers is

identical.  $\epsilon_{CFRP,i}^{in}$  are the strains in concrete fibers adjacent to CFRP fibers at the threshold moment  $M_{in}$ .  $\epsilon_{CFRP,i}^{adjusted}$  are the adjusted CFRP strains for a moment greater than  $M_{in}$ .

### 2.3.4 General Moment-Curvature Response

Figure 2.9 shows a moment-curvature ( $M - \theta$ ) relationship that results from typical analyses of a PSC girder with and without bonded CFRP laminates. The relationship for the case with CFRP laminates shows key points of behavior such as at transfer, loss, threshold moment points (point at which concrete deck is cast or CFRP is bonded), and ultimate point. After casting the CIP deck, the girder exhibits increased stiffness, which further increases when the CFRP is attached. Once the CFRP ruptures, the flexural strength of the cross-section drops sharply then gradually flattens out as the crack in the CFRP laminates travels up the web. The strengthened cross section does not fail completely, but exhibits a post-failure capacity equal to the strength of the original cross section.

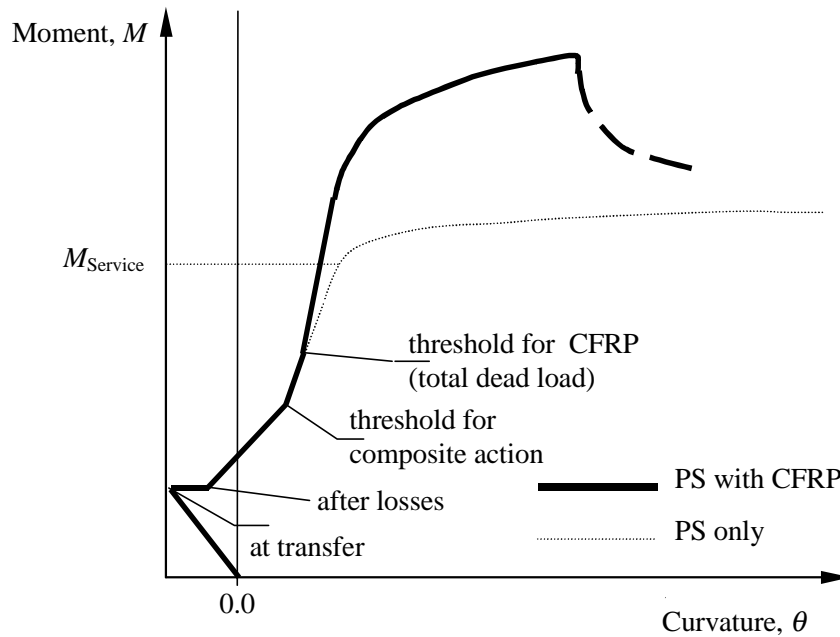


**Figure 2.9:** Idealized moment-curvature relationships for PSC girders strengthened with CFRP laminates.

## 2.4 Constitutive Properties of Component Materials

The assumed constitutive properties for the component materials are shown in Fig. 2.10. The stress-strain response of CFRP is assumed to be elastic-perfectly brittle whereas the stress-strain curve for steel is elastic-plastic with a post yield strain hardening of 1%. Prestressing strands are

modeled assuming a Ramberg-Osgood function. The Ramberg-Osgood coefficients are taken as  $a = 0.025$ ,  $b = 118$ , and  $c = 10$  for low relaxation strands (Collins and Mitchell 1991). A nonlinear stress-strain relationship is assumed for concrete fibers, which is described next.

#### 2.4.1 Concrete in Compression

The concrete compressive stress-strain curve is taken after Thorenfeldt (1987) and Popovics (1973):

$$f_c = \frac{nf'_c(\varepsilon_{cf}/\varepsilon'_c)}{n-1+(\varepsilon_{cf}/\varepsilon'_c)^{nk}} \quad (2.9)$$

Where:

$f_c$  is the concrete stress.

$f'_c$  is the unconfined compressive strength (cylinder strength).

$\varepsilon_{cf}$  is the concrete strain.

$\varepsilon'_c$  is the concrete strain at  $f'_c$ .

$n = 0.8 + f'_c/17$  ( $f'_c$  in MPa units)

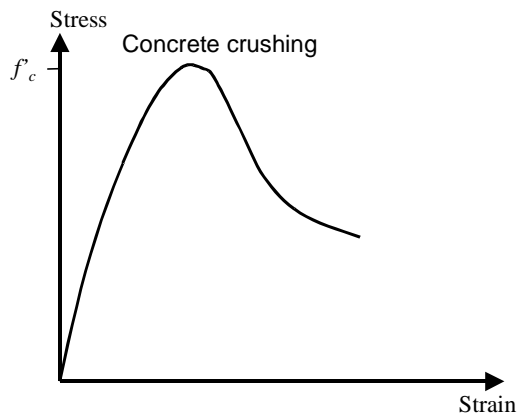
$k = (0.67 + f'_c/62) > 1$  for  $(\varepsilon_{cf}/\varepsilon'_c) > 1$ . Otherwise  $k = 1$ . ( $f'_c$  in MPa units)

Concrete strength is taken to be  $0.85 f'_c$  instead of  $f'_c$  in the analyses. Use of the 0.85 factor is well established in the literature and accounts for (a) basic differences between concrete in a test cylinder versus a reinforced concrete beam due to geometry, steel reinforcement, method of load application, rate of loading, ...etc.; and (b) variations in concrete compaction, water-cement ratio, and curing conditions.

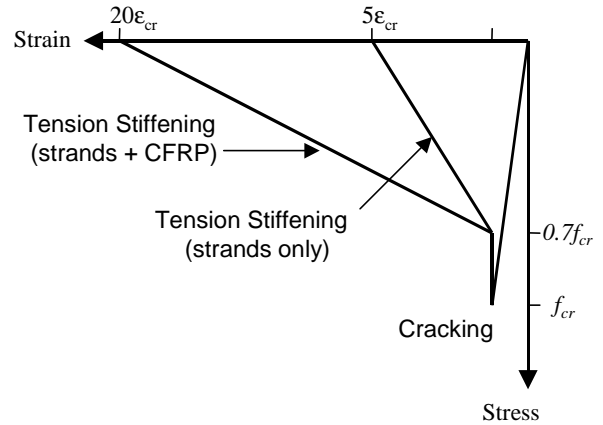
#### 2.4.2 Concrete Cracking

Concrete is assumed to crack when it reaches its tensile strength calculated according to the ACI 318 Code (1999). After concrete cracks, tension stiffening occurs in concrete reinforced with CFRP or steel bars. Tension stiffening accounts for load transfer mechanisms that exist between reinforcement (steel bars or CFRP fabric) and surrounding concrete and is generally represented by a gradual degradation in the concrete tensile strength after cracking. It is reasonable to assume that CFRP will generate a greater concrete tension stiffening effect compared to steel bars because it is directly attached to a large concrete surface area. Based on a calibration to beam test results by Shahawy and Beitelman (1999) tension stiffening due to steel bar reinforcement alone is assumed to decrease linearly from 70% of the cracking stress to zero at five times the concrete

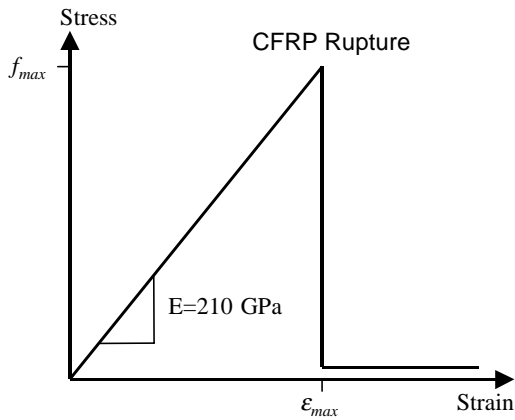
cracking strain. Tension stiffening due to the presence of both steel and CFRP combined is assumed to degrade linearly from 70% of the cracking stress to zero at 20 times the concrete cracking strain. These models are shown in Fig. 2.10b.



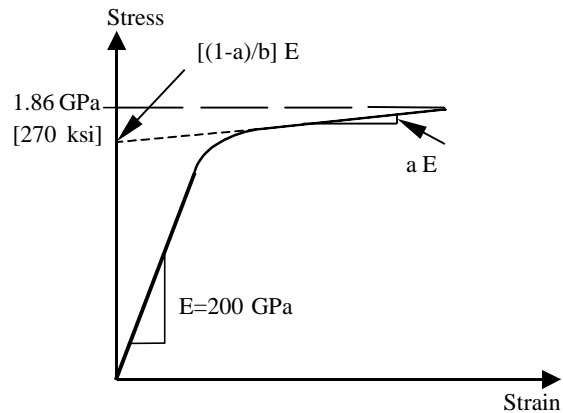
(a) Concrete in compression



(b) Concrete in tension



(c) CFRP in tension



(d) Prestressing strands

**Figure 2.10:** Monotonic constitutive models for component material

## 2.5 Time-Dependent Behavior of Component Materials

Much work has been done on time-dependent analysis of concrete structures. Bazant (1988) provides a general review of material models and analysis techniques for concrete structures undergoing creep and shrinkage. Rao and Jayaraman (1989) provide a more specific review of

models used for the analysis of reinforced and prestressed beams undergoing creep and shrinkage. Among the material models most commonly used are the incremental quasi-elastic stress-strain model and the age-adjusted effective modulus model. In the former, which is more rigorous and accurate, the stress-strain relation for the time step is treated as a quasi-elastic relation, and the structural problem is solved through a sequence of linear steps. In the age-adjusted effective modulus model, the problem is solved in one time step making use of an effective quasi-elastic stress-strain relationship. The model proposed in this paper falls under the first category and is described in the following sections.

### 2.5.1 Fatigue Response of Concrete

Cyclic loading on concrete produces an effect that is similar to creep, i.e. increase in concrete strain with increasing number of cycles. However, tests have demonstrated that strain accumulation due to a varying load is greater than creep due to a constant load equal to the average of the cyclic load. The difference is dependent on a number of parameters, including stress range, maximum stress, ambient temperature, and humidity (Neville 1996).

Experiments have shown that the stress-strain response of concrete varies with the number of load repetitions ('Considerations' 1974, Neville 1996, Holmen 1982). It starts out with the usual concave shape and quickly transitions to a straight-line then gradually to a characteristic convex shape. Test observations indicate that the closer the concrete is to failure, the more convex its stress-strain response (Figure 2.11).

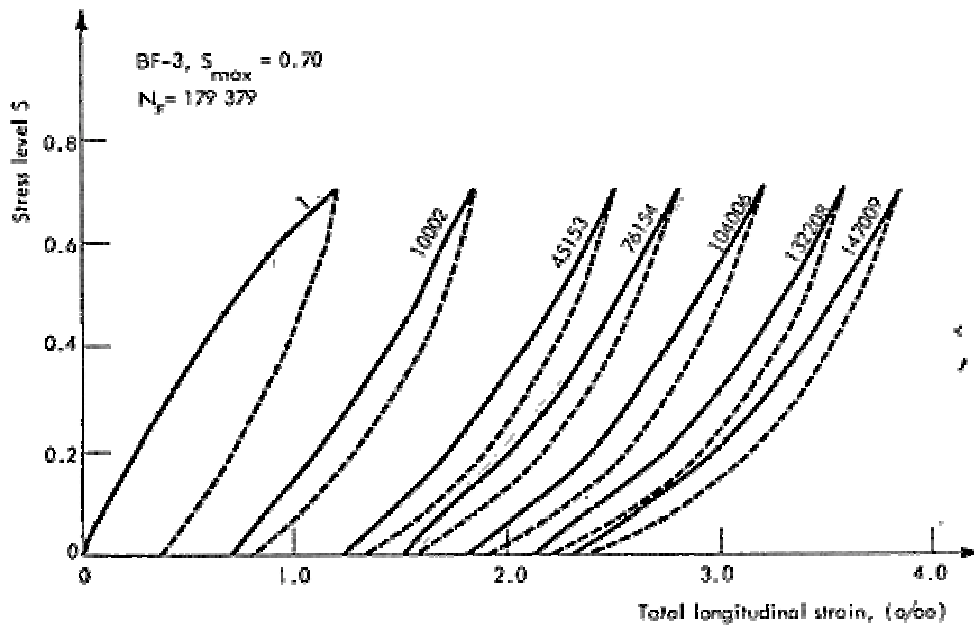


**Figure 2.11:** Compressive behavior of concrete subjected to repeated loading

Since concrete in most structures will typically be subjected to relatively low stress levels under service conditions and will generally not be susceptible to high cycle fatigue failure during the design life, it is reasonable to assume the straight-line constitutive model depicted in Fig. 2.12 for fatigue calculations. Making use of the straight-line assumption and uniaxial concrete fatigue test data provided by Holmen (1982) and Bennet and Raju (1971) the following concrete material model is proposed. The model is suitable for a loading frequency ranging from 0.83 to 15 Hz ('Considerations' 1974 and Holmen 1982).

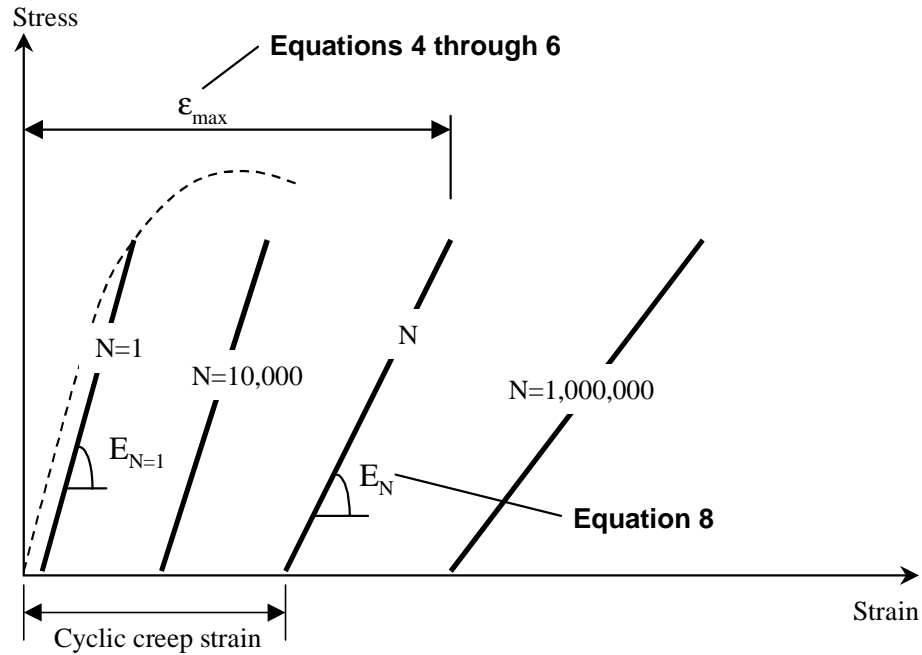


**Figure 2.12:** Proposed constitutive model for concrete subjected to fatigue loading.

Holmen proposed that the total maximum strain at any time and at any number of cycles is the sum of two components. The first component is related to the endurance of the specimen,  $\epsilon_e$ , and the second part is a function of the loading time,  $\epsilon_t$ , and is essentially a creep strain. In other words:

$$\epsilon_{\max} = \epsilon_e + \epsilon_t \quad (2.10)$$

It was observed from the tests that strain development follows three distinct phases; a rapid increase from 0 to about 10 percent of the total fatigue life, a uniform increase from 10 to about 80 percent, then a rapid increase until failure. Holmen (1982) proposed the following expressions to describe the first and second phases:

For  $0 < \frac{N}{N_F} \leq 0.1$

$$\epsilon_{\max} = \frac{1}{E_{\text{sec}}} \left| S_{\max} + 3.18(1.183 - S_{\max}) \left( \frac{N}{N_F} \right)^{0.5} \right| + 0.413 \times 10^{-3} S_c^{1.184} \ln(t + 1) \quad (2.11)$$

For  $0.1 < \frac{N}{N_F} \leq 0.8$

$$\epsilon_{\max} = \frac{1.11}{E_{\text{sec}}} \left| 1 + 0.677 \left( \frac{N}{N_F} \right) \right| + 0.413 \times 10^{-3} S_c^{1.184} \ln(t + 1) \quad (2.12)$$

where:

$\epsilon_{\max}$  maximum total strain

$E_{\text{sec}}$  initial secant modulus =  $\frac{S_{\max}}{\epsilon_0}$

$\epsilon_0$  maximum total strain in the first load cycle

$S_{\max}$  ratio of maximum stress to concrete strength

$S_c$  characteristic stress level =  $S_m + \text{RMS}$

$S_m$  mean stress ratio =  $\frac{1}{2} (S_{\min} + S_{\max})$

$S_{\min}$  ratio of minimum stress to concrete strength

$N$  number of load cycles

$N_F$  number of load cycles to failure for a specified probability of failure. For example, for a 50% probability of failure, and for  $S_{\min}=0.05$ , the number of cycles to failure can be calculated from  $\log N_F = 1.839 S_{\max}^{-3.033}$  (Holmen 1982)

$t$  duration of alternating load in hours

RMS root mean square value =  $\sqrt{\frac{1}{T_0} \int_0^T x^2(t) dt}$

$x(t)$  stress as a function of time,  $t$

$T_0$  total time, i.e. duration of loading.

According to Holmen (1982), the RMS value for sinusoidal loading is given by

$$RMS = \frac{1}{2\sqrt{2}}(S_{\min} + S_{\max}) \quad (2.13)$$

Based on calibration to test results in Bennet and Raju (1971) and Holmen (1982), the following equation is proposed for the effective modulus of elasticity.

$$E_N = \left(1 - 0.33 \frac{N}{N_F}\right) E_{\text{sec}} \quad (2.14)$$

where:

$E_N$  is the effective concrete modulus of elasticity at N cycles.

Knowing  $S_{\max}$ ,  $\epsilon_{\max}$ , and  $E_N$  defined using Eqs. 2.10 through 2.14, a relationship can be constructed that represents the compressive stress-strain response of concrete as a function of the applied stresses and number of load cycles. Concrete under tension is assumed to have no significant tensile strength during cyclic fatigue calculations. The proposed stress-strain curve is shown in Fig. 2.12.

### **2.5.2 Additional Model Assumptions**

The proposed concrete fatigue model makes use of a number of additional assumptions. It is assumed that the concrete water content and ambient temperature associated with a particular specimen to be analyzed are comparable to those in Holmen's tests. It is further assumed that the model, which is calibrated to uniaxial data, is applicable to concrete subject to a strain gradient. Test results indicate that a strain gradient can influence the fatigue behavior of concrete, typically resulting in a slower rate of strength degradation with increasing number of cycles ('Considerations' 1974). However, fatigue tests on eccentrically loaded concrete are limited, and there is insufficient information to calibrate the proposed model to account for this effect. It is also assumed that the shrinkage strain is negligible compared to the cyclic fatigue strain. This is justifiable since the proposed model is mostly useful for analyzing beams subjected to accelerated fatigue loading, in which the duration of the test is rather short - two to three weeks.

### **2.5.3 Fatigue Response of Steel, CFRP, and Epoxy**

Experimental results presented in Barsom and Rolfe (1987) suggest that the modulus of elasticity for steel remains unchanged until just before failure by high cycle fatigue. Furthermore, test data in Hull (1981) and Hollaway and Leeming (1999) suggests that the behavior of CFRP is virtually unaffected by fatigue loading. Hence, the modulus of elasticity for both steel and CFRP is assumed to remain unchanged during cyclic loading. Furthermore, the epoxy between the CFRP laminates and concrete is assumed to be rigid and unaffected by cyclic loading. This is a



reasonable assumption for beams in which failure initiates in the high moment zone, where shear stresses in the epoxy are low.

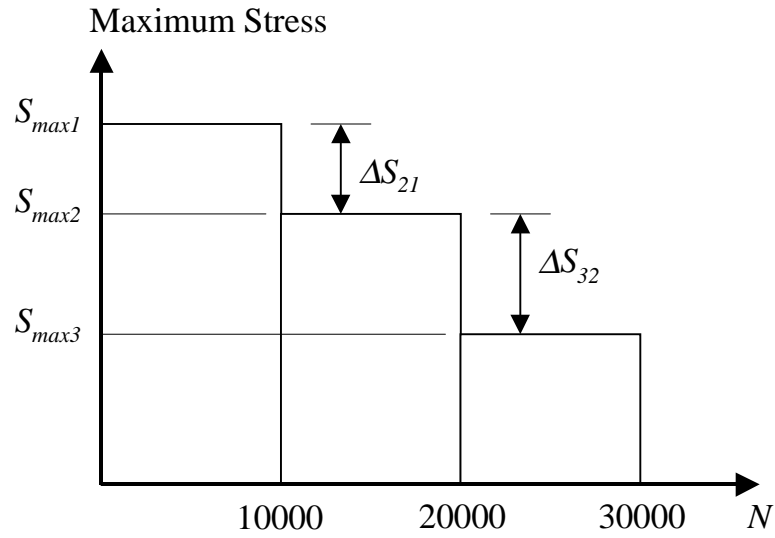
## 2.6 Fatigue Calculations

As fatigue loading progresses, the stress-strain response of each concrete fiber changes as a function of the number of cycles and maximum and minimum stresses generated within the fiber. To simulate the fatigue behavior of a cross-section, the analysis is conducted in increments of cycles, say 10,000 cycles each, and the concrete constitutive model is updated at the end of each block of cycles. It is assumed that the concrete model does not change within each set of cycles.

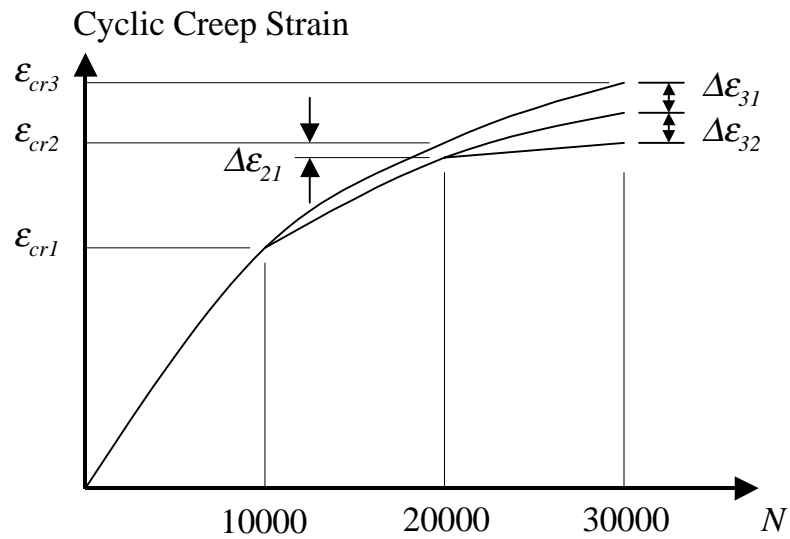
The maximum and minimum stresses in each fiber can change considerably during the analysis, affecting the cyclic creep strain calculation and the corresponding constitutive relationship. As shown in Figure 2.12, the cyclic creep strain is equal to  $\epsilon_{\max}$  minus the elastic component of strain. The change in stress levels during the analysis is taken into account using the principle of superposition. The principle of superposition states that the creep strain response (in this case cyclic creep strain) of concrete to a sum of two stress histories is the sum of the responses to each of them taken separately. The superposition principle is generally deemed reasonably accurate when applied to concrete within the service stress range (Bazant 1988).

A fatigue simulation starts by conducting a monotonic moment-curvature analysis of the beam cross-section. The purpose of this step of the analysis is to obtain the maximum and minimum stresses in each fiber corresponding to the application of the maximum and minimum moments. These stresses are utilized to construct concrete constitutive models for each individual fiber using Eqs. 2.10 through 2.14. The developed constitutive model for each fiber is assumed to represent fiber behavior at the beginning and during the following (second) block of cycles. Using the constructed constitutive models, a second monotonic analysis is conducted to calculate the moment-curvature response of the section during the second block of cycles. The maximum and minimum stresses calculated from the second monotonic analysis are used as input stresses for the third set of cycles and new stress-strain curves for each fiber are constructed using Eqs. 2.10 through 2.14. The process described above is repeated to compute the response of the cross-section for any number of cycles.

The sequence of steps taken by the program to update the cyclic creep strains can be better understood by examining Fig. 2.13. At the beginning of the first block of 10,000 cycles, the maximum stress in a particular fiber is say,  $S_{\max 1}$ , and the cyclic creep strain is zero. At the beginning of the second block of cycles, the maximum stress in the same fiber drops to  $S_{\max 2}$  by an amount  $\Delta S_{21}$  and the accumulated cyclic creep strain is  $\epsilon_{cr1}$ . At the beginning of the third block of cycles, the maximum stress in the fiber drops to  $S_{\max 3}$  by an amount  $\Delta S_{32}$  and the accumulated cyclic creep strain is  $\epsilon_{cr2} - \Delta \epsilon_{21}$ . The quantity,  $\epsilon_{cr2}$ , is calculated as if the stress,  $S_{\max 1}$ , had been acting for 20,000 cycles. According to the superposition principle, the correction  $\Delta \epsilon_{21}$  is algebraically added (in this case subtracted because the stress is dropping) and represents the accumulated creep strain due to  $\Delta S_{21}$  acting for 10,000 cycles, between the ends of cycle increments 1 and 2. The process can then be repeated for subsequent blocks of cycles. The solution method requires some bookkeeping to keep track of corrections, which increase with the number of cycle increments. Nevertheless, programming the process is quite straightforward.



(a)



(b)

**Figure 2.13:** Principle of superposition for cyclic creep strain calculations

## 2.7 Beam Deflection Calculation

Beam deflections are calculated using the stiffness approach. The stiffness method relates nodal displacements to nodal forces through the global stiffness matrix. Displacements at nodes (translational and rotational) are unknown and are solved for incrementally to account for nonlinear behavior. Since only beam structures are of interest, nodal degrees of freedom are

limited to vertical translations and rotations, i.e. the beams are considered axially rigid (Fig. 2.14). The stiffness matrix of the beam is

$$k = \frac{EI}{L^3} \begin{bmatrix} 12 & 6L & -12 & 6L \\ 6L & 4L^2 & -6L & 2L^2 \\ -12 & -6L & 12L & -6L \\ 6L & 2L^2 & -6L & 4L^2 \end{bmatrix} \quad (2.15)$$

where  $EI$  is the flexural stiffness and  $L$  is the member length.

Prior to an analysis, the moment-curvature response for each finite element is calculated using the fiber section method. The moment-curvature response is obtained for both positive and negative bending and is used to compute the flexural stiffness of each element. The slope of the moment-curvature curve is the tangential  $EI$  (Figure 2.15). Since most bridges have cross-sections that do not vary much over the length, many finite elements in a particular problem will have similar properties. Hence the cross-section analysis needs to be run for only a few representative elements.

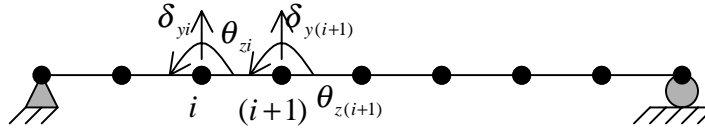


**Figure 2.14:** Degrees of freedom of beam elements used in this research

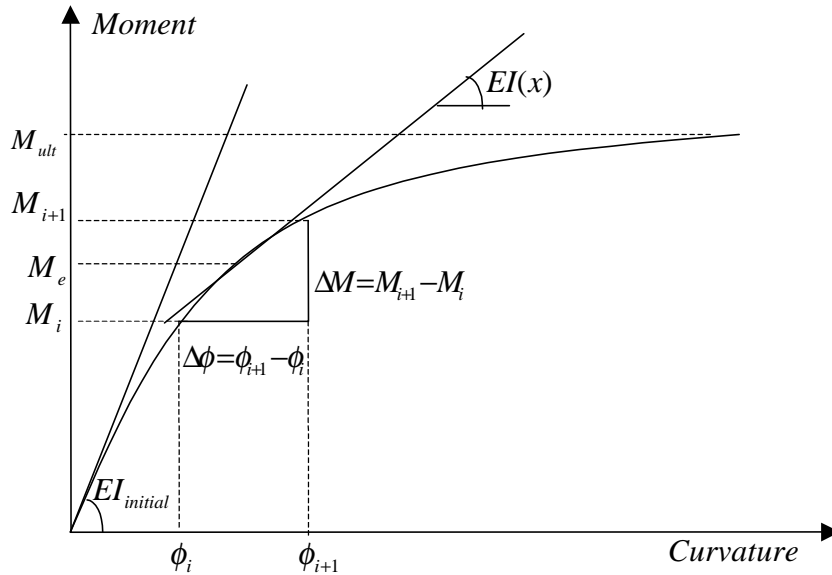


**Figure 2.15:** Calculation of flexural stiffness from moment-curvature relationship

The solution process is of the Euler type, i.e. simple incremental. After each load increment is applied, the condition of the structure is evaluated and the stiffness matrix is updated. No attempt is made to iterate on the unbalanced forces resulting from this process. Acceptable accuracy can be achieved because the applied load increments are kept small. Although the solution process is well known, it is summarized here for completeness.

1. The incremental load vector, which is a small fraction of the total applied load, is assembled. The applied load increments are kept constant throughout the analysis.
2. For the first load increment, the member flexural stiffness is equal to the initial value of  $EI$  calculated from the moment-curvature response.
3. Once the global stiffness matrix and incremental force vector are assembled, the incremental nodal displacements are computed. The total nodal displacements are then updated by adding the incremental displacements to the total displacement vector.
4. The incremental member displacements are extracted from the incremental global displacements, and the incremental member forces are obtained by multiplying the member stiffness matrix by the incremental member displacements. The total member forces are then updated by adding the incremental forces to the total member force vector.
5. The new member forces are used to calculate the member flexural stiffness from the moment curvature relationships.
6. The member stiffness matrix is then updated and analysis steps 3 through 6 are repeated until a specified maximum load is reached or until the ultimate load is reached.

## **2.8 Computer Implementation - T-DACS Program**

The static and fatigue analysis procedures described in this chapter have been implemented in a computer program T-DACS (Time-Dependent Analysis of Composite Sections), which was developed and runs within MatLab. T-DACS is verified and exercised in Chapter 4 by comparing analytical results to test data in Shahawy and Beitelman (1999, 2000) and Barnes and Mays (1999). Numerical studies using T-DACS show that accuracy of the analysis does not increase significantly when the number of cycles per step is less than 10,000, and so all calculations in this work are conducted using 10,000 cycle increments.

## **2.9 Computer Implementation - MACS Program**

T-DACS is rather cumbersome to use because it runs within MatLab, and needs text input. A more user friendly computer program was developed to run the static fiber section model only; i.e. it computes monotonic moment-curvature and load-deflection response. This program (MACS - Monotonic Analysis of Composite Sections) was developed within the Visual Basic programming environment and has a sophisticated a graphical user interface.

Visual Basic was chosen for development of MACS because it provides a flexible programming environment that allows the creation of user-friendly software. In VB, coding is stored in forms and modules. Forms are windows that appear on the screen. Visual Basic allows the user to move from one window (form) to another to enter data or receive results in a user-friendly manner. Modules are where most of the VB coding is stored. Algorithms with numerically intensive calculations are implemented within these modules.

MACS was developed by linking two existing pieces of code: the monotonic portion of T-DACS and a program that performs structural analysis of beams using the stiffness method developed by Okeil (1999). Modifications were done to the linked code to allow the execution of nonlinear analyses. The program stores input data in files with extension \*.*bd*t and saves the analysis results in two output files; namely *PD.dat* and *MPhi.dat*. The former contains load-mid-span deflection data, while the latter stores the moment-curvature data.

Figure 2.16 shows the main window of the program that allows the user control over dependent windows. Figure 2.17 shows the first dependent form that is used to enter cross section type, geometric and material properties of reinforcing bars, concrete, CFRP and prestressing steel bars. In order to minimize input errors, reinforcing steel bars, CFRP and prestressing steel bars groups are inactive by default until the user activates them by clicking on a check box. The program is capable of analyzing cross sections with any or all of these reinforcement groups combined. Figures 2.18 and 2.19 show windows that allow the user to enter beam name, span length and loading configurations and to make necessary changes in the input data. During the analysis the load-deflection and moment-curvature relationships are plotted and updated as the analysis proceeds (Fig. 2.20). After the analysis is completed, detailed plots of load-deflection and moment-curvature relationships are displayed as a part of the main window as shown in Figs. 2.21 and 2.22. The window also shows the moment and curvature values at cracking, steel yielding, ultimate capacity of the cross section, failure type under positive and negative bending and the time spent during the analysis. Displacement, bending moment and shear force diagrams also plotted as shown in the Fig. 2.23.

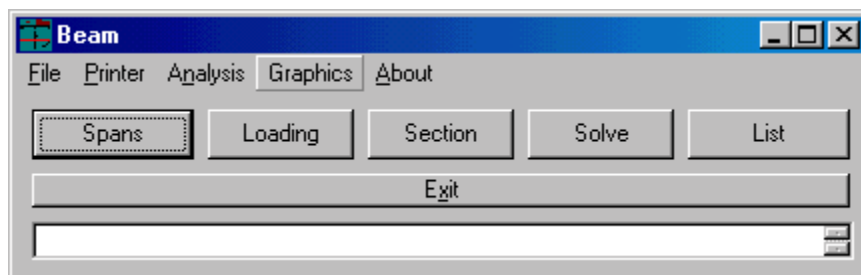


**Figure 2.16:** Main window that controls input data and analysis results

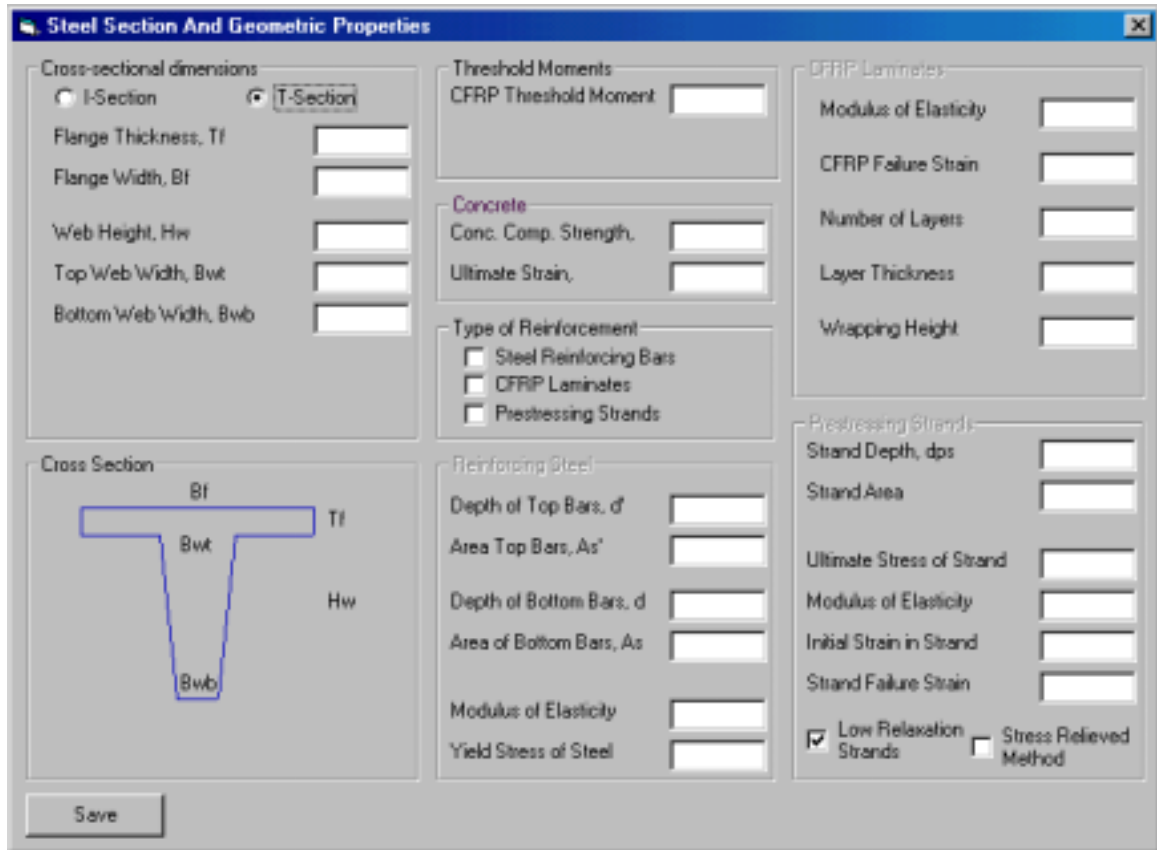


Figure 2.17: Reinforcement types, geometric and material properties window

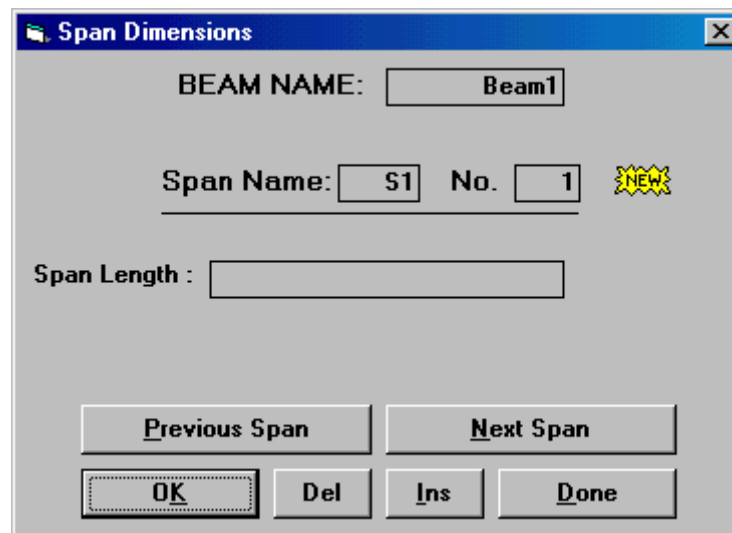


Figure 2.18: Input window for beam name and length

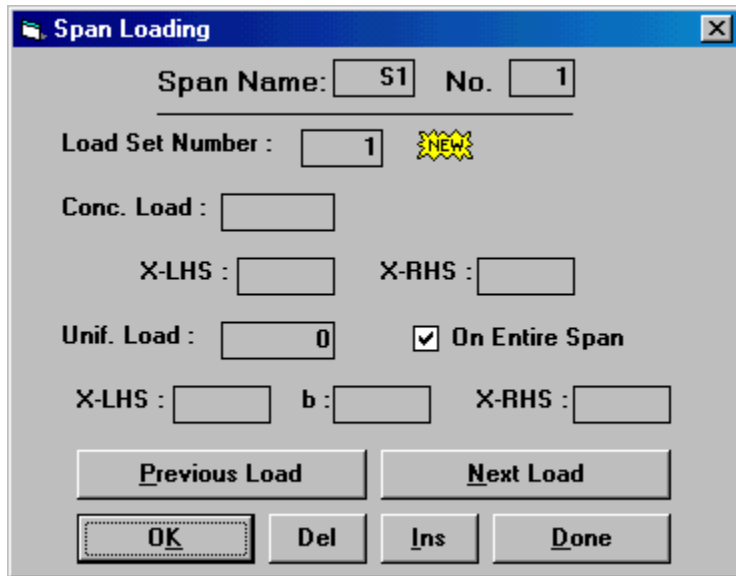


Figure 2.19: Input window for definition of loading

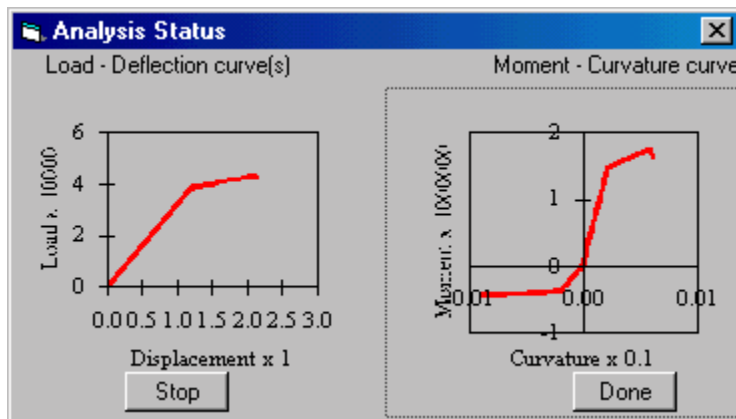
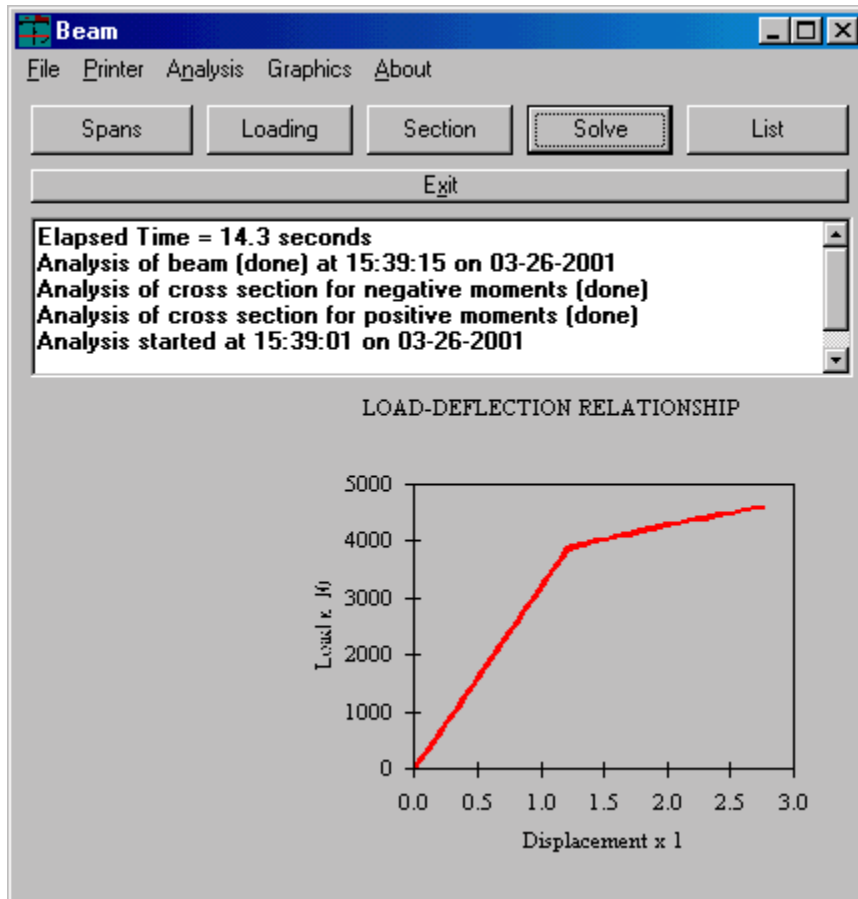
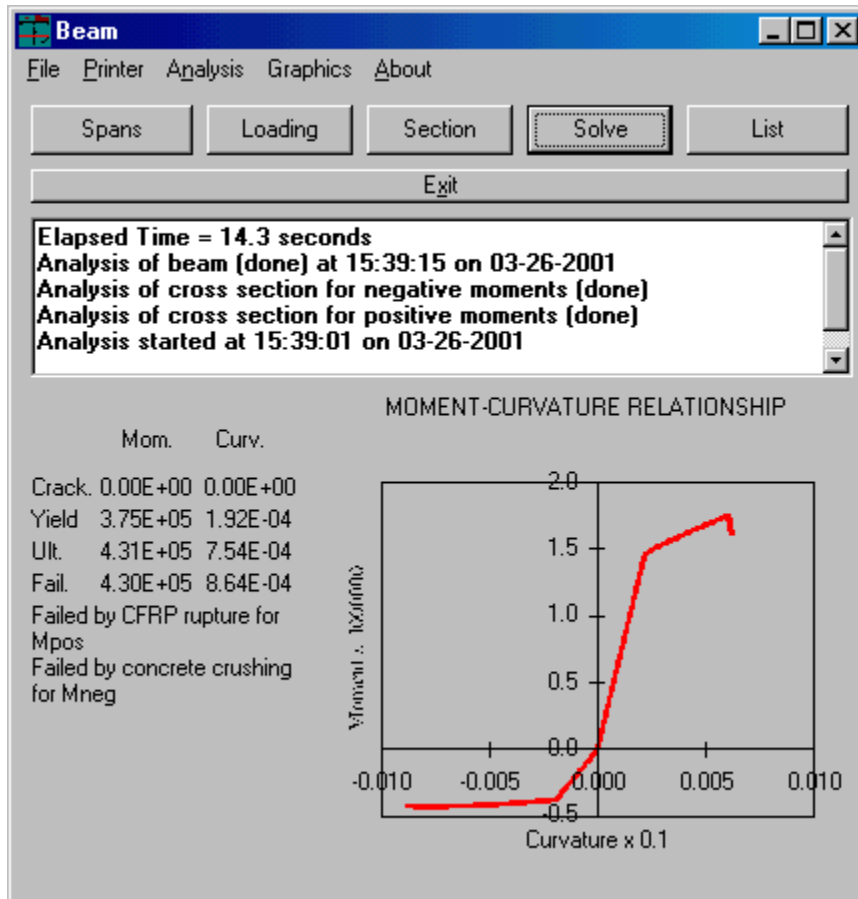


Figure 2.20: Status window that runs during the analysis



**Figure 2.21:** Mid-span load-deflection results window





**Figure 2.22:** Positive and negative moment-curvature relationship of the cross-section

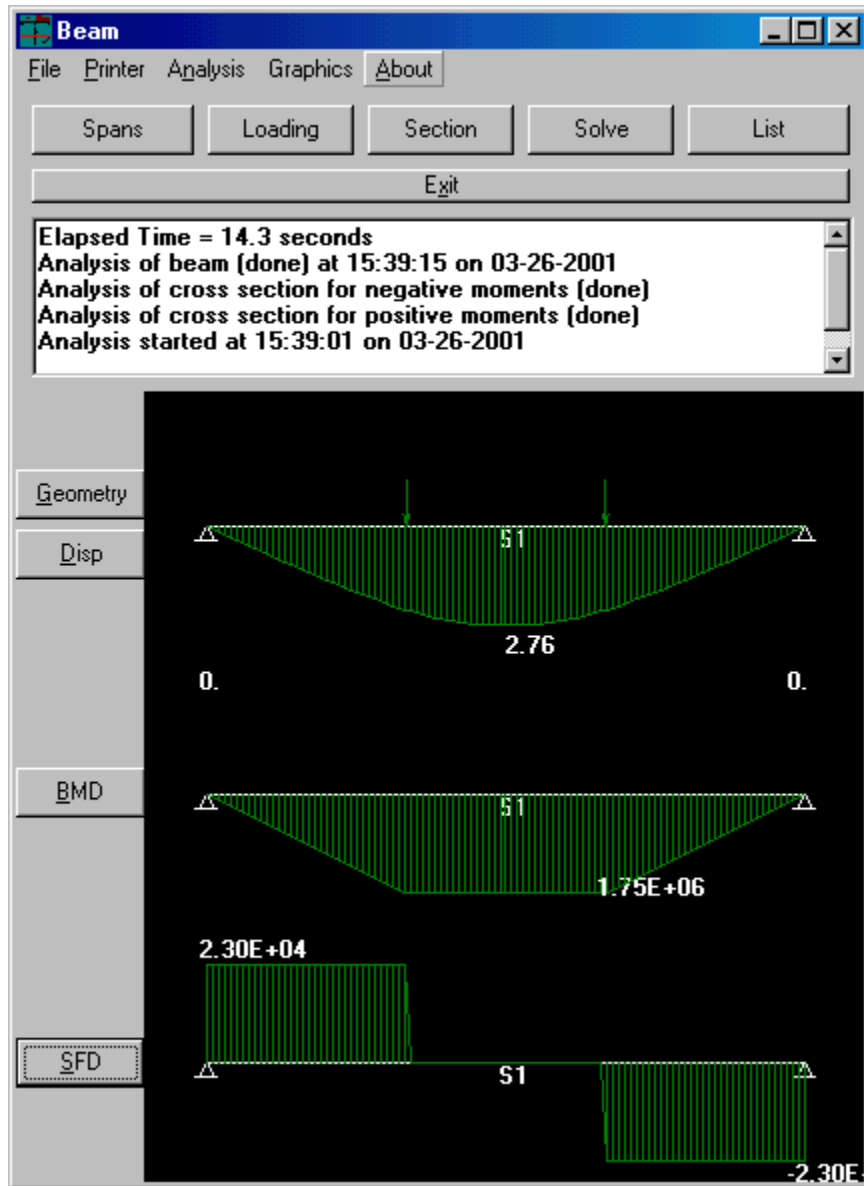


Figure 2.23: Displacement, bending moment and shear force diagrams

## 3 SHORT-TERM CFRP LAMINATE STRENGTH

### 3.1 Introduction

Despite the fact that fiber reinforced polymer materials are no longer considered new products, established methods for estimating the design tensile strength are absent. ACI's state-of-the-art report (1996) acknowledges the issue; however, it falls short in recommending values or a specific method for estimating the design tensile strength of the product. This position is understood since products vary greatly by manufacturer, fiber type, fiber structure, and resin type. The state-of-the-art report suggests that loading conditions for the CFRP product be determined in advance and that the material characteristics corresponding to those conditions be obtained in consultation with the manufacturer. The work of Bakht et al. (2000) suggests the use of coupons for estimating the strength of FRP materials. While some researchers investigating uses of CFRP materials for strengthening applications have performed coupon tests to estimate the tensile strength of CFRP laminates (e.g. Ritchie et. al. 1991), there are some instances in the literature where laminate strength was assumed equal to the manufacturer reported fiber strength. This could be unconservative since the strength of a single fiber or dry strand is generally greater than the laminate strength. Nevertheless, an unconservative estimate of laminate strength is inconsequential if the modes of failure under study do not involve laminate rupture, but rather concrete and bond related failures.

Fibers are assembled together to form tows or yarns, which are then woven into a fabric that forms the laminate. Experimental testing and analyses (Bullock 1974, Harlow and Phoenix 1981, Batdorf and Ghaffarian 1984, Duva et al 1996, Mahadevan et al 1997, and Yushanov and Bogdanovich 1998) have shown that the strength of the final composite product (i.e. laminate),  $\sigma_{\text{laminate}}$  is normally much lower than the strength of the fiber,  $\sigma_{\text{fiber}}$ , in some cases, as low as 40-50%. The above listed researchers have investigated the relationship between  $\sigma_{\text{fiber}}$  and  $\sigma_{\text{laminate}}$  and presented techniques for estimating laminate strength from fiber characteristics. However, these methods have yet to be adopted by structural engineers designing structures strengthened with CFRP laminates.

In this chapter, the Weibull theory is used to establish a relationship between the fiber tensile strength and the tensile strength of CFRP laminates attached to a concrete girder. Such a relationship facilitates the design process and enables structural engineers to estimate laminate strength from fiber properties published by the manufacturer. While coupon and component tests are valid means for estimating the short-term tensile strength of CFRP sheets, they are not practical for everyday use and, as will be illustrated in this work, composite strength is affected by the coupon size. To verify the theory presented in this chapter, the short-term tensile strength of CFRP sheets calculated using the proposed theory is compared to published experimental results of concrete T-beams strengthened with a varying amount of CFRP laminates. Good agreement is found between theoretical calculations and test results.

### 3.2 Weibull Theory for Composite Materials

The tensile strength of composite materials is assumed to follow the Weibull Theory. This assumption is well established in the literature (Harlow and Phoenix 1981, Batdorf and Ghaffarian 1984, Batdorf 1994) and has been verified experimentally through tests of composite specimens with different size and stress distribution (Bullock 1974, Kaminski 1973, Lavoie 1997), especially for unidirectional and  $0^\circ/90^\circ$  laminates. The basic concepts of the Weibull theory can be found in many textbooks (e.g. Batdorf 1994) and are summarized below for completeness.

If the average number of flaws per unit length of a fiber of a Weibull material is  $n$ , and the length of a fiber is  $L$ , the expected number of flaws in the entire length,  $Q$ , is  $nL$ . Weibull theory expresses the number of flaws per unit length,  $n$ , in terms of the applied stress,  $\sigma$ , a shape parameter,  $m$ , and a scale parameter,  $\sigma_o$ :

$$n(\sigma) = \left( \frac{\sigma}{\sigma_o} \right)^m \quad (3.1)$$

which leads to the following expression for the expected number of flaws for a fiber of a Weibull material of length  $L$  subjected to a strength less than  $\sigma$

$$Q = L \left( \frac{\sigma}{\sigma_o} \right)^m \quad (3.2)$$

To study the effect of the length of the fiber on the failure strength of a Weibull material, the expected number of flaws,  $Q$ , has to be investigated. Failure takes place if there is a probability that one complete flaw exists; i.e.  $Q = 1$ . By setting  $Q = 1$  in Eq. 3.2, the following expression is obtained for the expected failure stress:

$$\sigma_f = \sigma_o L^{-1/m} \quad (3.3)$$

Figure 3.1 shows the effect of the length of the fiber on the expected failure stress of a Weibull material. It is clear that the strength of a fiber decreases as its length increases.

To generalize the theory, an infinitesimal fiber length,  $\Delta L_j$ , is considered. The probability that the segment contains a flaw, which is equal to the probability of failure of the segment, is

$$(\Delta P_f)_j = n \Delta L_j \quad (3.4)$$

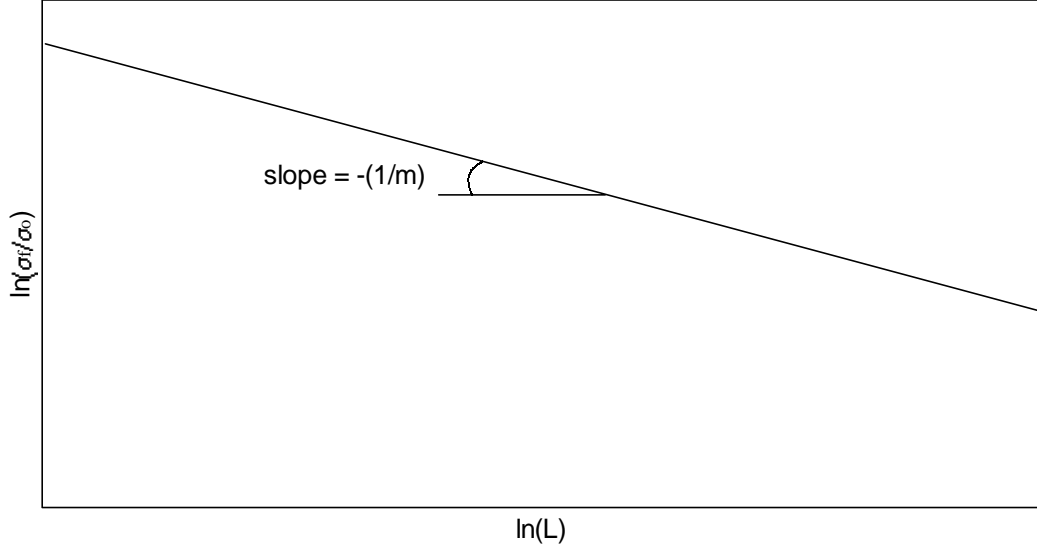


**Figure 3.1:** Effect of fiber length on failure stress (Weibull size effect)

The probability of failure of an entire fiber of length  $L$  (comprised of  $N$  segments) is therefore

$$P_f = 1 - \prod_{j=1}^N \left[ 1 - (\Delta P_f)_j \right] \quad (3.5)$$

For infinitesimal segment lengths  $\Delta L_j$ , the probabilities of failure  $(\Delta P_f)_j = n\Delta L_j$  are also infinitesimal, and hence the probability of failure of an entire fiber can be approximated as

$$P_f = 1 - \prod_{j=1}^N \exp\left[-(\Delta P_f)_j\right] = 1 - \exp\left[-\sum_{j=1}^N (\Delta P_f)_j\right] = 1 - \exp[-nL] \quad (3.6)$$

Making use of Eq. 3.1, Eq. 3.6 can be expressed in the following alternative form.

$$P_f = 1 - \exp\left[-\int_L (\sigma/\sigma_o)^m dL\right] \quad (3.7)$$

Equation 3.6 expresses the probability of failure,  $P_f$ , of a single fiber of a Weibull material in terms of its length,  $L$ , and the applied tensile stress,  $\sigma$ . It is useful to have a general form for the probability of failure expressed in terms of the volume instead of the length. This can be done by modifying Eq. 3.7 to read as follows.

$$P_f = 1 - \exp \left\{ - \int_V \left( \frac{\sigma}{\sigma_o} \right)^m dV \right\} \quad (3.8)$$

The relationships in Eq. 3.7 and Eq. 3.8 are usually referred to as the Weibull cumulative distribution functions. The shape and scale parameters in these equations are determined by calibration to test results and are related to the mean,  $\mu_\sigma$ , and coefficient of variation, COV, through the following expressions.

$$\mu_\sigma = \sigma_o \Gamma \left[ \frac{1+m}{m} \right] \approx \sigma_o \quad (3.9)$$

$$\text{COV} = \sqrt{\frac{\Gamma \left[ \frac{2+m}{m} \right]}{\Gamma^2 \left[ \frac{1+m}{m} \right]} - 1} \approx \frac{1.2}{m} \quad (3.10)$$

where  $\Gamma[ ]$  is the gamma function. The approximations in Eqs. 3.9 and 3.10 have been made by several researchers including Batdorf (1994) and yield good results for the practical range of application.

Harlow and Phoenix (1981) provided an "exact" formulation based on the chain-of-bundles model for the strength of *composite materials* comprised of many fibers. In their model, it is assumed that the composite material is formed of a chain of bundles in which each bundle consists of a number of fibers. Each of the fibers is assumed to have a Weibull distribution for the tensile strength; i.e. a Weibull material. Failure occurs when the weakest link of the entire formation reaches its load carrying capacity. The formulation of the problem provides a relationship between the failure of the composite material and the size of the specimen. The work of Harlow and Phoenix is laborious and is limited to two-dimensional applications. This led to several approximations of the exact behavior (Batdorf and Ghaffarian 1984, Duva et al 1996, Mahadevan et al 1997, Yushanov and Bogdanovich 1998, and Batdorf 1994). The following section summarizes the approximate method adopted in this research.

### 3.3 Application of Weibull's Theory to CFRP Laminates Used to Strengthen RC and PC Beams

The tensile strength of CFRP laminates used to strengthen concrete girders can be estimated by assuming that the fibers follow the Weibull theory. This goal will be achieved in two steps. The first step deals with the size effect aspect of the behavior. After establishing a relationship between the strength of an individual fiber and a uniformly stressed laminate, a second treatment is needed to account for stress gradients.

### 3.3.1 Size Effect

The size effect is accounted for following the approximate theory reported by Batdorf and Ghaffarian (1984). It is assumed that the number of flaws,  $Q_i$ , in a composite product that is uniformly-stressed and uniaxially-reinforced by a group of Weibull material fibers is

$$Q_i = NL \left( \frac{\sigma}{\sigma_o} \right)^{im} \prod_{k=1}^{i-1} c_k^m n_k \lambda_k \quad (3.11)$$

in which  $N$  is the number of fibers in the final product,  $L$  is the length of each fiber. The product of  $NL$  represents the entire volume of fibers in the composite; i.e. this formulation accounts for the volume or size effect.  $\sigma$  is the uniform stress acting on the composite product,  $n_k$  is the number of fibers immediately adjacent to a ruptured fiber that are affected by its failure,  $\lambda_k$  is the effective length of the overloaded region affected by the rupture,  $c_k$  is the stress concentration factor in that region,  $\sigma_o$  and  $m$  are the scale and shape parameters of the Weibull distribution representing the single fiber, and finally  $i$  is the number of adjacent fibers that are ruptured at the time of failure of the composite product. In the case of  $i=1$ , it is said that a singlet has formed. The formation of a singlet causes stresses in the adjacent fibers to increase due to stress concentrations. When an adjacent fiber ruptures,  $i$  increases to two and the condition is that of a doublet. As the stress increases, triplets and quadruplets ...etc. form. Once  $Q_i$  reaches unity, i.e. it is probable that a complete flaw exists in the product, failure is eminent. Solution of Eq. 3.11 leads to the following relationship between the failure stress,  $\sigma_{\text{uniform}}$ , of a uniformly stressed laminate and that of the scale parameter,  $\sigma_o$ , of a single fiber

$$\frac{\sigma_{\text{uniform}}}{\sigma_o} = \left[ NL \prod_{k=1}^{i-1} c_k^m n_k \lambda_k \right]^{-1/im} \quad (3.12)$$

The value of  $m$  and  $\sigma_o$  in the previous equation can be estimated using Eqs. 3.9 and 3.10. When applied to  $0^\circ/90^\circ$  laminates, the total fiber length  $NL$  in Eq. 3.12 pertains to fibers aligned in the direction of the beam axis only. Transverse fibers do not participate significantly in flexural strengthening applications, and their contribution to the size effect will be negligible.

While  $N$  and  $L$  are physical quantities that can be easily estimated,  $n_k$ ,  $\lambda_k$ ,  $c_k$  are harder to quantify. Batdorf and Ghaffarian (1984) report that measured values for  $\lambda_k$  are around 0.1 mm. The number of adjacent fibers affected by a rupture at any stage,  $n_k$ , is taken between 2 and 15. The stress concentration factor,  $c_k$ , can be dealt with as a random variable (Harlow and Phoenix 1981) or a simplified form can be used as reported by Batdorf (1994).

$$c_k = 1 + 0.5k \quad (3.13)$$

The size effect expressed by Eq. 3.12 is illustrated in Fig. 3.2. The plot makes use of Eq. 3.13 and assumes that  $\lambda_k = 0.1$  mm and  $n_k = 8$  for all values of  $k$ . It should be noted that the failure surface (upper bound) of all possible  $i$ -plets defines whether failure is due to a singlet, doublet, etc. For example at  $\ln(NL/\lambda) = 10$ , singlets first form and as the stress increases doublets form. The material cannot resist stresses beyond the doublet level (failure surface bound) since it is clear from the figure that at this level triplets and beyond provide less resistance. The failure surface obtained from this approximate method is in good agreement with the more exact failure surface based on the theory of Harlow and Phoenix (1981).

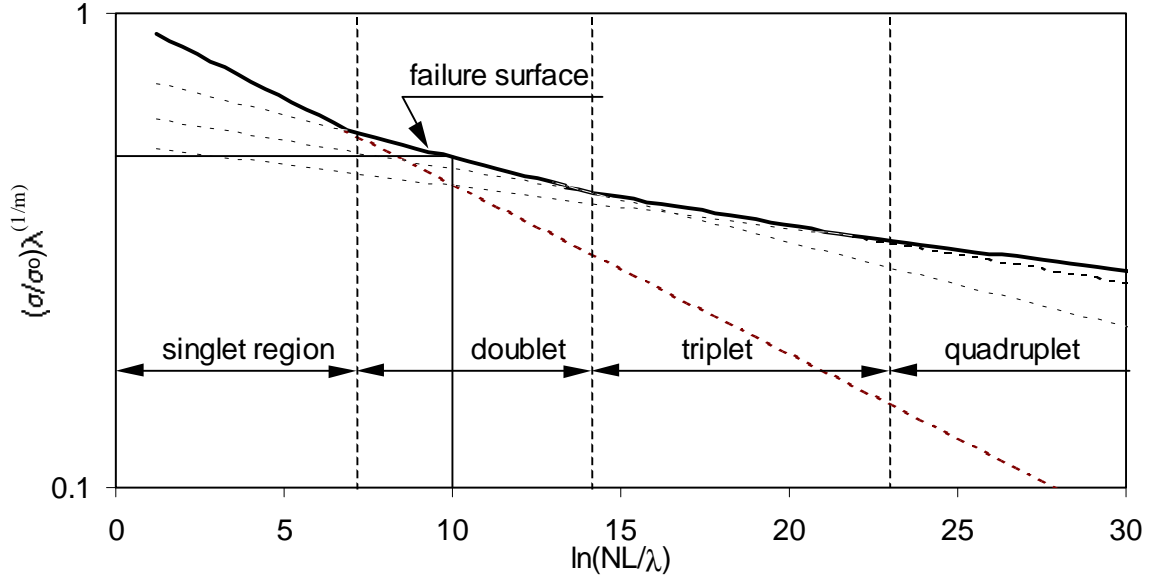


**Figure 3.2:** Effect of composite size on damage sequence based on approximate method. ( $n_k = 8$ ,  $\lambda_k = 0.1$  mm,  $c_k = 1 + 0.5k$ )

### 3.3.2 Stress Gradient Effect

The previous derivation assumes that the composite is uniformly stressed. In many cases the stress distribution in the laminate is not uniform and another treatment of  $\sigma_{\text{uniform}}$  is needed to adjust the results derived in the previous section. For the case of a composite laminate subjected to a stress gradient (such as that attached to the web of a beam), the probability of failure can be expressed in integral form as follows

$$P_f^{\text{beam}} = 1 - \exp \left\{ - \int_V \left( \frac{\sigma}{\sigma_o} \right)^{im} dV \right\} \quad (3.14)$$



The difference between Eq. 3.14 and Eq. 3.8 is that  $m$  is replaced with  $im$ , where  $i$  is the number of  $i$ -plets expected at failure. This modification follows directly from the work of Batdorf and Ghaffarian (1984) and is necessary to account for the decrease in coefficient of variation of the laminate strength that has been observed experimentally (Bullock 1974).

For the case of a composite laminate subjected to a uniform stress, Eq. 3.14 yields

$$P_f^{\text{uniform}} = 1 - \exp \left\{ - \left( \frac{\sigma_{\text{uniform}}}{\sigma_o} \right)^{im} V_{\text{uniform}} \right\} \quad (3.15)$$

where  $V_{\text{uniform}}$  is the volume of the uniformly stressed composite, and  $\sigma_{\text{uniform}}$  is the uniform stress it is subjected to.

The relationship between the failure strength of a uniformly stressed composite and that of a nonuniformly stressed composite is established by equating the expressions for the probability of failure; i.e.  $P_f^{\text{beam}} = P_f^{\text{uniform}}$ . The following section establishes the value of failure stress for the constant moment case and for several other common configurations.

### 3.3.3 Constant Moment Case

The derived expressions are for CFRP laminates that are wrapped around the web of a concrete girder. The wrap-around detail is considered in this derivation because it has been shown to provide better performance than attaching the CFRP sheets to the bottom of the girder. Wrapping the girder web with CFRP reduces the possibility of concrete delamination and bond failure between the concrete and CFRP (Shahawy and Beitelman 1999). In deriving the following expressions it was assumed that the stress at the top laminate fiber is equal to zero as shown in Fig. 3.3. This assumption is justified because the top of the laminate is close to the neutral axis. For the cases where CFRP sheets are only attached to the bottom of the girder (e.g. slab bridges), a value of zero can be used for  $V_{\text{web}}$  below. The coordinate system used in deriving the following expressions is shown in Figs. 3.3 and 3.4.

The stress state is different in the bottom part (having volume  $V_{\text{bottom}}$ ) of the CFRP sheet than it is in the webs (having volume  $V_{\text{web}}$ ). Hence, the integral portion of Eq. 3.14 will be evaluated separately.

#### Bottom Contribution:

A uniform stress distribution is assumed for the bottom part, since no stress variations exist in this case. The integral in Eq. 3.14 is determined as

$$\int_{V_{\text{bottom}}} \left( \frac{\sigma}{\sigma_o} \right)^{mi} dV = \int_{x=0}^{x=L} \int_{y=0}^{y=t} \int_{z=-b/2}^{z=b/2} \left( \frac{\sigma}{\sigma_o} \right)^{im} dz dy dx = btL \left( \frac{\sigma}{\sigma_o} \right)^{im} = V_{\text{bottom}} \left( \frac{\sigma}{\sigma_o} \right)^{im} \quad (3.16)$$

### Web Contribution:

A linear stress distribution is assumed for the web parts:

$$\sigma(x, y, z) = -\frac{y}{h_{CFRP}} \sigma \quad (3.17)$$

Accordingly the integral in Eq. 3.14 is determined as

$$\begin{aligned} \int_{V_{web}} \left( \frac{\sigma}{\sigma_o} \right)^{im} dV &= \int_{x=0}^{x=L} \int_{y=0}^{y=-h_{CFRP}} \int_{z=0}^{z=t} \left( \frac{y}{h_{CFRP}} \frac{\sigma}{\sigma_o} \right)^{im} dz dy dx = \frac{h_{CFRP} t L}{(im+1)} \left( \frac{\sigma}{\sigma_o} \right)^{im} \\ &= \frac{V_{web}}{(im+1)} \left( \frac{\sigma}{\sigma_o} \right)^{im} \end{aligned} \quad (3.18)$$

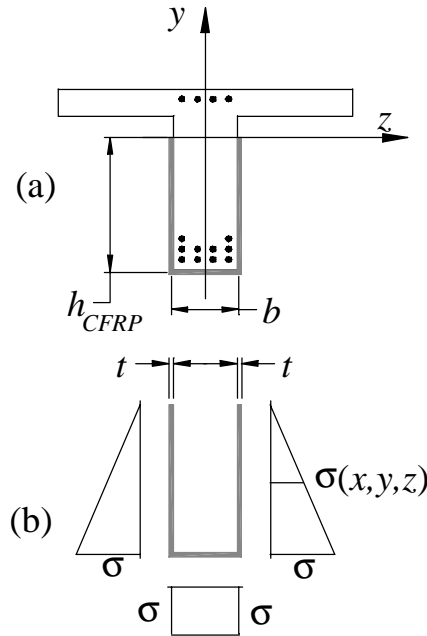


**Figure 3.3:** Normal stress distribution in CFRP sheets due to flexure (a-wrap-around detail, b-normal stress distribution on bottom and web parts).

**Total (Web and Bottom) Contribution:**

Adding both integrals

$$\int_V \left( \frac{\sigma}{\sigma_o} \right)^{im} dV = V_{\text{bottom}} \left( \frac{\sigma}{\sigma_o} \right)^{im} + 2 \frac{V_{\text{web}}}{(im+1)} \left( \frac{\sigma}{\sigma_o} \right)^{im} = \left( V_{\text{bottom}} + 2 \frac{V_{\text{web}}}{(im+1)} \right) \left( \frac{\sigma}{\sigma_o} \right)^{im} \quad (3.19)$$

In the previous expressions,  $V_{\text{bottom}}$  is the volume of the bottom part of the wrapped laminate, and  $V_{\text{web}}$  is the volume of the laminate attached to each side of the web.

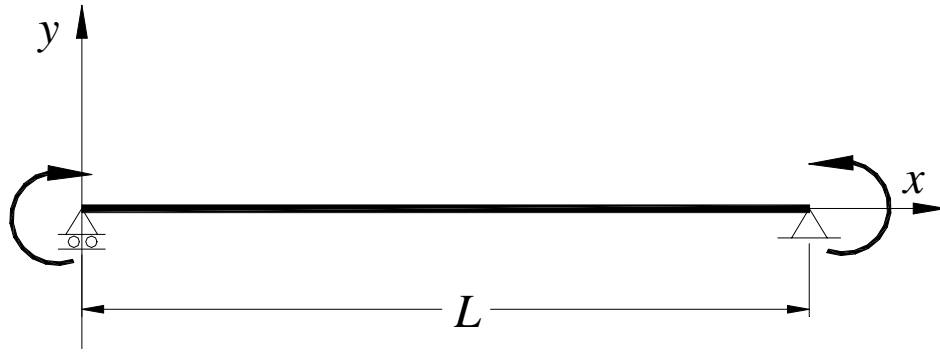


**Figure 3.4:** Coordinate system for integration purposes (Case of constant moment)

Using Eq. 3.14, the probability of failure can be expressed in terms of the volumes of the CFRP parts.

$$P_f^{\text{beam}} = 1 - \exp \left\{ - \left( \frac{\sigma_{\text{beam}}}{\sigma_o} \right)^{im} \left[ V_{\text{bottom}} + 2 \frac{V_{\text{web}}}{(im+1)} \right] \right\} \quad (3.20)$$

The ratio between the failure stress of the beam laminate,  $\sigma_{\text{beam}}$ , and that of a uniformly stressed laminate,  $\sigma_{\text{uniform}}$ , can be obtained by setting  $P_f^{\text{beam}} = P_f^{\text{uniform}}$  which will lead to

$$V_{\text{uniform}} \left( \frac{\sigma_{\text{uniform}}}{\sigma_o} \right)^{im} = \left( V_{\text{bottom}} + 2 \frac{V_{\text{web}}}{(im+1)} \right) \left( \frac{\sigma_{\text{beam}}}{\sigma_o} \right)^{im} \quad (3.21)$$

This results in the following expression relating the failure stress of a uniformly stressed composite and that of a composite sheet wrapped around the web of a beam subjected to constant bending moment.

$$\frac{\sigma_{\text{beam}}}{\sigma_{\text{uniform}}} = \left( \frac{(im+1)V_{\text{uniform}}}{(im+1)V_{\text{bottom}} + 2V_{\text{web}}} \right)^{1/im} \quad (3.22)$$

In Eqs. 3.20 and 3.21, both uniformly and nonuniformly stressed laminates must be of similar size to develop the same type of  $i$ -plet failure.

### 3.3.4 Concentrated Load at Mid-Span (Fig. 3.5)

Following the procedure for accounting for stress gradients described above, an expression can be obtained for the case of a beam subjected to a concentrated load acting at midspan. In this case the stress varies linearly in the longitudinal direction with a peak at midspan. This leads to the following expression for the stress in the bottom part of the CFRP sheet

$$\sigma(x, y, z) = \frac{2x}{L} \sigma \quad (3.23)$$

and similarly the next expression for the web parts:

$$\sigma(x, y, z) = -\frac{2x}{L} \frac{y}{h_{\text{CFRP}}} \sigma \quad (3.24)$$

These stress expressions lead to the following relationship between  $\sigma_{\text{uniform}}$  and  $\sigma_{\text{beam}}$

$$\frac{\sigma_{\text{beam}}}{\sigma_{\text{uniform}}} = \left( \frac{(im+1)^2 V_{\text{uniform}}}{(im+1)V_{\text{bottom}} + 2V_{\text{web}}} \right)^{1/im} \quad (3.25)$$

### 3.3.5 Four Point Loading (Fig. 3.5)

The integrals for both the web parts and the bottom part are evaluated in two steps since each part comprises of two regions; a constant moment region, and a linear moment region. The CFRP sheet volumes will be designated using a superscript for the part they represent; e.g.  $V_{\text{web}}^{\text{linear}}$  and  $V_{\text{web}}^{\text{constant}}$ . The following relationship is obtained:

$$\frac{\sigma_{\text{beam}}}{\sigma_{\text{uniform}}} = \left( \frac{(im+1)^2 V_{\text{uniform}}}{(im+1)^2 V_{\text{bottom}}^{\text{constant}} + (im+1)[V_{\text{bottom}}^{\text{linear}} + 2V_{\text{web}}^{\text{constant}}] + 2V_{\text{web}}^{\text{linear}}} \right)^{1/im} \quad (3.26)$$

### 3.3.6 Uniformly Distributed Load (Fig. 3.5)

A general closed-form solution for the integral is only possible in terms of the gamma function,  $\Gamma[ ]$ . The evaluation of the integral leads to the following stress relationship

$$\frac{\sigma_{\text{beam}}}{\sigma_{\text{uniform}}} = \left( \frac{2(im+1)^2 V_{\text{uniform}}}{\pi^{1/2} \frac{\Gamma[2+im]}{\Gamma[3/2+im]} \{(im+1)V_{\text{bottom}} + 2V_{\text{web}}\}} \right)^{1/im} \quad (3.27)$$

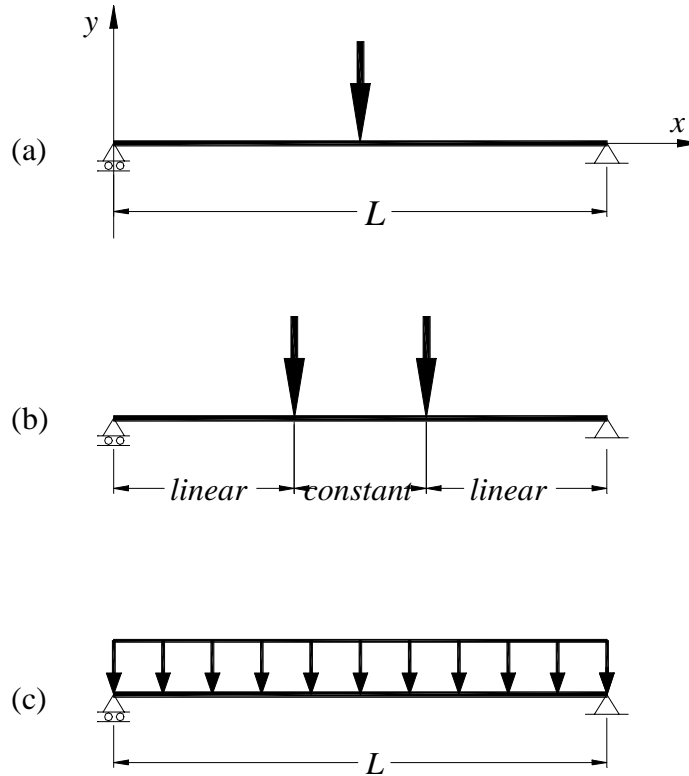


**Figure 3.5:** Common loading configurations: (a) concentrated load, (b) four-point loading, (c) uniform load.

### 3.4 Verification of Theory

The experimental work reported by Shahawy and Beitelman (1999) is used to verify the applicability of the theory to strengthening schemes involving the use of CFRP sheets. The tested beams serve the purpose of the verification study because the CFRP laminates ruptured in the high flexure region. Many of the experimental results reported in the literature cannot be used for verification because other modes of failure were observed (concrete crushing, delamination of CFRP, ...etc.). Figures 3.6 and 3.7 show the dimensions of the tested beams. The properties of the CFRP fibers of which the laminates were woven are given in Table 3.1. Table 3.2 gives the reinforcing steel and concrete properties for each of the studied beams.

### 3.4.1 Short-term Tensile Stress

The first step in the process is to find  $\sigma_{\text{uniform}}$  based on fiber strength provided by the manufacturer,  $\sigma_{\text{fiber}}$ . At this stage, it will be first assumed that the total volume (803 mm x 5791 mm x  $t_{\text{CFRP}}$  [31.6in x 228in x  $t_{\text{CFRP}}$ ]) of the CFRP laminates is uniformly stressed. The number of longitudinal yarns in a single layer of CFRP laminate is equal to (14+3.6+14) in x (6) yarns/in = 190 with 12,000 fibers in each yarn; i.e.  $N = 2275200$  fibers. The data provided by the manufacturer (Table 3.1) does not give the COV of CFRP fibers. It was therefore assumed that COV is 6.86% which corresponds to values of  $m = 18$  and  $\sigma_o = 546$  ksi according to Eqs. 3.9 and 3.10. The choice of  $m = 18$  is based on a review of the experimental results reported by several researchers (Bullock 1974, Kaminski 1973, and Lavoie 1997), which showed that for FRP fibers  $m$  ranges between 10 and 29. The length of each fiber is  $L = 5791$  mm [228 in]. Using  $n_k = 8$ ,  $\lambda_k = 0.1$  mm, and  $c_k$  as suggested in Eq. 3.13, it was found that a triplet failure ( $i = 3$ ) will take place for W-1L5, and that  $\sigma_{\text{uniform}}/\sigma_o$  is equal to 0.5435 according to Eq. 3.12.

**Table 3.1:** Properties of CFRP Laminates (Provided by manufacturer)

Property	Value
Fiber Tensile Strength ( $\sigma_{\text{fiber}}$ )	3.65 GPa [530 ksi]
Modulus of Elasticity (Tension)	231 GPa [33,500 ksi]
Filament Diameter	7 $\mu\text{m}$
Filaments/yarn	12,000
Yarn density	0.23/mm [6/inch]
Ultimate Elongation	1.4%

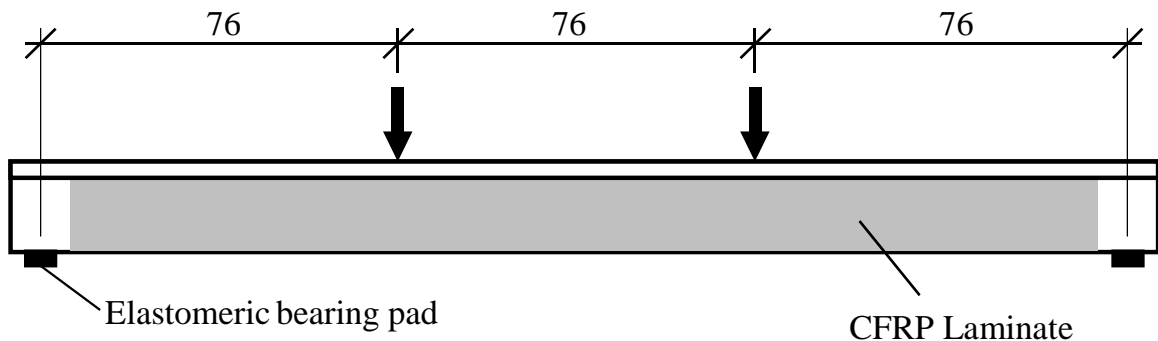


**Figure 3.6:** Loading setup for FDOT girders (dimensions in inches)

**Table 3.2:** Comparison of Failure Moments

Specimen	Material Strength, MPa [ksi]			Flexural Capacity ( $M_{max}$ )		
	Yield Stress ( $f_y$ )	Concrete Strength ( $f'_c$ )	CFRP Strength ( $\sigma_f$ )	Experiment kN-m [kip-in]	Analysis kN-m [kip-in]	Difference* (%)
W-1L5	441[64]	35.9 [5.2]	2200[314.4]	211.4 [1871]	205.0 [1813]	-3.1
W-2L5-A		37.2 [5.4]	2140[310.4]	259.5 [2300]	243.5 [2155]	-6.3
W-2L5-B		35.1 [5.1]	2140[310.4]	259.9 [2300]	242.2 [2143]	-6.8
W-3L5		35.1 [5.1]	2120[308.1]	282.5 [2500]	278.5 [2464]	-1.4
W-4L5		35.1 [5.1]	2110[306.4]	305.1 [2700]	313.1 [2770]	+2.6
Average						-3.0

\* (+) indicates unconservative prediction, (-) indicates conservative prediction

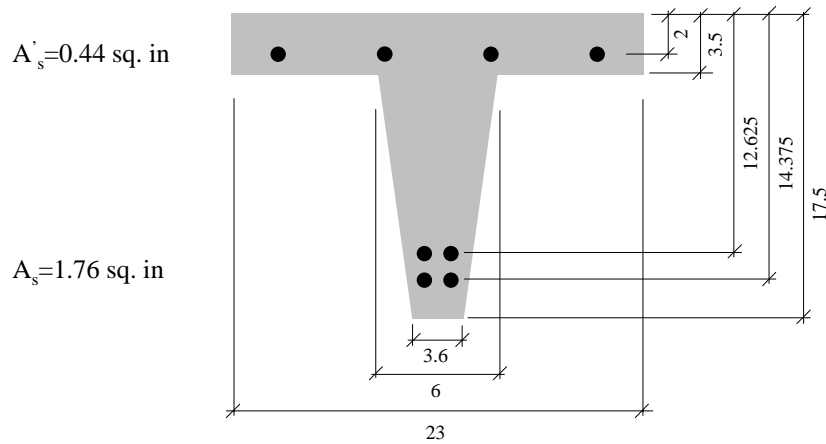


**Figure 3.7:** Cross-section details (dimensions in inches)

Since failure happened due to the formation of a triplet flaw (i.e.  $i = 3$ ), then  $im = 3 \times 18 = 54$  is used in the following stress gradient calculations. The effect of the stress gradient in the web portions is accounted for in the second step, which is performed by substituting the cross-sectional properties into Eq. 3.26. The result is  $\sigma_{beam}/\sigma_{uniform}$  equal to 1.059. Combining both effects leads to a  $\sigma_{beam}/\sigma_o$  ratio of 0.576; i.e.  $\sigma_{beam} = 2.17$  Gpa [314.4 ksi]. It is clear that the size effect has a much greater impact on the short-term strength of the composite sheet than the stress gradient effect has. The same procedure was repeated for the other specimens using the appropriate number of fibers for each case (e.g.  $N = 6825600$  fibers for W-3L5). The failure stress predicted by the theory is used as input for a fiber section analyses of the test beams.

### 3.4.2 Comparison of Flexural Capacities

The verification study is conducted by performing fiber-section analyses of the specimen cross-sections. The analyses are conducted using the computer program discussed in Chapter 2. Table 3.2 summarizes the results of the verification study. The designation of the beams describes the number of CFRP layers used and concrete strength; e.g. W-3L5 is strengthened with 3 layers and has a nominal concrete compressive strength of  $f'_c = 5$  ksi. It can be seen from Table 3.2 that the flexural capacities ( $M_{max}$ ) obtained from the analyses and the values observed from the tests are in good agreement (average difference of -3.0%). The maximum difference is -6.8%. The flexural capacity as predicted by the analysis based on the suggested short-term tensile strength is on the conservative side for all beams except Beam W-4L5 where the analysis predicts a slightly higher  $M_{max}$  ( $\Delta M_{max} / M_{max} = +2.6\%$ ).

While this verification study is rather limited, it does suggest that the proposed method can be used to reasonably estimate the short-term tensile strength of CFRP laminates. Nevertheless, further verification of the method should be sought through comparisons to additional tests of beams with different size and load configurations.

### 3.5 Design Implications

The work described in this report has important implications regarding the applicability of coupon test results. Coupon tests are typically conducted using relatively small specimens, and may therefore lead to unconservative estimates of strength if the size effect is not properly considered. For coupons to be representative of the final structure, they should be large enough to develop the same type of multi-plet that is expected in the actual-size structure. While such a size may be relatively small, the size of the specimen should be studied before the results can be considered reliable for design purposes. The methodology described in this chapter and represented by Eq. 3.12 and Fig. 3.8 can be used for this purpose.

An alternative approach that is more suited for implementation in design guidelines is to develop design charts from which engineers can extract the short-term strength of CFRP laminates. Figure 3.8 is a plot of the relationship between the total length of fibers in a composite,  $NL$ , and the strength ratio,  $\sigma_f / \sigma_o$  calculated according to Eq. 3.12. The plot is obtained using the same parameters used to compute Fig. 3.2, i.e.  $m = 18$ ,  $c_k$  from Eq. 3.13,  $\lambda_k = 0.1$  mm, and  $n_k = 8$  for all values of  $k$ . These parameters are chosen following Batdorf and Ghaffarian (1984) and Batdorf (1994) and were found to give reasonable results in the verification study described in the previous section.

The input to the developed design chart is the total length of all the fibers in the composite structure,  $NL$ , and the output is the ratio of the short-term tensile strength,  $\sigma_f$ , to the scale factor,  $\sigma_o$ , which can be taken equal to  $\sigma_{fiber}$  for all practical purposes following the approximation in Eq. 3.9. To illustrate the method, the dimensions of verification beam W-1L5 will be used. The total length of fibers can be estimated as  $5791$  (mm)  $\times$   $190$  (yarn)  $\times$   $12,000$  (fibers/yarn)  $= 13.2 \times 10^9$  mm. The corresponding short-term tensile strength is



$\sigma_{f,max} = 0.5435 \times 3.65 = 1.984$  GPa [287.7 ksi] and a triplet failure type is expected ( $i = 3$  from chart). This stress still needs to be adjusted to account for the stress gradient effect using  $i = 3$  (previously calculated to be 1.059). The stress gradient effect is typically less than 10% and can be conservatively ignored when estimating the short-term tensile strength of CFRP laminates. The developed chart is suitable for general-purpose carbon fiber reinforced polymer laminates. Similar charts can be developed for other types of CFRP laminates.

The chart in Fig. 3.8 is developed assuming that the reported fiber strength is for fibers with a gauge length of 25.4mm [1in]. This gauge length is frequently used in fiber and dry strand tests (McMahon 1973). In cases where the manufacturer reports a different gauge length, the reported stress can be adjusted to the 25.4mm [1in] gauge length strength using the following factor, which stems from Eq. 3.7.

$$\text{Gauge Length Factor} = \frac{\sigma_{fiber1}}{\sigma_{fiber2}} = \left( \frac{L_1}{L_2} \right)^{-1/m} \quad (3.28)$$

The tensile strength computed from the chart represents the short-term strength. The design tensile strength should account for additional reductions due to environmental exposure conditions (temperature, humidity, and chemical exposure) as well as load characteristics (long term and repeated).

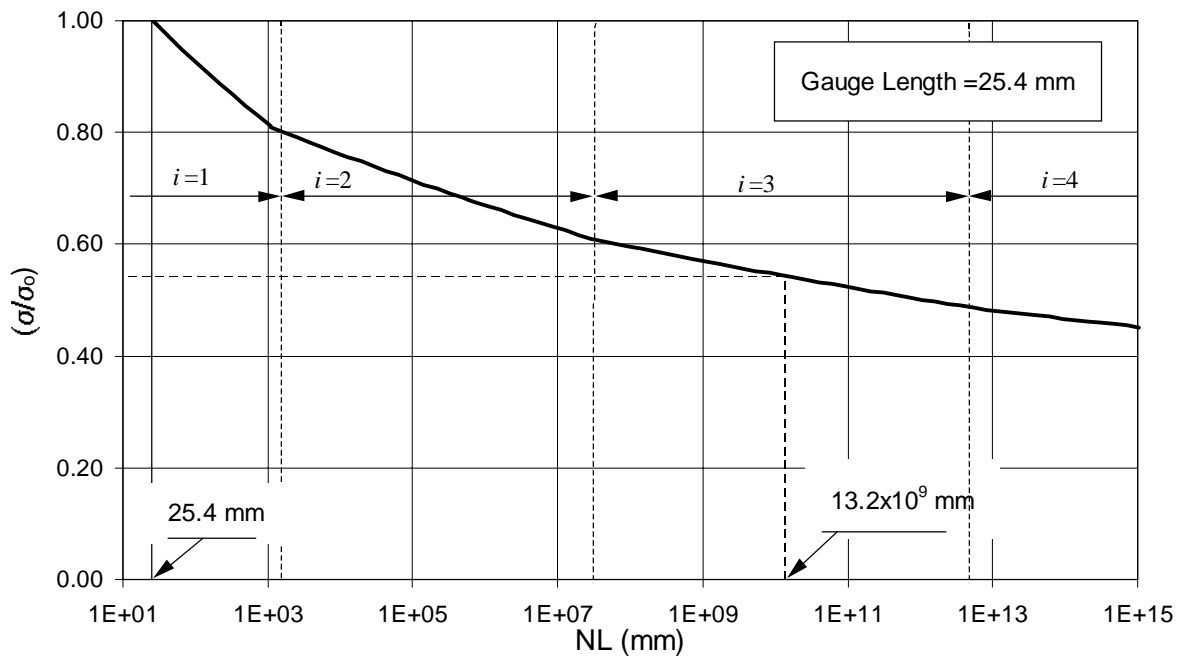


**Figure 3.8:** Proposed chart for predicting the short-term tensile strength of uniformly stressed CFRP sheets.

### **3.6 Summary and Conclusions**

The short-term tensile strength of CFRP laminates used for strengthening concrete girders can be estimated by applying the Weibull Theory. Two steps are needed to calculate the short-term tensile strength. The first step accounts for the size effect and predicts the tensile strength of a uniformly stressed volume that shares the size of the CFRP used in the real structure. The second step accounts for the effect of stress gradients. Expressions that account for the stress gradient effect in several common load configurations are derived and presented. Analytical results calculated using the developed theory are compared to published test results of reinforced concrete T-beams strengthened with CFRP laminates. Good agreement is found between theoretical calculations and test results. The work described herein suggests that coupon tests may lead to unconservative estimates of strength if the size effect is not properly considered. Based on the work presented in this chapter, a design tool is provided in the form of a chart, which can be used to estimate the effect of size on the short-term tensile strength of CFRP laminates.

## 4 STATIC AND FATIGUE BEHAVIOR

### 4.1 Introduction

Information on the short-term behavior of RC beams strengthened with CFRP laminates is relatively abundant and well documented (Plevris et al 1994 and 1995, Shahawy et al 1996, and Saadatmanesh and Malek 1998). However, data on long term behavior, especially fatigue response, is still rather limited. Meier et al. (1992) conducted some of the earliest fatigue tests on RC beams strengthened with hybrid glass/carbon laminates. The test results showed that in addition to improving the short-term behavior of the RC beams, the use of CFRP also improved fatigue behavior. Inoue et al. (1995) conducted fatigue tests of rectangular RC beams strengthened with CFRP plates. They observed that the behavior of the beams became quite complex leading to several possible secondary modes of failure after the steel reinforcing bars ruptured due to high-cycle fatigue. They concluded that CFRP reinforcement was beneficial to the fatigue performance of the beams, reducing crack width, and improving its distribution prior to failure. Shahawy and Beitelman (1999) conducted accelerated fatigue testing of several RC T-beams strengthened with a varying number of CFRP laminates including a test specimen that was cycled to about half its fatigue life then rehabilitated using CFRP. Test results showed that the application of the CFRP laminates significantly extended the fatigue life of the reinforced concrete beams, including the beam that had accumulated fatigue damage prior to rehabilitation using CFRP. These test results along with other fatigue tests reported by Barnes and Mays (1999) highlight the benefits of using CFRP laminates and plates to rehabilitate deficient reinforced concrete bridge girders.

This chapter discusses the static and accelerated fatigue behavior of reinforced concrete beams strengthened with CFRP. The computer program developed in Chapter 2 is first verified by comparing its results to experimental data in Shahawy and Beitelman (1999, 2000) and Barnes and Mays (1999). The program is then used to conduct parametric studies of CFRP strengthened beams. Based on the analyses, design considerations are suggested for the repair and/or strengthening of reinforced concrete beams using CFRP laminates.

### 4.2 Shahawy and Beitelman's (1999, 2000) Tests

Tests of reinforced concrete beams strengthened with CFRP laminates were conducted at the FDOT Structures Lab (Shahawy and Beitelman 1999 and 2000). The four-point flexural tests were designed to study the effect of concrete strength and number of laminates on the fatigue behavior of reinforced concrete beams rehabilitated with CFRP laminates. The test program consisted of both static and fatigue tests of 23 specimens. Figures 3.6 and 3.7 (Chapter 3) show the test setup and cross-section details, while material properties are listed in Tables 3.1 and 3.2. The CFRP fabric utilized in the tests was composed of unidirectional dry carbon material formed by weaving individual yarns into a fabric. The strength of the composite laminates was calculated to be 310 ksi by assuming the strength of the carbon fibers to follow a Weibull

statistical distribution as described in Chapter 3. Further details about the test setup may be found in Shahawy and Beitelman (1999 and 2000).

Two series of specimens were tested. The first series (Shahawy and Beitelman 1999) was subjected to fairly low moments ranging from 44 to 89 kN-m which correspond to 25 to 50% of the flexural capacity of the reinforced-concrete cross section. The second series (Shahawy and Beitelman 2000) was subjected to moments that were somewhat higher ranging from 44 to 132 kN-m which correspond to 25 to 75% of the flexural capacity of the reinforced concrete cross section. The stirrups in the first series were tack welded to the main bar reinforcement, which caused the bar reinforcement in the control beam (without CFRP strengthening) to fracture early on in the cyclic load history. The beams in the second series did not have any tack welding.

All specimens subjected to monotonic loading failed by fracture of the CFRP laminates in the high moment zone. Specimens subjected to cyclic loads failed in the high moment region by high-cycle fatigue fracture of the main steel reinforcement.

#### **4.2.1 Monotonic Analyses of Shahawy and Beitelman's (1999, 2000) Specimens**

A series of monotonic fiber element analyses were carried out. The analyses were conducted for the control beam and beams with 0, 1, 2, 3, and 4 CFRP laminates. Analytically calculated moment vs. curvature results for all cross-sections are plotted in Figs. 4.1 through 4.5 along with the measured response. It is clear from the figures that the analytical response correlates well with the experimental data at all stages of behavior up to failure. The calculated moment vs. curvature responses for all specimens are plotted together in Figure 4.6. The following observations can be made from the figures:

1. At concrete cracking, there is a pronounced change in slope of the moment curvature response of the control beam.
2. The cracking moment for beams with CFRP laminates is almost the same irrespective of the number of CFRP laminates and is larger than the cracking moment of the control beam.
3. There is another pronounced change in the moment curvature slope when the lowermost steel yields. This is shortly followed by another sudden change when the second layer of steel yields.
4. Moment capacity is greatly affected by the number of CRPF laminates. The strength increase per laminate is almost constant.
5. Cross-sections with different layers of CFRP reach their ultimate strength at approximately the same curvature.
6. There is a sudden drop in the moment-curvature response when the moment capacity is attained. The drop corresponds to rupture of bottommost layer of CFRP laminates and becomes larger as the number of layers increase.
7. Immediately after the sudden drop in moment-curvature response, there is a more gradual reduction in strength. This portion of the response corresponds to the rupture of the CFRP

laminates on the sides of the web. In other words, fracture of the CFRP laminates is travelling up the web. The curve is jagged because of the relatively coarse fiber discretization. Each little drop in the descending curve corresponds to a fiber fracturing. The curve would become smoother as the discretization becomes finer.

The effect of the number of CFRP laminates on the moment strength is shown in Figure 4.7. It is clear from the figure that there is excellent correlation for all cases. The effect of the number of CFRP laminates on the yield moment strength is shown in Figure 4.8. Although the comparison is not as good as for the moment strength, the results are still very good.

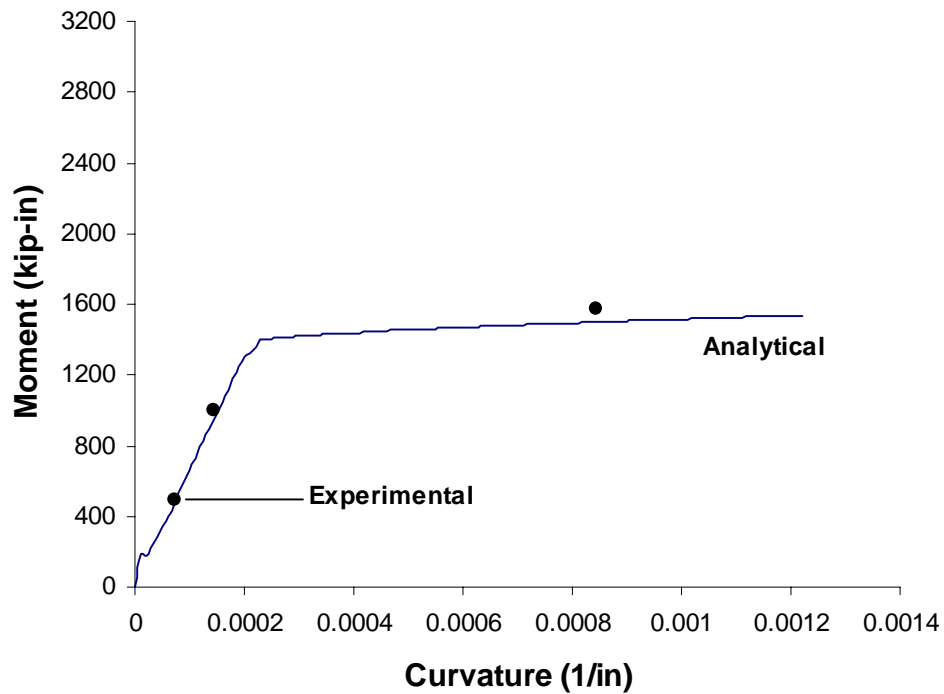


**Figure 4.1:** Experimental vs. analytical moment curvature. Specimen C-L0-5

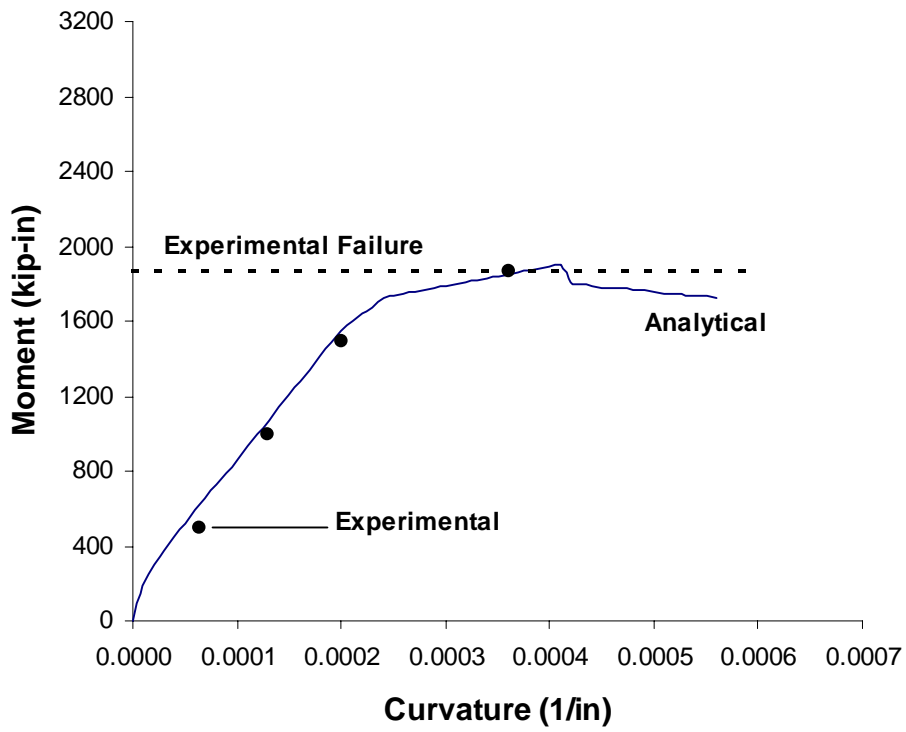


**Figure 4.2:** Experimental vs. analytical moment curvature. Specimen W-L1-5

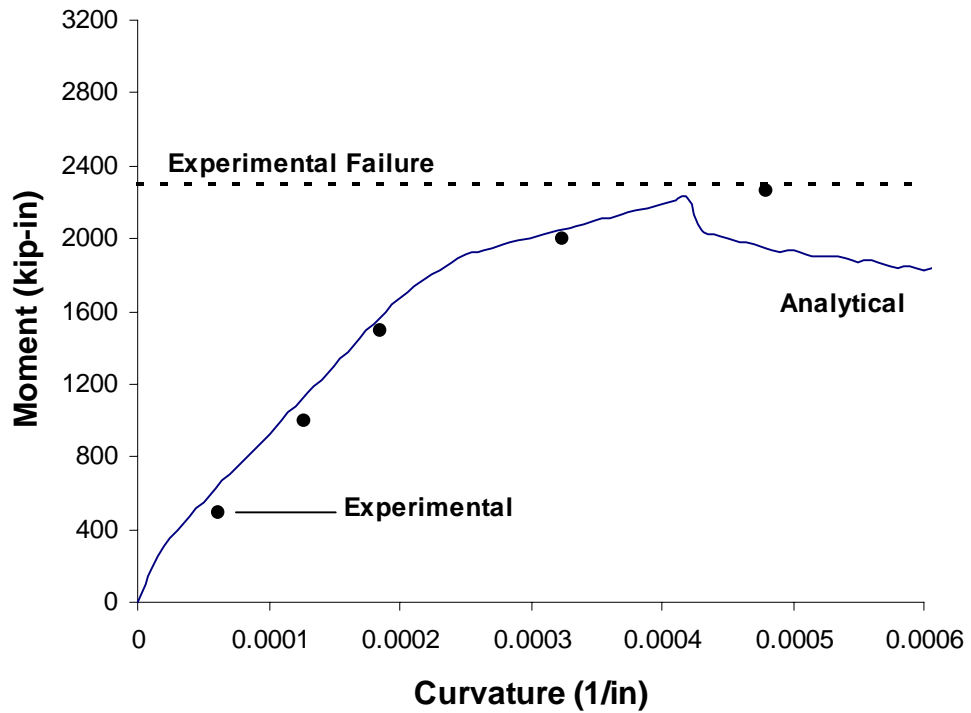


**Figure 4.3:** Experimental vs. analytical moment curvature. Specimen W-L2-5

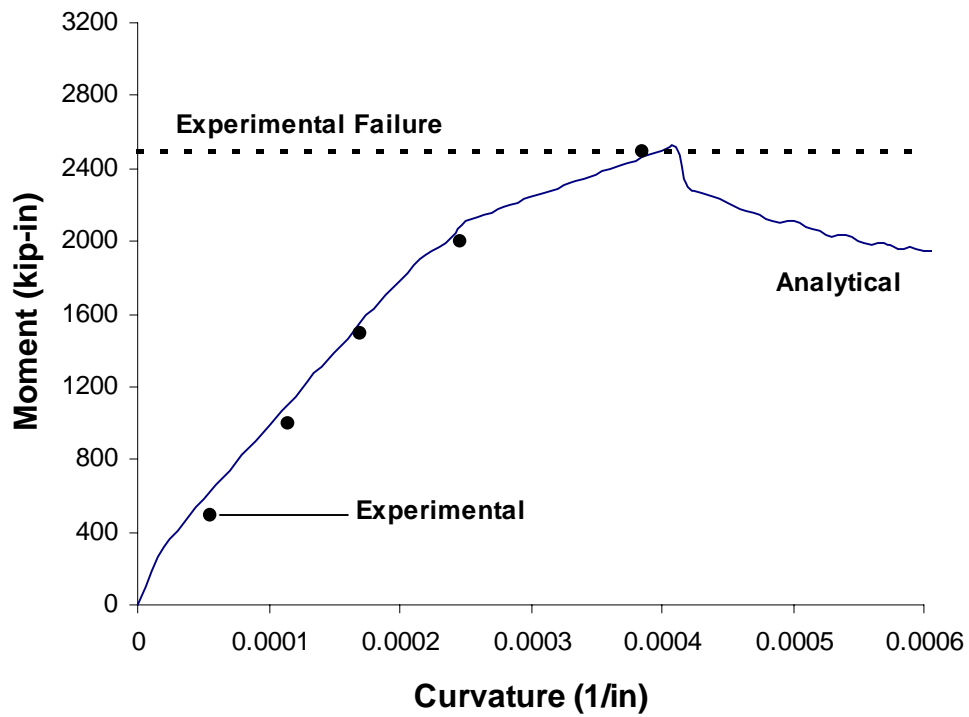


**Figure 4.4:** Experimental vs. analytical moment curvature. Specimen W-L3-5

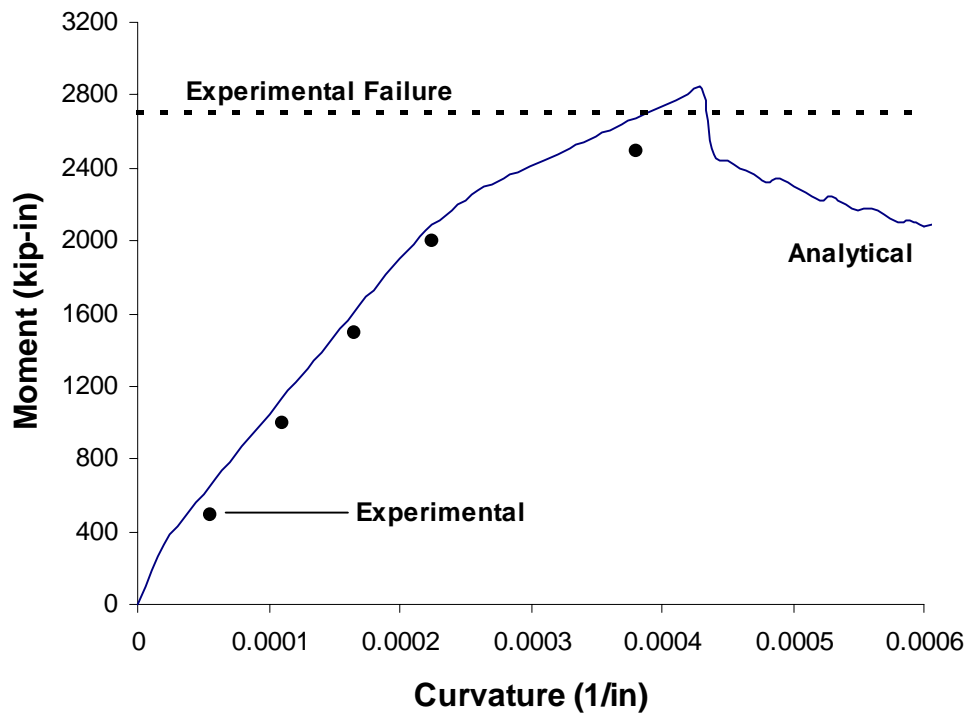


**Figure 4.5:** Experimental vs. analytical moment curvature. Specimen W-L4-5

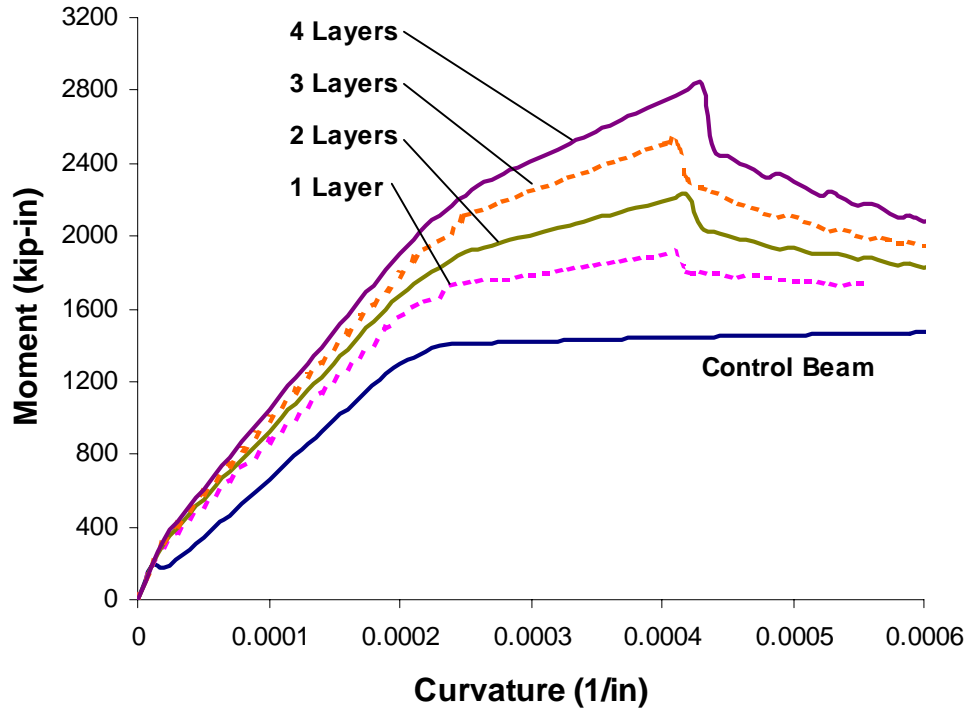


**Figure 4.6:** Moment curvature relationships for beam with different number of CFRP layers.

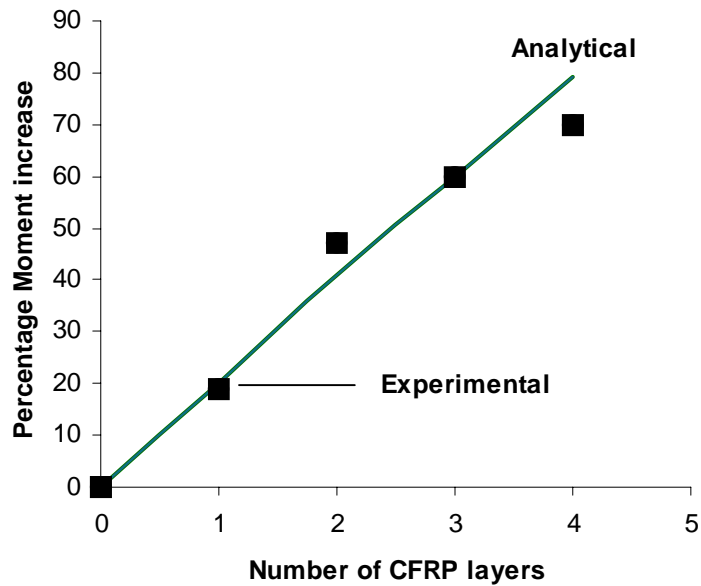


**Figure 4.7:** Analytical and experimental ultimate moment increase vs. number of CFRP layers



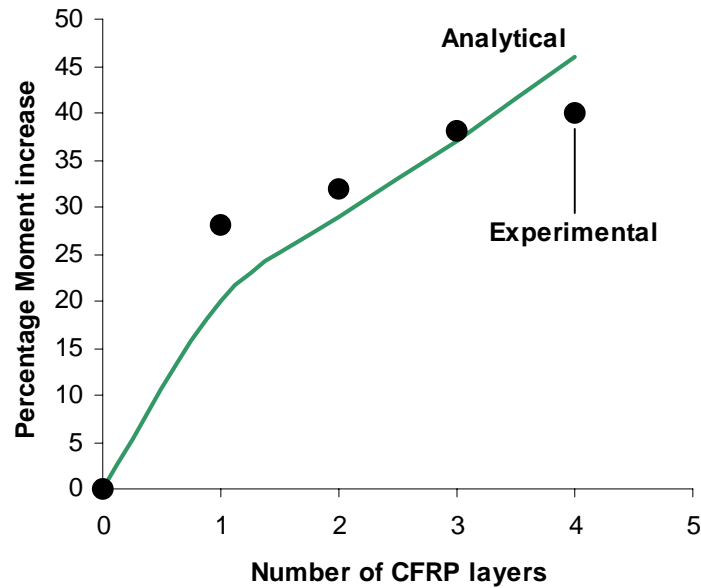


**Figure 4.8:** Analytical and experimental yield moment increase vs. number of CFRP layers

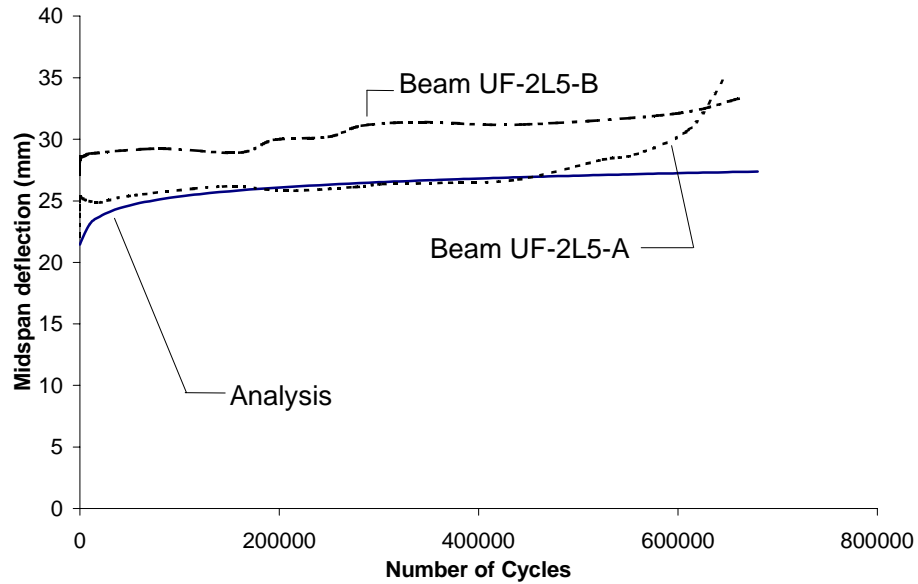
#### 4.2.2 Cyclic Analyses of Shahawy and Beitleman's (1999, 2000) Specimens

The measured and computed mid-span deflections for beams with 2 and 3 CFRP layers are plotted versus the number of cycles in Fig. 4.9. In the figure, beams in which only the end designation is different (i.e. A or B) are identical in all respects, and were tested in the same manner (Shahawy and Beitleman 1999 and 2000). It is clear from the figure that the computed response compares favorably to the measured deflections, with the exception of Beam F-3L5-A, which suffered a sudden jump in deflection at about 1.7 million cycles. This sudden increase in deflection is attributed to an early fatigue fracture of one of the reinforcing bars. However, in spite of the loss of one of the bars, the beam was still capable of sustaining the applied load for over 3 million cycles.

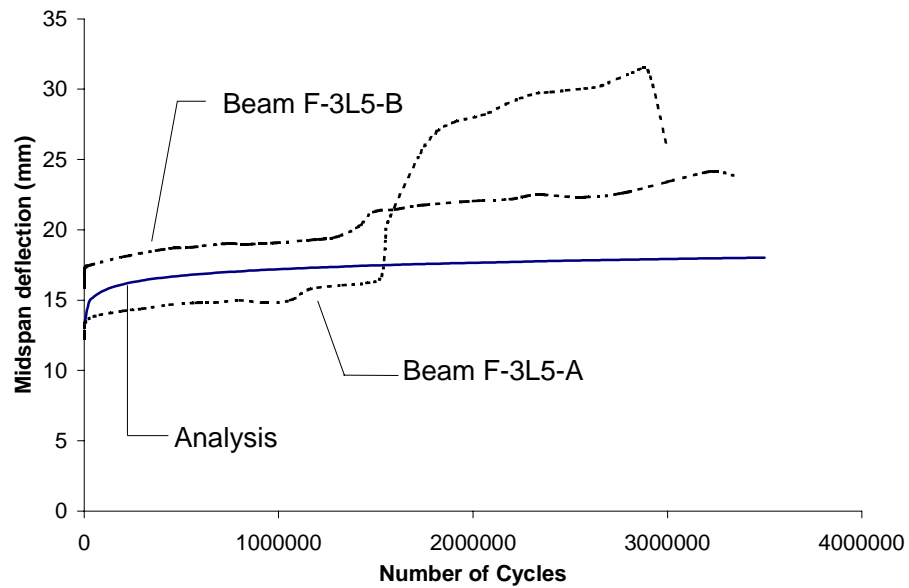
The internal redistribution of stresses due to cyclic creep within a cross section is illustrated in Fig. 4.10. The calculated stress in the topmost concrete fiber of the specimen with 2 CFRP layers is plotted versus the number of cycles in Fig. 4.10(a). As is typical of creep behavior, the concrete stress drops rapidly during the initial loading cycles then flattens out. The stress in the steel exhibits an opposite trend, rising rapidly then slowing considerably as can be seen in Fig. 4.10(b). The overall rise in steel stress is mild, increasing from 324 MPa to 340 MPa - a less than 5% increase. The stress in the carbon fiber also increased by about the same percentage. The increase in steel and CFRP stresses in all the other specimens was also less than 5%.

Time dependent moment vs. curvature plots for specimens C-L0-5 and W-L1-5 are shown in Figures 4.11 and 4.13. It is clear from the figures that the moment vs. curvature plot is shifting to the right as N increases. The shift also appears to be rather uniform. This was observed in the test results for applied cycles almost up to failure. The steel stresses at minimum and maximum

applied moments for specimens C-L0-5 and W-L1-5 are shown in Figures 4.12 and 4.14. As discussed in the previous paragraph, the stresses appear to be increasing slightly as  $N$  increases. An important observation from the figure is that the stress range is almost constant at any  $N$ .

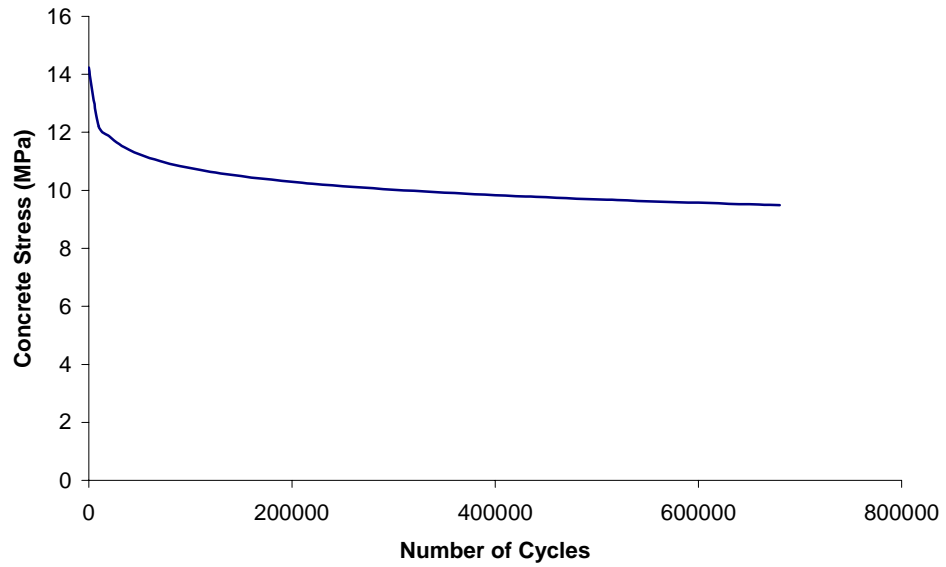


(a)

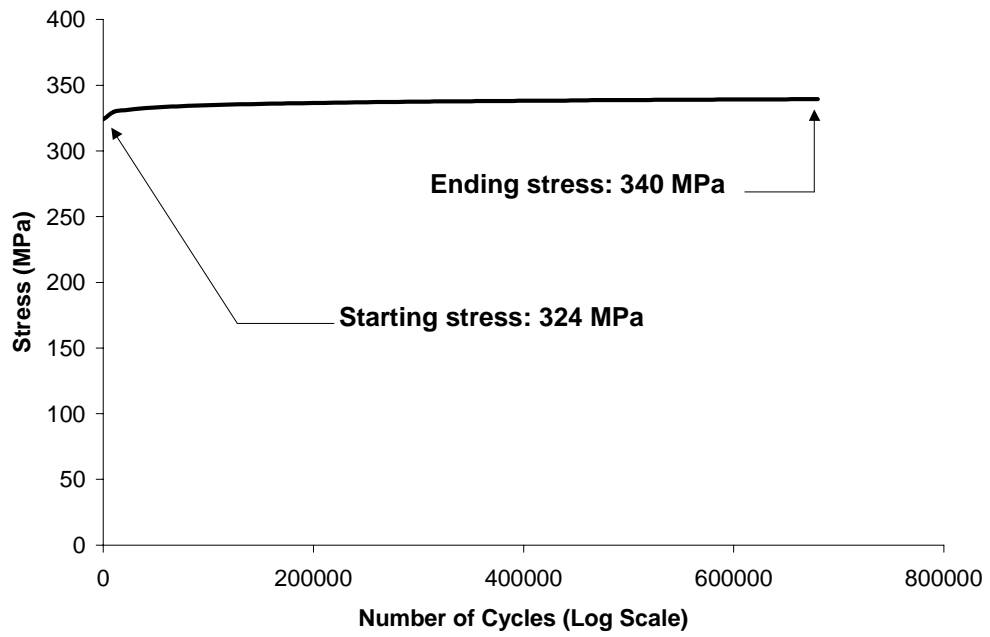


(b)

**Figure 4.9:** Calculated versus experimental mid-span deflection for (a) beams with 2 CFRP layers (Shahawy and Beitelman 2000) and (b) beams with 3 CFRP layers (Shahawy and Beitelman 1999).



(a)



(b)

**Figure 4.10:** Calculated stresses in (a) top concrete fiber and (b) bottom steel layer versus number of cycles for beam with 2 CFRP layers

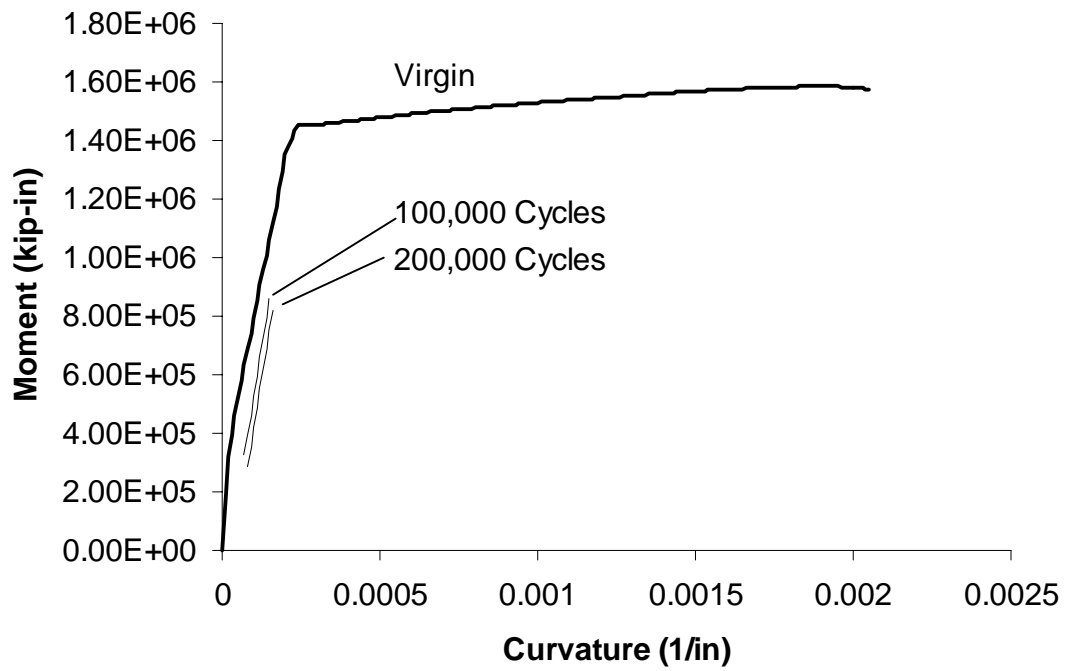


**Figure 4.11:** Time-dependent analysis for Specimen C-L0-5

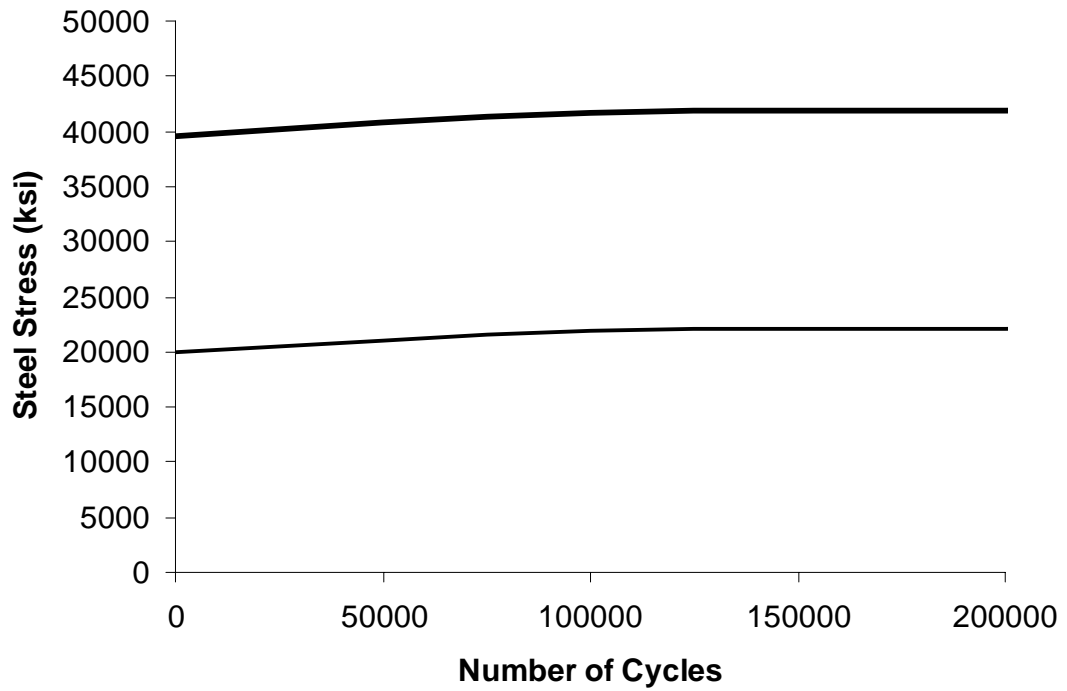


**Figure 4.12:** Stress in bottom steel layer as a function of number of cycles. Specimen C-L0-5

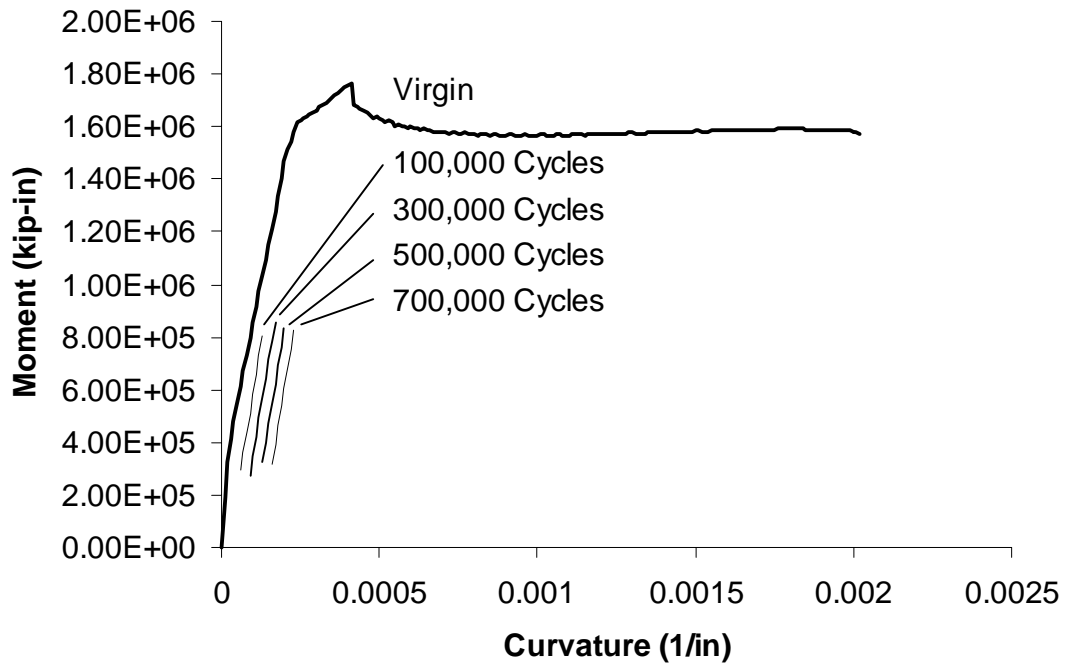


**Figure 4.13:** Time-dependent analysis for Specimen W-L1-5

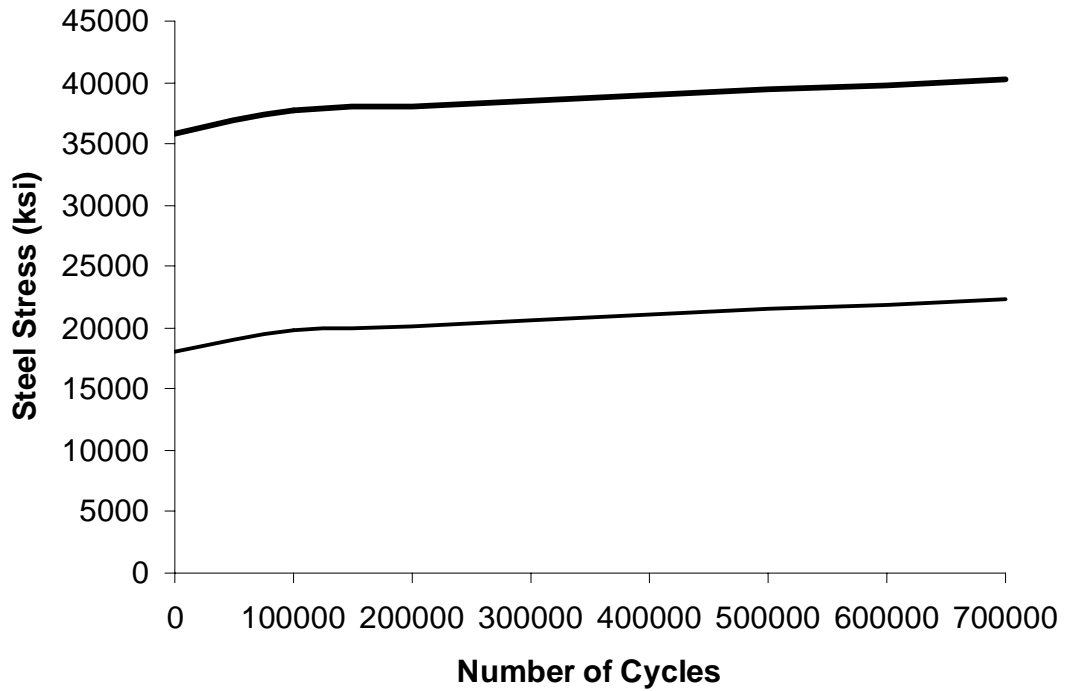


**Figure 4.14:** Stress in bottom steel layer as a function of number of cycles. Specimen W-L1-5

### 4.2.3 Fatigue Life of Shahawy and Beitleman's (1999, 2000) Specimens

As discussed in the previous section, it was observed from the analyses that even though the steel stress increases mildly as the number of applied cycles increases, the stress range, which is the difference between maximum and minimum stresses in the reinforcement, was essentially unchanged. In other words, the stress range acting over the life of the specimen can be estimated with good accuracy from a cracked section analysis. Such analyses are conducted and the results are shown in Table 4.1 along with the observed number of cycles to failure. The modular ratios for steel and CFRP are assumed to be 7.4 and 8.4 respectively.

It is clear from the table that the addition of CFRP laminates appreciably increases the cracked moment of inertia, and results in a corresponding reduction in the steel stress range and the maximum concrete and CFRP stresses. For example, adding two layers of CFRP laminates increases the cracked moment of inertia by 20%, and decreases the steel stress range by 20%. For the control section in the unwelded series, the top fiber stress ranges from 0.81 to 2.41 ksi for the given loading conditions. Holmen's equations for number of cycles to failure do not apply directly since  $S_{min}=0.155$  and  $S_{max} = 0.46$ . For a given  $S_{max}$  and a 50% probability of failure, he proposed two equations: one for  $S_{min}=0.05$ , and another for  $S_{mean} = 0.5$  (Holmen 1982). Nevertheless, substituting into both equations indicates that the number of cycles to failure of the concrete is several orders of magnitude greater than the number of cycles to failure observed in the tests. Hence it is certain that the control beam did not fail due to concrete fatigue. Furthermore, because  $S_{max}$  is low and the corresponding fatigue life so large, concrete deterioration due fatigue is unlikely to have appreciably affected the behavior of the beam.

**Table 4.1:** Properties of sections (calculated from cracked section analysis)

Specimen	Moment of Inertia (in <sup>4</sup> )	Steel Stress Range (ksi)	Max. Concrete Stress (ksi)	Max. CFRP Stress (ksi)	Cycles to Failure
Welded Specimens					
C-0L5-FA	1630	17.9	1.62	-	295,000
F-2L5-A&B	1952	14.5	1.48	44.6	1,800,000
F-3L5-A&B	2106	13.2	1.43	41.0	3,100,000
Unwelded Specimens					
C-0L5-FA	1630	35.8	2.41	-	390,000
F-2L5-A&B	1952	28.9	2.20	67.0	650,000
F-3L5-A&B	2106	26.4	2.14	61.4	920,000
UF-4L5-A	2255	24.3	2.07	56.6	1,300,000

Since concrete fatigue did not contribute to the failure of the control beam, it is reasonable to assume that the steel precipitated the failure. This is confirmed in Figure 4.15 in which the steel fracture surfaces are characteristic of high cycle fatigue failures. For comparison, Figure 4.16 shows a typical fatigue fracture of a reinforcing bar. This is a #11, grade 60 bar that was

embedded in a concrete beam subjected to repeated loading until the bar failed. The fatigue crack is the smooth portion of the fracture surface. The jagged region is where the bar finally fractured in tension after the propagating fatigue crack weakened the bar. Note that the fatigue crack did not initiate at the lower most point of the bar as expected (where the stress is highest), but actually started along the side of the bar, at the base of the transverse lugs. Pictures of the fractured bars in the FDOT tests (shown in Figure 4.15) have similar failure characteristics. It is clear from both figures that the failures are steel bar fatigue failures.



(c)



(d)

**Figure 4.15:** Different views of the failure surfaces of steel reinforcement.

The  $S_r$ - $N$  curves for all test specimens are plotted in Figure 4.17. Corley et al (1971) conducted an extensive experimental investigation to determine the fatigue strength of deformed reinforcing bars. The experimental program covered many variables and involved hundreds of tests. The dotted lines plotted in Figure 4.17 bound the data presented in Corley et al (1971). It is clear from the figure that the unwelded specimens fall within these bounds, while the tack-welded beams falls well below the lower bound for Corley's data. This is expected since tack-welding causes stress-risers, which significantly reduce fatigue life. An obvious conclusion that can be drawn from Figure 4.17 and Table 4.1 is that increasing the number of CFRP layers reduces the steel stress range leading to an enhancement in fatigue life.

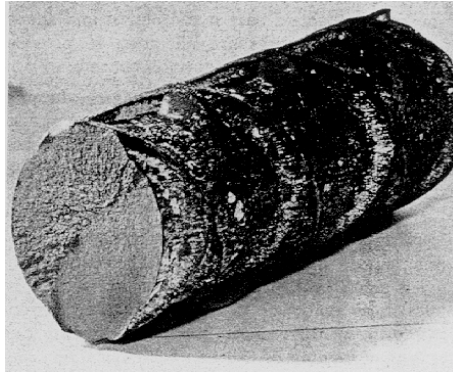


**Figure 4.16:** Typical fatigue fracture of reinforcing bar

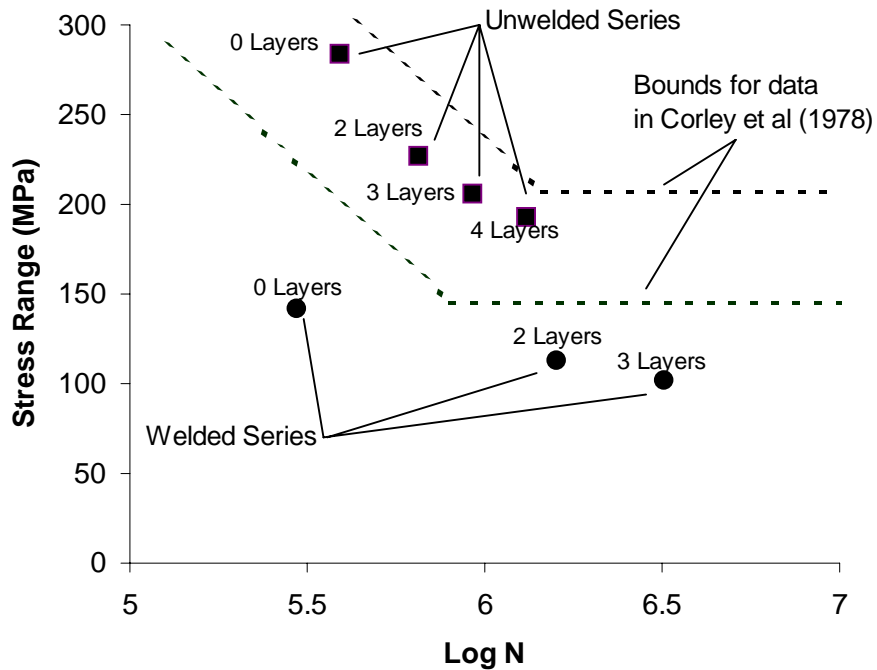


**Figure 4.17:**  $S_r$ -N Curve for Shahawy and Beitelman's (1999, 2000) fatigue tests

### 4.3 Analysis of Barnes and Mays' (1999) Specimens

Further verification of the program is sought by comparing analysis results to test data in Barnes and Mays (1999) who also conducted accelerated fatigue tests of a series of reinforced concrete beams. The 2300-mm long beams, which had a rectangular cross-section (130-mm wide, and



230-mm deep), were subjected to a cyclic load in four-point bending at a frequency of 1Hz. Unidirectional CFRP (Toray T300) plates were bonded to the bottom surface of the beam. Figures 4.18 and 4.19 show the calculated and measured mid-span deflection plotted versus the number of cycles for the control beam (Beam 2) and another beam reinforced with a CFRP plate (Beam 4), respectively. The upper two curves in either figure correspond to the deflection at the maximum applied load, whereas the lower two curves correspond to the lower load. Once again, the analysis results compare favorably to the test results.

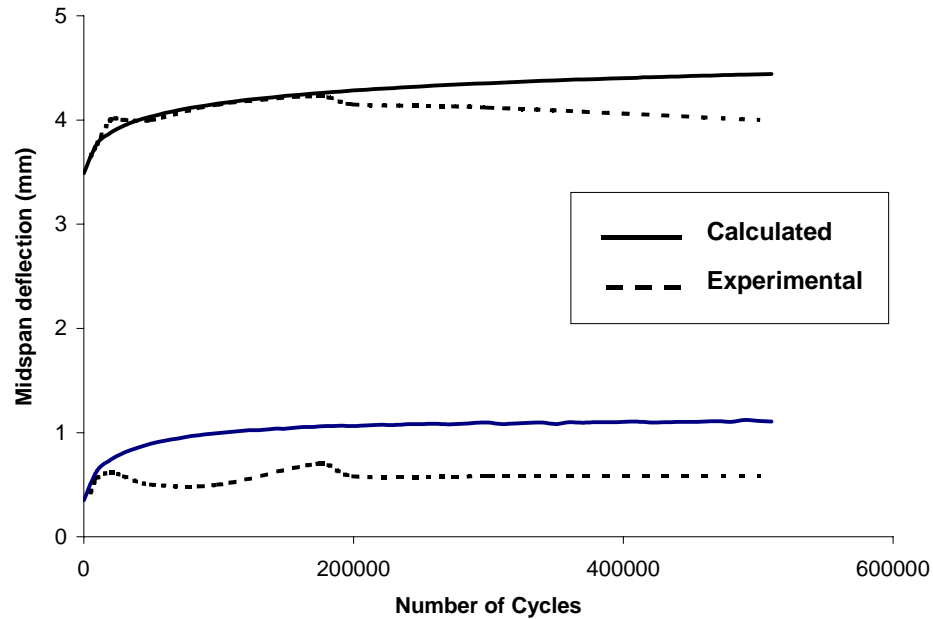
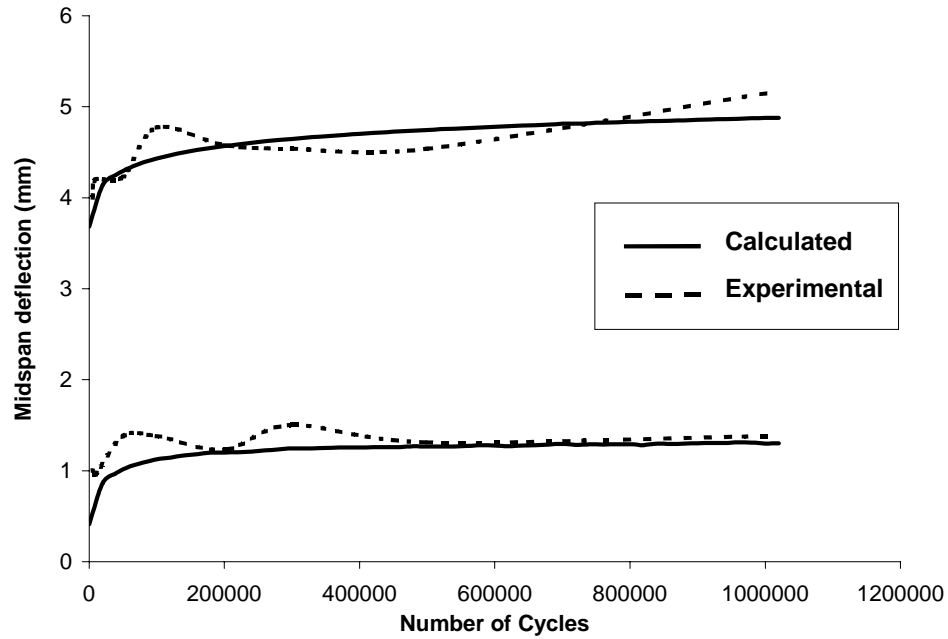


**Figure 4.18:** Calculated versus experimental mid-span deflection for Beam 2 (Barnes and Mays 1999).

#### 4.4 Design Considerations

There is growing consensus among structural engineers that CFRP laminates are suitable for repairing or strengthening reinforced concrete beams subjected to flexure. An example of a repair situation is when a structure suffers damage such as corrosion of a few steel reinforcing bars or prestressing strands and needs to be returned to its original strength. The latter case is normally encountered when an existing structure needs to be strengthened to meet increased strength demands, e.g. due to heavier traffic loads. In either case, the CFRP is usually attached to the structure while still subjected to dead load. Under such conditions, the steel bars are already significantly stressed. Since CFRP ruptures at a strain that is considerably higher than the steel yield strain, it is conceivable that steel reinforcement in a flexurally repaired/strengthened beam may yield under service conditions, i.e. application of the dead plus full live load. Steel yield under service conditions must be avoided because it can cause a reduction in the effective stiffness of the member and can result in excessive permanent deformations, both of which lead to severe serviceability problems.



(b)

**Figure 4.19:** Calculated versus experimental mid-span deflection for Beam 4 (Barnes and Mays 1999).

This situation can be easily remedied during design of the rehabilitation scheme by limiting the steel stress ( $\sigma_s$ ) under service conditions such that

$$\sigma_s < \alpha \beta f_y \quad (4.1)$$

where both  $\alpha$  and  $\beta$  are factors that are less than 1.0. The reduction factor  $\alpha$  takes into consideration the increase in steel stress, which results from the time-dependent redistribution of stresses due creep, shrinkage, and cyclic fatigue. Analyses by Moustafa (1986) and Rao and Jayaraman (1989) of rectangular reinforced concrete sections show that reinforcing steel stresses increase by less than 3.1% as a result of creep and shrinkage. Cyclic fatigue analyses presented in this paper of the test specimens of Shahawy and Beitelman (1999, 2000) and Barnes and Mays (2000) show that the beams suffer less than 5% increase in steel stresses until failure. In general, the steel stress increase is dependent upon the time elapsed, number of cycles the bridge has been subjected to prior to rehabilitation, ambient temperature and humidity conditions, etc. and therefore it is difficult to draw a firm conclusion from these numbers regarding a precise and conservative value for  $\alpha$ . Until further research is conducted, it is recommended that the factor  $\alpha$  be taken as 0.90.

The reduction factor  $\beta$  accounts for the possibility that the tensile strength of steel is less than the assumed nominal stress. A review of the literature shows that steel reinforcement strength is normally distributed, has a strength bias of 1.125 (i.e. mean strength is higher than the nominal design value by 12.5%), and a coefficient of variation, COV (ratio of standard deviation to mean) of 10% (Plevris et al. 1995). For a designer to have 95% confidence that the steel yield stress will not fall below the nominal strength, the design stress,  $f_{des}$ , should be restricted to

$$f_{des} = \text{mean} - 1.645 \times \text{standard deviation} \quad (4.2)$$

Using the values of the bias and COV listed above, it turns out that the reduction factor  $\beta$  should be 0.96 ( $1.125 f_y - 1.645 \times 0.10 f_y = 0.961 f_y$ ).

Substituting the recommended values of  $\alpha$  and  $\beta$  into Eq. 4.1 results in  $\sigma_s < 0.86$  - say  $\sigma_s < 0.85 f_y$ . In other words, a designer involved in the design of a rehabilitation scheme should limit the steel stress under service conditions to 85% of the yield strength.

#### 4.5 Summary and Conclusions

The computer program T-DACS is exercised in this chapter. The program is shown to compare well to test results for all aspects of behavior. A study of the internal stresses obtained from T-DACS showed that cyclic fatigue leads to an internal redistribution of stresses similar to that obtained under static creep. The analyses show that the steel reinforcement stress in the specimens of Shahawy and Beitelman (1999, 2000) and Barnes and Mays (2000) increased by less than 5% during the fatigue life of the test beams. To account for the increase in steel stresses due to cyclic fatigue as well as shrinkage, creep under dead loads and the variability in reinforcing steel strength, it is recommended that the service steel stress be limited such that  $\sigma_s < 0.85 f_y$  for repair and/or strengthening of reinforced concrete girders using CFRP laminates. The 0.85 factor is affected by a variety of parameters and further research is needed to refine it.

# 5 RELIABILITY OF REHABILITATED BRIDGE GIRDERS

## 5.1 Introduction

With the exception of a few studies, most of the research conducted on CFRP strengthened structures has been done in a deterministic manner, and the statistical variations associated with the main design variables have been largely ignored. Reliability-based techniques can be used to account for the randomness in important variables that affect the strength of CFRP strengthened concrete girders. The use of such methods in structural engineering has greatly increased in the past few years as reliability-based models have become better understood and more widely accepted. The recent surge in applications of the theory of reliability to structural engineering problems may be attributed to two main reasons. First, design codes have, and still are, being changed from the *Allowable Stress Design* approach to the *Strength Design* approach. Strength Design provisions in modern design codes are calibrated through reliability-based methods to ensure that the probability of failure,  $P_f$ , does not exceed a target level (Nowak 1995 and Kariyawasam et al. 1997). This approach allows designers to more rationally evaluate the possibility of structural collapse as opposed to Allowable Stress Design, which usually results in hidden reserve strength. The second reason driving the increasing popularity of structural reliability is that it makes possible a new trend in thought whereby structural systems are characterized in a probabilistic manner rather than using deterministic strength to achieve a more rational balance between safety and life cycle costs (Val et al. 1997, Thoft-Christensen 1998, and Estes and Frangopol 1999).

One of the earliest studies of the reliability of concrete structures strengthened with CFRP was conducted by Pelvris et al (1995). In their approach, a virtual design space comprised of a number of random parameters was created and used to study flexural reliability of RC beams strengthened with CFRP. Pelvris et al proposed the use of a reduction factor for CFRP material strength,  $\phi_{\text{CFRP}}$ , together with a general resistance factor,  $\phi$ , for overall member flexural strength. The developed reliability model was used to calibrate the resistance factors for a variety of design situations. Although material level reduction factors are adopted by several design codes, their use constitutes a divergence from current U.S. practices in which a single overall, albeit behavior specific, reduction factor is used. Furthermore, the choice of design factors implied that the study was limited to only reinforced concrete beams in buildings.

In this chapter, the reliability of reinforced and prestressed concrete bridge girders strengthened with CFRP laminates is investigated. The study focuses on cross-sectional flexural behavior and has two specific goals: a) determine resistance models for RC and PSC cross sections rehabilitated with CFRP laminates, and b) develop appropriate design factors.

## 5.2 Reliability Index

The performance of a structure in flexure, shear, ...etc., can be represented by a limit state function, also known as a performance function,  $Z$ . In its simplest form, the limit state function is the difference between the random resistance of the member,  $R$ , and the random load effect acting on the member,  $Q$ .

$$Z = R - Q \quad (5.1)$$

A general limit state function involves a number of random variables,  $X_1, X_2, \dots, X_n$ , representing dimensions, material properties, loads ...etc. Accordingly,  $Z$  becomes a random vector  $g(\cdot)$  where

$$Z = g(X_1, X_2, \dots, X_n) \quad (5.2)$$

Such a general limit state function represents a failure surface, which divides the design space into safe and unsafe designs as can be seen in Fig. 5.1 for a simple 2-dimensional design space. The probability of failure,  $P_f$ , for the limit state under consideration can be represented by the *Reliability Index*,  $\beta$ . The relationship between the reliability index and the probability of failure is

$$P_f = \Phi(-\beta) \quad (5.3)$$

where  $\Phi(\cdot)$  is the Cumulative Distribution Function (CDF) of the limit state function under consideration. The reliability index can be determined using the following expression

$$\beta = \frac{\mu_z}{\sigma_z} \quad (5.4)$$

where  $\mu_z$  and  $\sigma_z$  are respectively the mean value and the standard deviation of the Probability Density Function (PDF) of  $Z$ . Design codes are developed to result in structures with a  $P_f$  corresponding to a reliability index between 3.0 and 3.75. The range of  $\beta$  is due to many factors such as the importance of the structure, the expected mode of failure, the ratio of live loads to dead loads, ...etc. (Allen 1992).

## 5.3 First Order Reliability Method (FORM)

The mean and standard deviation ( $\mu_z$ ,  $\sigma_z$ ) of the joint PDF of  $Z$  in Eq. 5.1 are needed to determine the reliability index. Determining these values is not straight forward, especially for the case of a complex limit state function. Several methods are used to determine the reliability index (Ayyub and McCuen 1997) including the First Order Reliability Method (FORM) which is chosen to study the reliability of the analyzed cross sections. FORM is based on a first order Taylor series expansion of the limit state function, which approximates the failure surface by a

tangent plane at the point of interest. According to FORM, the mean and variance of  $Z$  are evaluated and given as

$$\mu_Z \cong g(\mu_1, \mu_2, \dots, \mu_n) \quad (5.5)$$

$$\sigma_Z^2 \cong \sum_{i=1}^n \sum_{j=1}^n \left( \frac{\partial Z}{\partial X_i} \right)_{\mu} \left( \frac{\partial Z}{\partial X_j} \right)_{\mu} \text{covariance}(X_i, X_j) \quad (5.6)$$

where the partial derivatives  $\left( \frac{\partial Z}{\partial X_i} \right)_{\mu}$  and  $\left( \frac{\partial Z}{\partial X_j} \right)_{\mu}$  are evaluated at the mean of the basic random variables. In the case of uncorrelated variables, Eq. 5.6 reduces to

$$\sigma_Z^2 \cong \sum_{i=1}^n \left( \frac{\partial Z}{\partial X_i} \right)_{\mu}^2 \sigma_{(X_i)}^2 \quad (5.7)$$

The most probable failure point is the mean. In the design space, this point is located on the failure surface  $Z$  (Eq. 5.1) such that distance from the origin of the design space to the tangent plane to the failure surface is shortest (see Fig. 5.1). To locate such a point, an iterative process is needed. The iterations are executed on transformed standard normally distributed random vectors using a specially developed MatLab computer program. A detailed description of the process can be found in Appendix A and Estes and Frangopol (1998).

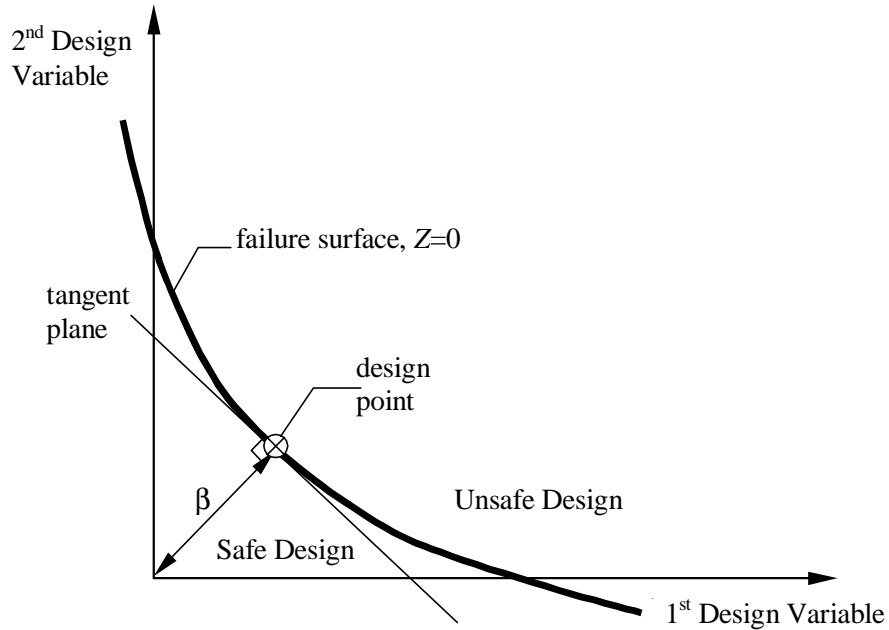


Figure 5.1: A simple reduced design space showing the design point, reliability index,  $\beta$ , and limit state function,  $Z$ .

## 5.4 Monte Carlo Simulations

One hundred and twenty thousand data sets were randomly generated for the RC and PSC bridges considered in this study and described later on in Sections 5.4 and 5.5. The data sets were generated by assuming appropriate probabilistic distributions for the uncertainties of the various parameters. A review of the literature on bridge and building structures was performed to identify the statistical properties of the various parameters affecting flexural behavior. Table 5.1 lists the range of statistical properties found in the literature. The table shows the bias (mean/nominal), coefficient of variation ( $COV = \text{standard deviation}/\text{mean}$ ), and distribution type assumed by other researchers including Lu et al. (1994), Nowak et al. (1994), Pelvris et al. (1995), Thoft-Christensen (1998), Val et al. (1998), Crespo-Minguillon and Casas (1999), Estes and Frangopol (1999), Stewart and Val (1999). It is obvious from Table 5.1 that there is no clear consensus on specific values for many of the parameters involved.

The bias and coefficient of variation adopted in the current study are also listed in Table 5.1. Based on the survey, all parameters were assumed to have a normal distribution except for the CFRP laminates, which were assumed to be a Weibull material. It is important to note that CFRP laminates have a relatively low bias and  $COV$  compared to steel or concrete. Both analytical and experimental results confirm this observation (Bullock 1974, Harlow and Phoenix 1981, Batdorf 1994, Bakht et al. 2000).

## 5.5 Reliability of Reinforced Concrete Bridge Girders

The reliability of RC bridge girders is evaluated through the following process. A pool of bridge designs that cover a wide range of design parameters is created. The pool is comprised of a number of reinforced concrete bridges with different spans designed according to AASHTO-LRFD (1998). Each of the bridge designs is assumed to have suffered various degrees of damage to the main steel reinforcement and is then strengthened back to its original design strength through externally bonded CFRP laminates. Monte Carlo simulations are conducted on each of the designed and rehabilitated bridges and use the resulting randomly generated data sets to develop a resistance model for cross-sectional flexural strength. The probability of failure of the designed sections and the reliability index,  $\beta$ , are determined using the specially developed computer program which implements the first order reliability method (FORM). The calculated probability of failure is used to calibrate the flexural resistance factor,  $\phi$ .

Since flexural behavior is the focus of this study, it is implicitly assumed that other modes of failure such as shear failure, laminate peel-off, and bond failure between laminates and concrete do not control behavior. Such modes of failure can be precluded by additional strengthening or through special detailing (Shahawy and Beitelman 1999).

**Table 5.1:** Statistical properties of variables involved in the study

Variable		Other Researchers			Current Study		
		Bias	COV (%)	Distribution Type	Bias	COV (%)	Distribution Type
Dimensions ( $h, d, b$ )		1.00 - 1.03	0.5 - 7.0	Normal	1.00	3.0	Normal
Area of steel ( $A_s$ )		1.00	0.0 - 4.0	Normal - Deterministic	1.00	1.5	Normal
Concrete strength ( $f'_c$ )		0.81 - 1.25	9.0 - 21.0	Normal - LogNormal	1.10	18.0	Normal
Strand strength ( $f_{pu}$ )		1.00 - 1.04	1.7 - 2.5	Normal - LogNormal	1.04	2.0	Normal
CFRP failure strain ( $\epsilon_{u,CFRP}$ )*	Analytical	1.33	7.4 - 10.0	Weibull	1.10	2.2	Weibull
	Experimental	--	2.2 - 5.1	--	--	--	--
Model Uncertainty ( $\alpha$ )		1.01 - 1.10	4.5 - 12.0	Normal	1.01	4.5	Normal
Uncertainty of Girder DF ( $\eta$ )		0.89 - 1.02	9.1 - 14.0	Normal	0.924	13.5	Normal
Wearing Surface Load ( $WS$ )		1.00 - 1.44	8.0 - 53.2	Normal	1.10	20.0	Normal
Dead Load ( $D$ )		1.00 - 1.05	8.2 - 25.0	Normal	1.05	10.0	Normal
Live Load ( $L$ )	Buildings	1.20	9.0 - 25.0	Extreme Event I	--	--	--
	Bridges	1.25-1.52	12.0 - 41.0	Normal - Modified Normal	1.35-1.38	18.0	Normal

\* Analytical results used by Pelvis et al. (1995); experimental results are reported in Bakht et al. (2000).





### 5.5.1 Design of RC Bridges

A broad range of realistic designs are required to investigate reliability and recommend resistance factors for reinforced concrete girders strengthened with CFRP laminates. Three simply supported bridges with the following spans are considered: 22,860mm (75ft), 18,288mm (60ft), and 13,716mm (45ft). The bridges are designated as RC75, RC60, and RC45, respectively. An interior girder for each bridge was chosen for this study and designed for flexure according to AASHTO-LRFD (1998).

The designed cross sections are then assumed to have lost a significant portion of the main reinforcing steel (possibly due to corrosion, vandalism, or collision by a truck). Three levels of damage are considered; namely a loss of 10%, 20% and 30% of the main steel. Rehabilitation schemes are then designed to return the damaged bridge sections to their original strength by externally bonding CFRP laminates to the beam stems. The CFRP laminates are wrapped around the stem of the beams and attached using epoxy adhesives. This technique has been shown to be successful for repair purposes as it reduces the likelihood of laminate peel-off or debonding (Shahawy and Beitelman 2000).

Although arbitrary, the chosen damage levels are realistic in that rehabilitation of the girders using CFRP is a feasible and practical alternative. The damaged bridges are referred to hereafter by appending D1, D2, or D3 (which correspond to 10, 20, or 30% damage) to the bridge designation listed above. For example, for the 60-ft span design, the damaged bridges are designated RC60-D1, RC60-D2, and RC60-D3 for 10, 20, and 30% damage levels respectively. Altogether, the number of bridge designs chosen for the reliability study is twelve. The inventory is comprised of 3 undamaged bridges, each having three variations reflecting the three damage levels considered.

### 5.5.2 Bridge Geometry, Material Properties, and Loading

Figure 5.2 shows the cross section used for all bridge spans. The supported road is 10059mm wide (33ft 2in). The bridge cross-section is comprised of a 191mm-thick (7.5in) slab monolithic with five girders spaced at 2134mm (ft). The concrete compressive strength is assumed to be  $f'_c=27.6\text{MPa}$  (4ksi) whereas the steel yield strength is  $f_y=414\text{MPa}$  (60ksi).

It is assumed that the laminates used for strengthening are similar to those successfully used by the Florida Department of Transportation (FDOT) for repair purposes (Shahawy and Beitelman 1999). The tensile strength of CFRP fibers is assumed to be  $\sigma_{\text{fiber}}=3.65\text{GPa}$  (530ksi). However, the laminate strength, which is different than the fiber strength, is estimated using the Weibull theory as discussed in Chapter 3. Application of this method to the designed bridges results in the laminate strengths listed in Table 5.2. The small variations in the design tensile strength of the CFRP laminates are due to differences in the volume of carbon fibers in the different designs; i.e. size effect. The theory also provides the coefficient of variation, *COV*, for the laminate strength, which turns out to be 2.2%.

The design bending moments for the interior girder are calculated for the dead loads and live loads according to the AASHTO-LRFD specifications (AASHTO 1998). The maximum of "Lane Load/Standard Truck" and "Lane Load/Tandem Load" cases is considered as shown in Fig. 5.3. The truck or tandem portion of the live load moments is increased by an impact factor of 33%.

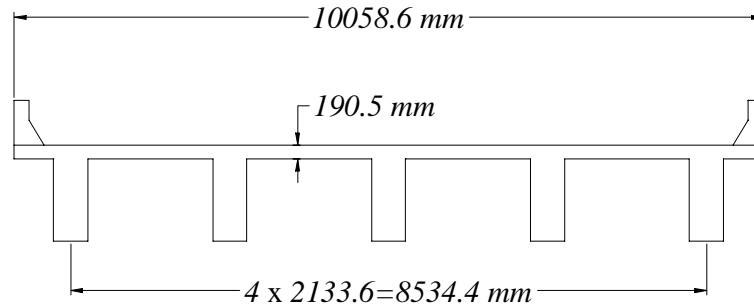


**Figure 5.2:** Cross section of 5-girder bridge

### 5.5.3 Design of RC Cross Sections

The designed cross sections of the interior girder of each bridge are shown in Fig. 5.4. The pure carbon thickness (in the CFRP laminates) required to return the damaged girders to their original strength is calculated using the fiber section model described in Chapter 2 and are given in Table 5.3. It is worthwhile to note that the expected failure mode of all the rehabilitated cross-sections is steel yielding followed by rupture of the CFRP. Concrete crushing is unlikely because of the presence of the concrete deck, which acts as a flange for the girders.

The stress in the main reinforcing bars due to service loads (dead, live, and impact;  $M_{\text{service}} = M_D + M_{L+IM}$ ) is also shown in the table and is well below the yield stress for all cases. It is important to ensure that the service steel stress is well below yielding since overloading the steel can lead to a reduction in the effective stiffness of the member and can result in excessive permanent deformations, both of which create severe serviceability problems. Chapter 4 discusses the maximum appropriate steel stress level for this type of serviceability check. Table 3 also shows the ratio of the flexural capacity provided by CFRP to the flexural capacity provided by steel reinforcement. For the 30% damage level, the CFRP laminates are providing about 45% of the moment capacity due to the steel reinforcement for all three spans.

**Table 5.2:** Usable tensile stress used in design of RC Bridges

Bridge Case	Damage	$\sigma_{CFRP}$ GPa [ksi]
RC75	10%	1.99 [289.2]
	20%	1.97 [285.7]
	30%	1.95 [283.5]
RC60	10%	2.01 [291.4]
	20%	1.98 [287.8]
	30%	1.97 [285.7]
RC45	10%	2.02 [292.7]
	20%	2.00 [289.3]
	30%	1.98 [287.4]

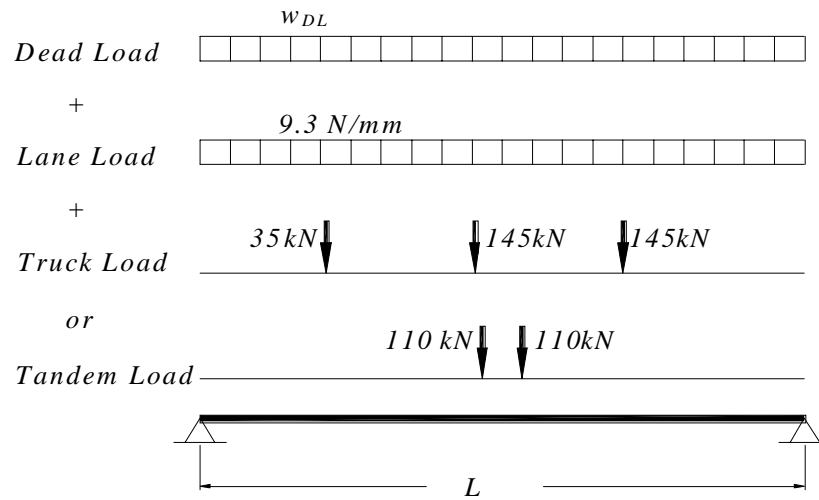
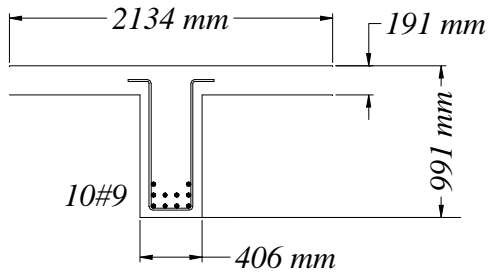
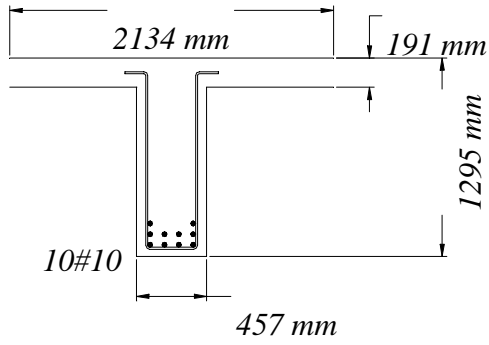


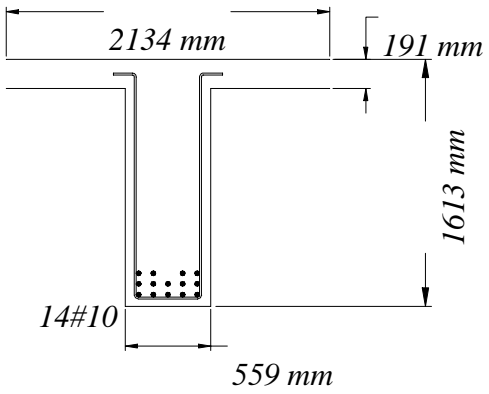
**Figure 5.3:** Loading cases considered in design of bridges



(a) RC45



(b) RC60



(c) RC75

**Figure 5.4:** Cross sections of undamaged interior bridge girders.

**Table 5.3:** Design summary of bridge cross sections

Bridge	Steel Damage Level	CFRP thickness (mm)	$\frac{M_{CFRP}}{M_{steel}}$	Steel Stress at Service (% of $f_y$ )
RC75	0%	--	--	66.2
	10%	0.145	0.12	72.4
	20%	0.280	0.26	80.0
	30%	0.420	0.44	89.5
RC60	0%	--	--	65.2
	10%	0.135	0.12	71.1
	20%	0.265	0.27	78.3
	30%	0.390	0.45	87.3
RC45	0%	--	--	64.8
	10%	0.130	0.13	70.3
	20%	0.247	0.27	77.1
	30%	0.365	0.45	85.4

#### 5.5.4 Monte Carlo Simulations for RC Bridges

Sixty thousand data sets were randomly generated for the designed RC bridges. Each of the generated random data sets was analyzed using the fiber section model discussed in Chapter 2. The resulting moment-curvature relationships for one of the designed RC cross section is shown in Fig. 5.5, where for clarity only 50 curves are drawn. Figure 5.6 shows an idealized moment-curvature relationship for an RC section strengthened with CFRP which is identified by major keypoints; cracking point, threshold moment point (point at which CFRP is bonded), yield point (point at which main steel yields), and ultimate point. Of interest in the reliability study is the flexural capacity (ultimate point) of the cross section. Figure 5.7 shows the distribution of the flexural resistance for Bridges RC60, RC60-D1, RC60-D2, and RC60-D3 combined. A Chi-squared goodness-of-fit study showed that all the distributions could be substituted with normal statistical distributions with reasonable accuracy.

Table 5.4 shows the results of the Monte Carlo simulations for all the bridges considered in the study. The information in Table 5.4 is referred to in the literature as the *Resistance Model* (Nowak and Collins 2000). Resistance models are especially helpful in reliability studies when the problem is highly nonlinear, as in this case where parameters such as steel yielding, concrete cracking and crushing, CFRP rupture, and CFRP initial condition all contribute to making the ultimate flexural strength a nonlinear function.

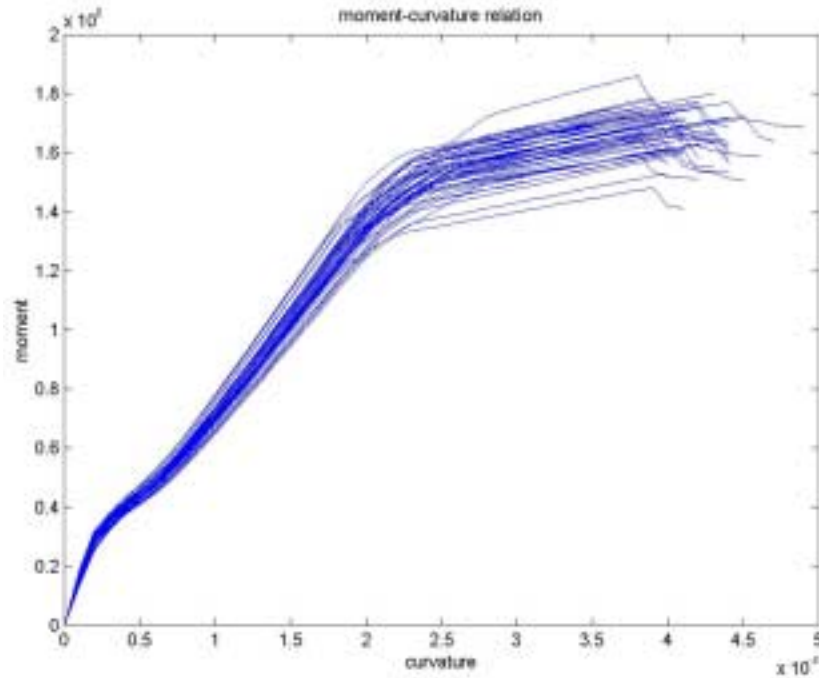


**Figure 5.5:** Moment-curvature relationship obtained from Monte Carlo simulation (50 cases shown)

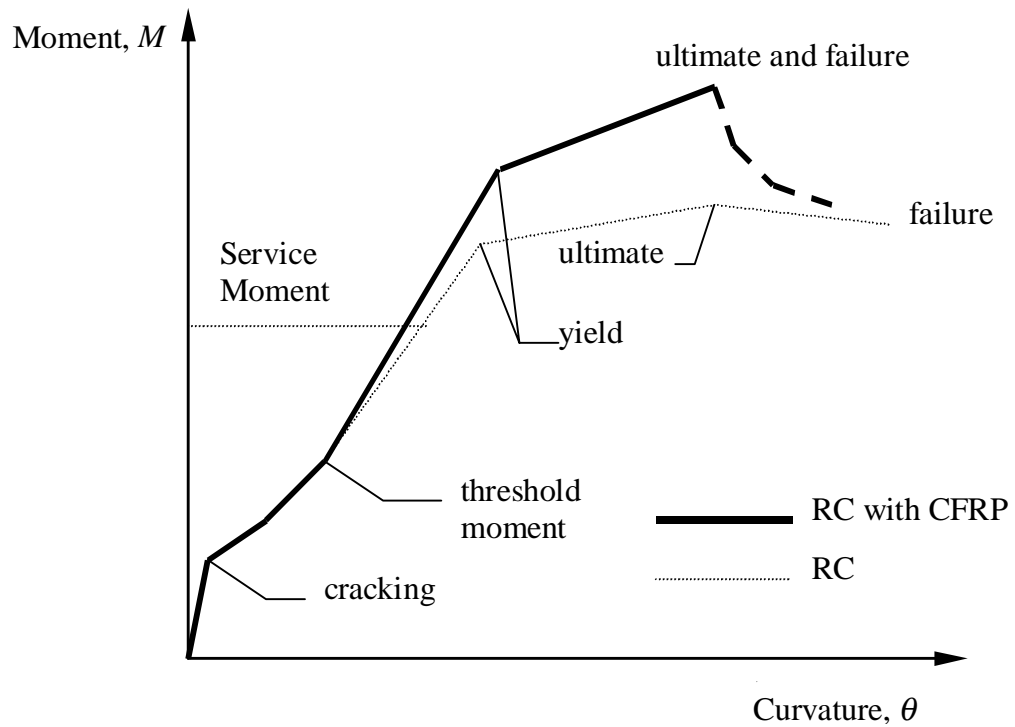
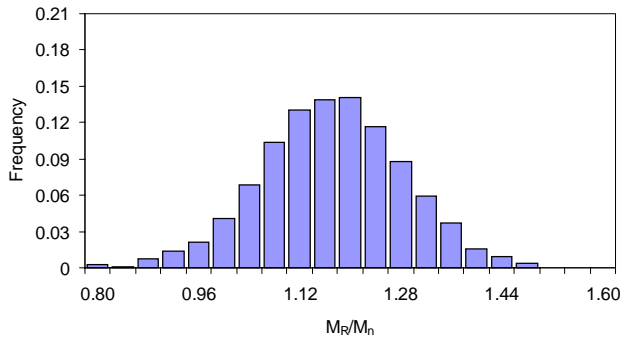
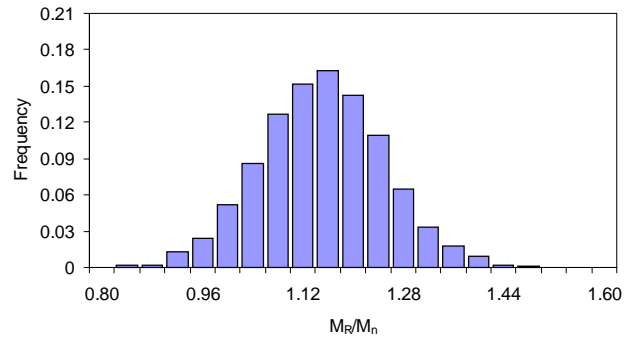


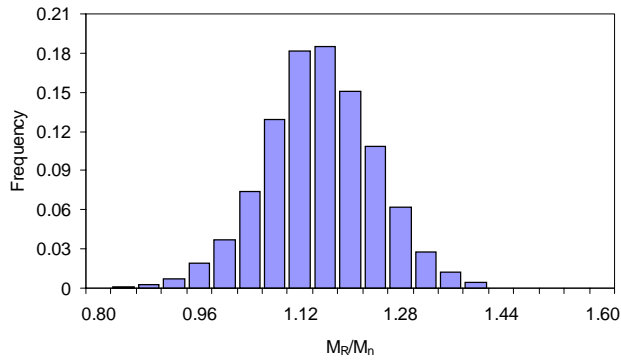
**Figure 5.6:** Idealized moment-curvature relationship



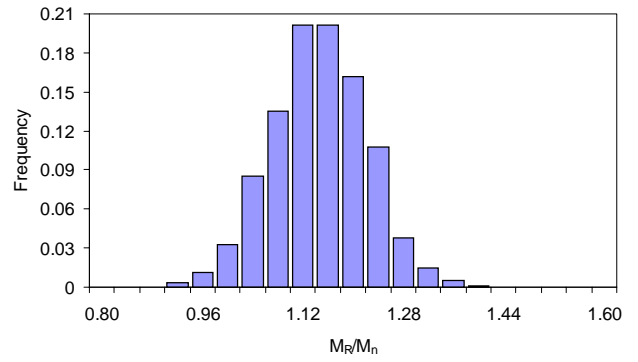
(a) RC60



(b) RC60-D1



(c) RC60-D2



(d) RC60-D3

**Figure 5.7:** Histograms of flexural resistance for Bridges RC60, RC60-D1, RC60-D2, and RC60-D3.



**Table 5.4:** Results of Monte Carlo simulation (moment units in kNm)

Case	$M_L/M_D$	$M_n$	$M_R$			Reliability Index $\beta$
			Value	Bias	COV (%)	
<b>RC45</b>	1.78	2260	2590	1.149	9.73	3.37
<b>RC45-D1</b>			2570	1.138	8.62	3.47
<b>RC45-D2</b>			2560	1.136	7.66	3.59
<b>RC45-D3</b>			2550	1.132	6.71	3.69
<b>RC60</b>	1.28	3900	4490	1.151	9.80	3.41
<b>RC60-D1</b>			4410	1.130	8.68	3.49
<b>RC60-D2</b>			4420	1.132	7.69	3.65
<b>RC60-D3</b>			4390	1.126	6.79	3.75
<b>RC75</b>	0.92	6420	7380	1.150	9.80	3.44
<b>RC75-D1</b>			7240	1.127	8.68	3.53
<b>RC75-D2</b>			7230	1.126	7.74	3.69
<b>RC75-D3</b>			7210	1.123	6.80	3.83

### 5.5.5 Results for RC Bridges

Due to the complexity of the problem, the limit state function used in this study is simplified as

$$Z = \alpha M_R - (M_D + \eta M_L) \quad (5.8)$$

Tables 5.1 and 5.4 give the bias and *COV* of the load and resistance models used in this study. The uncertainty of the analysis model is accounted for by using the random variable,  $\alpha$ , which, according to Ellingwood et al. (1980), has a bias = 1.01 and *COV* = 4.5% for RC sections in flexure. Comparisons of fiber section model results with experimental data show that these values are reasonable for RC sections strengthened with CFRP (Okeil et al. 2000). The live load moment is also treated to account for the dynamic impact and the number of loaded lanes. According to Nowak and Collins (2000) the static live load moment is increased by 10% to account for impact caused by two trucks for all lanes. The *COV* of the joint live load and dynamic load is suggested to be taken as 18%. The live load is also increased by 5% to account for the heavy traffic volume assumed in this study (ADTT=5000 and 2 loaded lanes). The uncertainty of girder distribution factors (DF) is also accounted for by the random variable,  $\eta$ . The bias and *COV* of  $\eta$  were taken as 0.924 and 13.5%, respectively according to Kennedy et al. (1992).

The calculated reliability index values are listed in Table 5.4 for all 12 cases. An examination of Table 5.4 shows that the reliability index for CFRP strengthened beams increases with the

increase of CFRP ratio in the cross section. This is expected since the failure mode is governed by rupture of the CFRP laminates which have a lower *COV* than steel or concrete. Nevertheless, it is important to point out that it is desirable for RC sections strengthened with CFRP laminates to have greater reliability because failure is more brittle.

### 5.5.6 Target $\beta$ for RC Bridges

LRFD design codes typically set the strength requirement in the following form

$$\phi R \geq \gamma_{Q_i} Q_i \quad (5.9)$$

where the resistance factor,  $\phi$ , and the load factors,  $\gamma_{Q_i}$ , are calibrated to ensure that a target reliability index is achieved. The target reliability index is maintained around 3.5 for structures designed according to AASHTO-LRFD (1998). The reliability study showed that  $\beta$  ranges between 3.37 and 3.44 for the unstrengthened RC sections, which is close to the code target. On the other hand, the reliability index for CFRP strengthened sections is greater than that for RC sections and ranges from 3.47 to 3.83. Although addition of CFRP improves the reliability index, the brittle nature of CFRP behavior imposes more stringent demands on the target reliability index.

Allen (1992) investigated the rationale behind defining a target reliability index. According to his proposed approach, the choice of  $\beta$  depends on the component behavior, system behavior, inspection level, and traffic category. He suggests that the target reliability index should be increased by  $\Delta\beta = 0.25$  for components that fail suddenly with little warning but maintain their post-failure capacity, and by  $\Delta\beta = 0.5$  for components that suffer a sudden and complete loss of capacity. RC sections provide ample warning if properly designed since steel yielding results in significant ductility. The introduction of CFRP laminates changes the behavior and causes failure (rupture of CFRP) to happen at smaller deformations. However, the section maintains a post-failure capacity equal to that of the unstrengthened cross section (see Fig. 5.6). Following Allen's argument, it is proposed to calibrate Eq. 5.9 such that the target reliability index for RC sections flexurally strengthened with CFRP  $\beta_{RC-CFRP}^{\text{target}}$  is

$$\beta_{RC-CFRP}^{\text{target}} = \beta_{RC} + 0.25 \quad (5.10)$$

where  $\beta_{RC}$  is the reliability index of the unstrengthened RC cross section. Calibrating Eq. 5.9 can be done by either changing the reduction factor,  $\phi$ , the load factors,  $\gamma_{Q_i}$ , or both. Since the used load factors are uniform for other AASHTO-LRFD (1998) provisions, it is more convenient to recalibrate the reduction factor.

Figure 5.8 shows the effect of changing the reduction factor,  $\phi$ , for Bridges RC60-D1, RC60-D2, and RC60-D3. The figure is a relationship between  $\phi$  and the sum of the squares of  $(\beta - \beta_{RC-CFRP}^{\text{target}})^2$ . The lowest point on the relationship curve is the optimum point that would maintain the smallest error for all cases and is determined by nonlinear regression. Results of the

optimization are given in Table 5.5. It can be seen that if all damaged cases are considered a  $\phi$  of 0.902 is needed to maintain  $\beta_{RC-CFRP}^{target}$ . When considering each damage level separately,  $\phi$  would be 0.881, 0.904, and 0.918 for the 10%, 20%, and 30% damage levels, respectively. Maintaining  $\phi$  at 0.9 would violate  $\beta_{RC-CFRP}^{target}$  for the low damage levels (10%). To reach a safe design that encompasses a wide range of damage levels,  $\phi$  is taken as 0.85. The next section shows the effect of using  $\phi = 0.85$  on the design of a wide range of damage levels and L/D ratios.

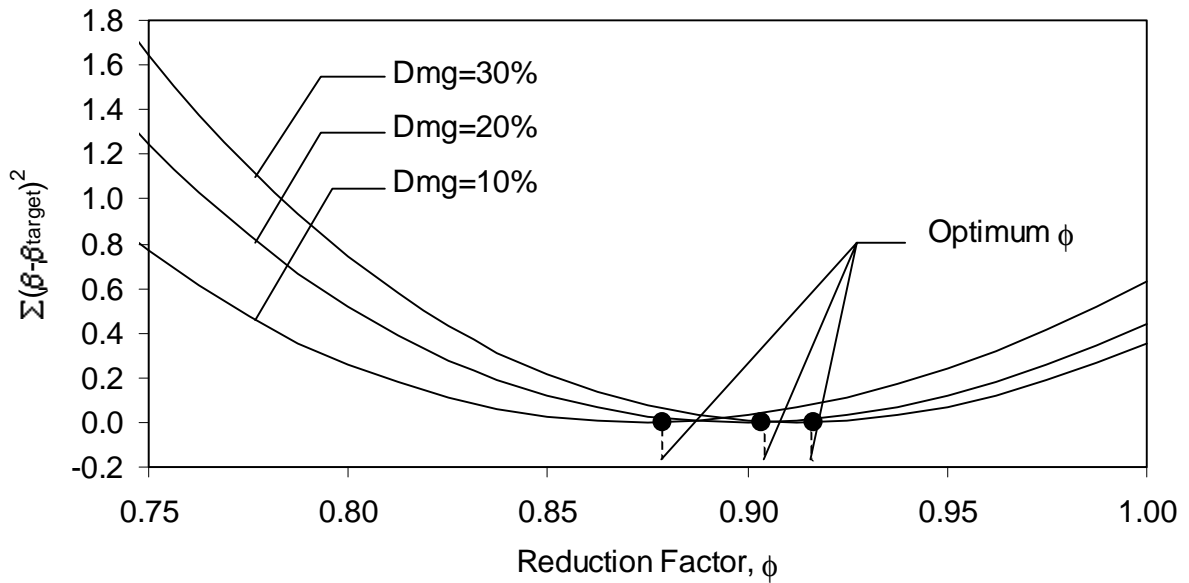


**Figure 5.8:** Determining reduction factor,  $\phi$ . (Bridges RC60-D1, RC60-D2, and RC60-D3)

### 5.5.7 Effect of $\phi = 0.85$ on RC Bridges

To study the impact of using  $\phi = 0.85$  for the design of RC sections strengthened with CFRP, the cross sections in Fig. 5.4 are used. Each cross-section is subjected to a range of  $M_L/M_D$  ratios varying from 0.0 (dead load only) to 4.0 (very high live load). The reliability index,  $\beta$ , is determined for all  $M_L/M_D$  ratios and damage levels using FORM. Figure 5.9 is a plot of the effect of  $M_L/M_D$  on the reliability index. It can be seen that using  $\phi = 0.85$  results in cross-sections with a reliability index,  $\beta$ , that conforms to what current codes normally target for a wide range of  $M_L/M_D$ .  $\beta$  falls below acceptable limits only in the case of unrealistically high  $M_L/M_D$  ratios. The figure again shows that the use of more CFRP enhances the reliability of the cross section because of the low *COV* of CFRP materials as discussed earlier.

**Table 5.5:** Optimum  $\phi$  to achieve  $\beta_{RC-CFRP}^{target}$

Case		Optimum $\phi$
RC45	D1	0.883
	D2	0.902
	D3	0.916
RC60	D1	0.879
	D2	0.904
	D3	0.917
RC70	D1	0.881
	D2	0.905
	D3	0.921
All D1 cases		0.881
All D2 cases		0.904
All D3 cases		0.918
All cases		0.902

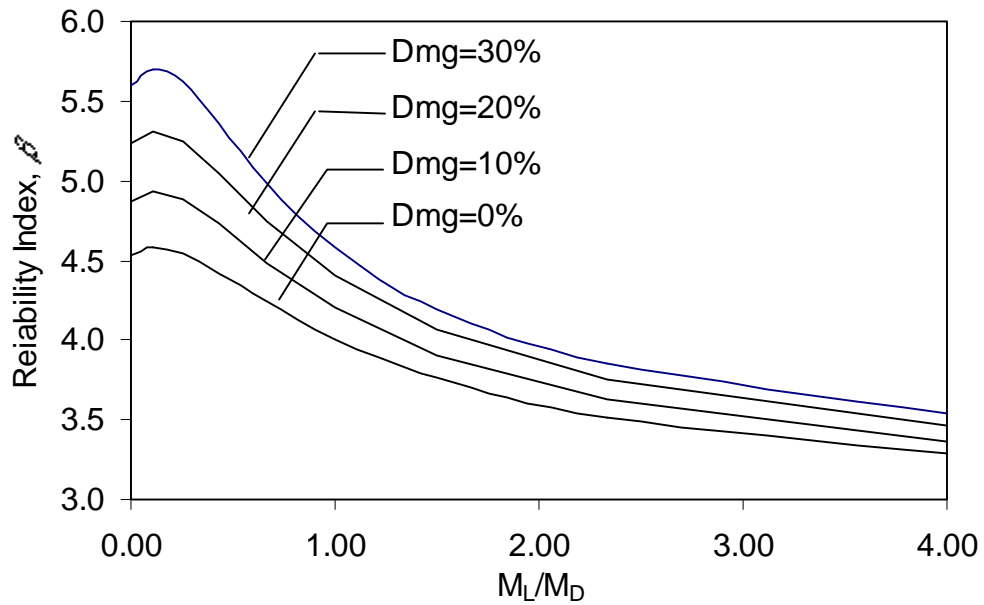


**Figure 5.9:** Effect of  $M_L/M_D$  on Reliability Index,  $\beta$ . (Bridge RC45,  $\phi=0.85$ )

### **5.5.8 Design Implications for RC Bridges**

A study using the developed resistance models showed that the reliability index of the strengthened cross sections is greater than that of the reinforced concrete sections and increases with increasing CFRP ratio. This is attributed to the low coefficient of variation for CFRP ultimate strength, which is lower than the coefficient of variation of the strength of steel or concrete. Although the reliability index improves with addition of CFRP, the flexural resistance factor is recommended as  $\phi=0.85$ , which is lower than that recommended by AASHTO-LRFD for RC sections under flexure. The reduced  $\phi$  value is calibrated to result in a larger target reliability index than is normally specified in recognition of the brittle nature of CFRP behavior.

## **5.6 Reliability of Prestressed Concrete Bridge Girders**

To evaluate the reliability of PSC girders, a number of realistic PSC bridge designs are generated, i.e. a design space is created. The designs have different spans and are based on current code provisions in AASHTO-LRFD (1998). Each of the bridge designs is assumed to have lost a variable number of prestressing strands and is then strengthened back to its original design strength through externally bonded CFRP laminates. As was done for the reinforced concrete bridges in Section 5.4, Monte Carlo simulations are performed on each of the designed and rehabilitated PSC bridges and the resulting data sets are used to develop resistance models for cross-sectional flexural strength. The developed resistance models are then used to calibrate the flexural resistance factor,  $\phi$ , to achieve a preset target probability of failure.

### **5.6.1 Design of PSC Bridges**

Three simply supported bridges with varying spans are designed according to AASHTO-LRFD (1998). These bridges form the core of the design space that is used as a basis for the reliability calculations. All bridges share the same road cross section shown in Fig. 5.10 (road width = 14180mm [46ft 6in], slab thickness = 205mm [8in], number of girders = 6, and girder spacing = 2440mm [8ft]), but have different span lengths (18290mm [60ft], 24380mm [80ft], and 30480mm [100ft]). The bridges are designated PS60, PS80, and PS100, with the numbers corresponding to the span length in feet. The concrete deck is assumed to be a cast-in-place (CIP) slab acting compositely with the girders.

Following the provisions of AASHTO-LRFD (1998), each of the bridges is first designed to resist the applied dead and live loads. Only interior girders are designed, and since all bridges have simple spans, only positive moments are accounted for. The precast prestressed AASHTO girder is assumed to resist the dead loads (self-weight of girders and slab), while the composite section (AASHTO girder and CIP slab) is assumed to resist live loads and additional dead loads (wearing surface and parapet load). Forces due to live loads are computed by superimposing the effect of a uniformly distributed lane load and the effect a standard truck or a tandem load whichever is greater (see Fig. 5.3). The truck/tandem portion of the live load moments are increased by an impact factor (IM) of 33% for the strength limit state and 15% for the fatigue limit state. When computing bending moments due to the standard truck for the strength limit state, the axle configuration used is based on a rear axle distance of 4300mm [14ft] (AASHTO minimum value). For fatigue calculations, a similar configuration is used, however, the rear axle

distance is taken as 9000mm [30ft]. Table 5.6 summarizes the bending moments computed for the design of an interior girder of each bridge. The table also lists the distribution factor (DF) for the cases of one-lane (used for fatigue limit state) and two-lane loading (used for service and strength limit states).

**Table 5.6:** Design moments for interior girder of reinforced concrete bridges.

Bridge	Distribution Factor		Service Moments (kN.m)				Factored Moment $M_u$ (kN.m)
	1 Lane	2 Lanes	Dead Load	Service III	Service I	Fatigue	
PS60	0.4927	0.6735	727	1900	2151	346	3358
PS80	0.4749	0.6657	1509	3301	3674	531	5600
PS100	0.4676	0.6684	2762	5298	5814	719	8678

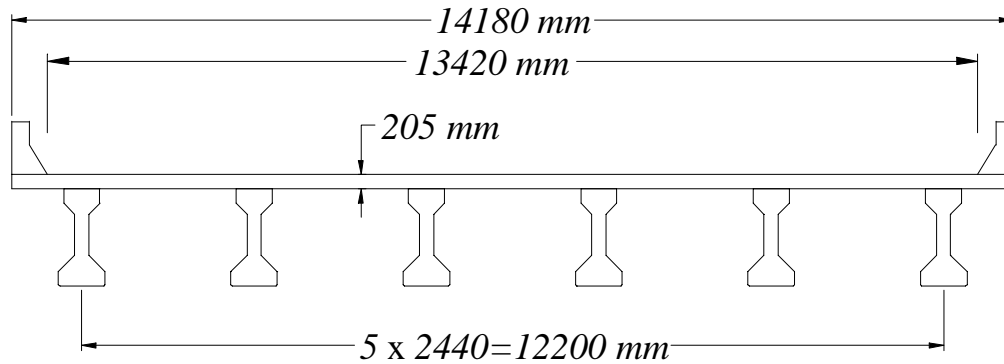


**Figure 5.10:** Cross section of 6-girder bridge

Flexural design of the cross section is performed using the fiber section program described in Chapter 2. The following material properties are assumed: compressive strength of CIP deck concrete = 27.6MPa [4-ksi], compressive strength of precast AASHTO girders = 48.3MPa [7-ksi], prestressing strands ultimate stress = 1860MPa [270-ksi] for 12.5 mm diameter 7-wire low relaxation strands. Details of the designed cross section are shown in Fig. 5.11. A summary of the design stresses at transfer and at different service levels is given in Table 5.7. It is noteworthy that the flexural capacity of the designed cross sections is more than needed (compare the last columns in Tables 5.6 and 5.7) because serviceability conditions control the

design (top cracking of girder at transfer, bottom cracking of girder at service, fatigue stress limit, ...etc.). This observation directly impacts the strengthening scheme described next.

To complete the design space, each girder designed above is assumed to have suffered some damage through the loss of a variable number of prestressing strands. The damaged girders are then strengthened to meet AASHTO LRFD standards through CFRP rehabilitation. For each unstrengthened girder in the core design space, three levels of damage are considered, D1, D2, and D3, which correspond to nominal strand losses of around 10, 20, and 30% respectively. A beam that suffered a damage level of D1 and then is strengthened using CFRP is designated as such by appending D1 to the naming system described above, e.g. PS60-D1. The three unstrengthened beams along with the nine strengthened beams (three strengthened designs for each original design) form a pool of bridge designs that account for design parameters of interest in this study. The developed pool of 12 designs forms the basis of the reliability calibration.

**Table 5.7:** Summary of design stresses and capacities.

Bridge	Cross Section			Concrete Stresses (MPa)					Fatigue Strand Stresses $\Delta f_{PS}$ (MPa)	Flexural Capacity $M_n$ (kN.m)
	Deck thickness (mm)	Girder Type	Number of Strands	Transfer		Ser. III	Service I			
				$f_{tgi}$	$f_{bgi}$	$f_{bg}$	$f_{tg}$	$f_{td}$		
PS60	205	II	26	-1.80	-21.57	+3.37	-16.74	-4.71	15.86	4050
PS80	205	III	34	-0.76	-19.66	+3.28	-15.94	-4.94	15.35	6756
PS100	205	IV	44	-1.58	-17.70	+3.50	-16.55	-5.12	13.92	10520

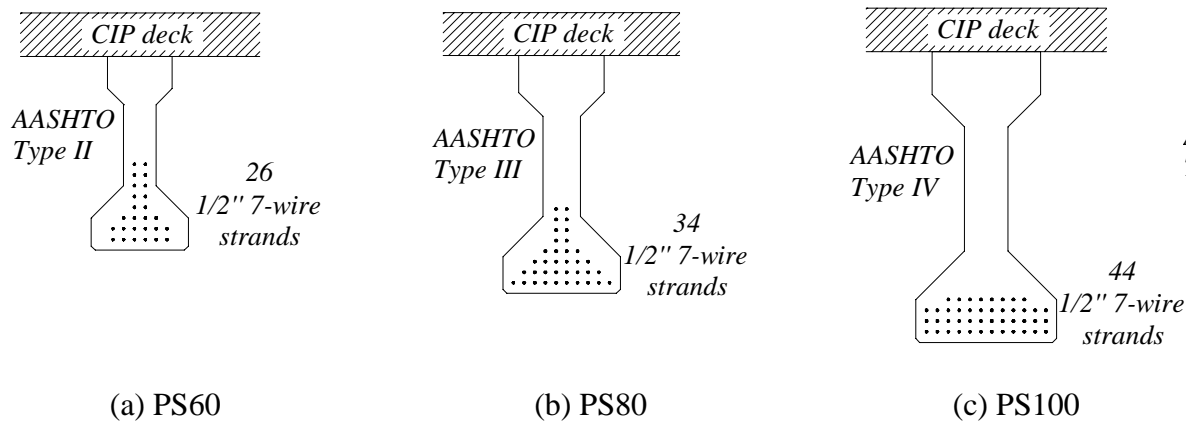


**Figure 5.11:** Cross sections of undamaged interior bridge girders.

The damage scenario considered in this research is representative of a feasible situation that can occur over the life of a girder where strands are lost to corrosion, vandalism, or impact between over height vehicles and girders. As a result of the assumed damage the affected girders may or may not violate strength requirements. However, the girders no longer satisfy code provisions pertaining to service limit state stresses and are therefore in need of repair. The three levels of damage investigated are carefully chosen to represent realistic situations where repairing a damaged beam is more economical than replacing it.

Rehabilitation is achieved through the use of externally bonded CFRP laminates that are wrapped around the stem of the beams. This technique has been shown to be effective by several investigators including Shahawy and Beitelman (2000). Since the repair method does not involve additional prestressing, the service stress levels specified by AASHTO can no longer be satisfied. These stress limits are imposed to insure that PSC girders do not have significant service cracks in the tension region, which can promote strand corrosion, and are therefore of no consequence since the bonded CFRP laminates cover up any existing cracks and will achieve this objective indirectly.

It is assumed that the CFRP laminates are similar to those used in the RC bridges in Section 1.4. As was done for the RC bridges, the usable tensile strength of the CFRP laminate is determined based on the Weibull Theory as discussed in Chapter 3. The results are shown in Table 5.8 for the different girder designs.

**Table 5.8:** Usable tensile stress used in design of PS Bridges

Bridge Case	Damage		$\sigma_{\text{beam}}$ Gpa [ksi]
	Strands	$A_{ps}$ (%)	
PS60-D1	3	11.54	1.97 [286]
PS60-D2	6	23.08	1.95 [283]
PS60-D3	9	34.62	1.92 [278]
PS80-D1	4	11.76	1.99 [289]
PS80-D2	8	23.53	1.96 [284]
PS80-D3	12	35.29	1.94 [281]
PS100-D1	5	11.36	1.97 [286]
PS100-D2	10	22.72	1.95 [283]
PS100-D3	15	34.09	1.92 [278]

As a result of being proportioned to satisfy service stresses, the bridges with the lowest level of damage (PS60-D1, PS80-D1, and PS100-D1) have sufficient remaining flexural capacity after strand loss to resist the applied factored loads. A minimum CFRP amount of one layer (with  $t_{\text{CFRP}} = 0.0109\text{mm}$ ) was nevertheless provided. The second and third damage levels (D2 and D3)



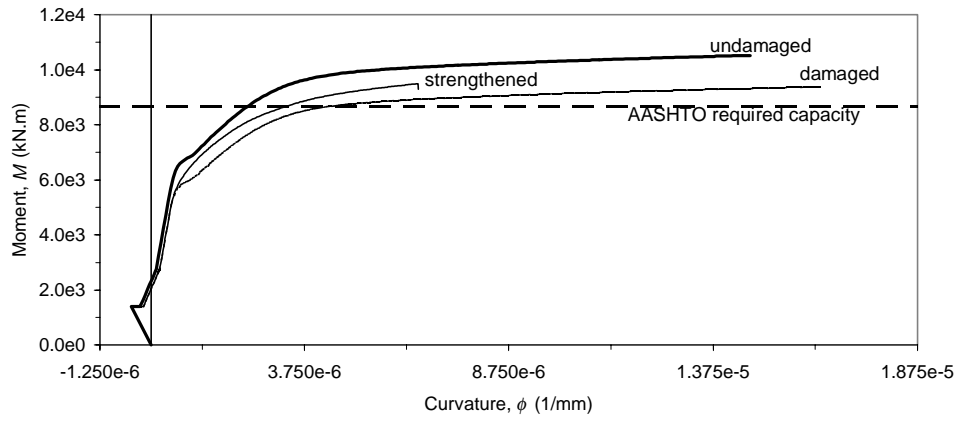
had a more significant deficiency in flexural capacity, and hence required more than one layer of CFRP laminates. Table 5.9 lists the ratio of the flexural capacity generated by CFRP to the flexural capacity provided by the remaining prestressing strands. This ratio is of importance for evaluation of results as will be seen later on in the Chapter. One of the other advantages of using CFRP for strengthening PS girders is that the service stresses in prestressing strands drop. This is shown in Table 5.9 which lists the strand stress at *Service I* limit state ( $M_{\text{Service I}} = M_D + M_{L+IM}$ ) for both damaged and strengthened cross sections. For the third damage level, it can be seen that the strand stress drops by around 12% after strengthening. This is beneficial to the behavior of the PSC beams from the fatigue point of view (as discussed in Chapter 4).

**Table 5.9:** Design summary of bridge cross sections

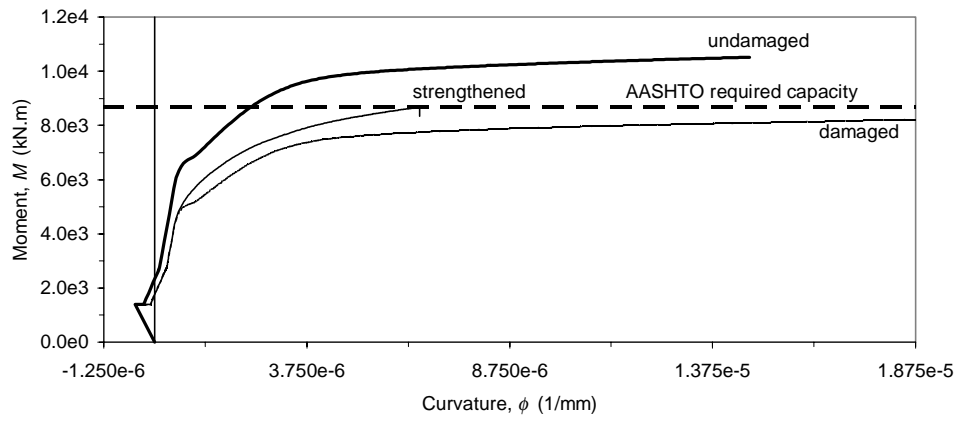
Bridge	CFRP thickness $t_{\text{CFRP}}$ (mm)	Flexural Capacity (kN.m)		$\frac{M_{\text{CFRP}}}{M_{\text{PS}}}$	Strand Stress at Service I		
		Damaged	Strengthened		Damaged (GPa)	Strengthened (GPa)	Diff. (%)
PS60	--	4050		--	1.13		--
PS60-D1	0.109*	3557	3683	0.0827	1.22	1.17	3.5
PS60-D2	0.179	3059	3357	0.1579	1.39	1.27	8.4
PS60-D3	0.381	2584	3358	0.4015	1.59	1.41	11.2
PS80	--	6756		--	1.12		--
PS80-D1	0.109*	5971	6095	0.0713	1.19	1.16	2.2
PS80-D2	0.198	5175	5606	0.1496	1.40	1.27	9.0
PS80-D3	0.430	4386	5607	0.3837	1.59	1.40	12.0
PS100	--	10520		--	1.12		--
PS100-D1	0.109*	9374	9495	0.0614	1.17	1.15	1.5
PS100-D2	0.184	8220	8678	0.1192	1.35	1.24	8.3
PS100-D3	0.433	7078	8677	0.3250	1.54	1.36	11.7

\* a minimum thickness is used equal to thickness of one layer.

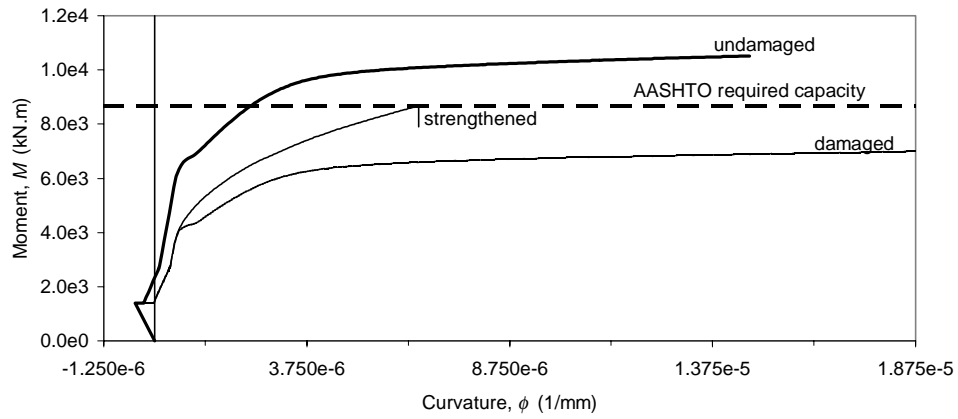
Figure 5.12 shows the moment curvature relationships for Bridge PS100. Each graph corresponds to one of the three damage levels. Three  $M - \theta$  relationships are included in each plot; the original  $M - \theta$  for the undamaged section (bold line),  $M - \theta$  for the damaged cross section before strengthening, and  $M - \theta$  for the strengthened cross section after bonding the CFRP laminates. Also shown is the required capacity according to AASHTO-LRFD (horizontal line). The plots clearly show that adding CFRP to the system increases the flexural capacity of the cross section. This is however, accompanied by a substantial reduction in the ductility. The loss of ductility is accounted for in the calibration of the strength reduction factor.



(a) 1<sup>st</sup> damage level (PS100-D1)



(b) 2<sup>nd</sup> damage level (PS100-D2)



(c) 3<sup>rd</sup> damage level (PS100-D3)

**Figure 5.12:** Moment - curvature relationships for interior girder (PS100)

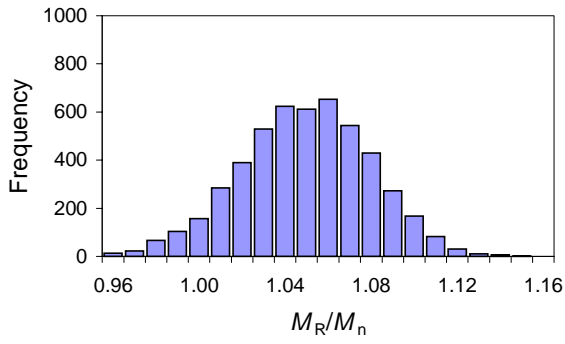
### 5.6.2 Resistance Models

As was done for the RC bridges, flexural resistance models are calculated by performing Monte Carlo simulations for the design space comprised of the original and strengthened cross sections. Five thousand data sets were randomly generated for each cross section, and therefore a total of sixty thousand cases were considered (4 cross sections [original + 3 strengthened] x 3 spans x 5000 data sets).

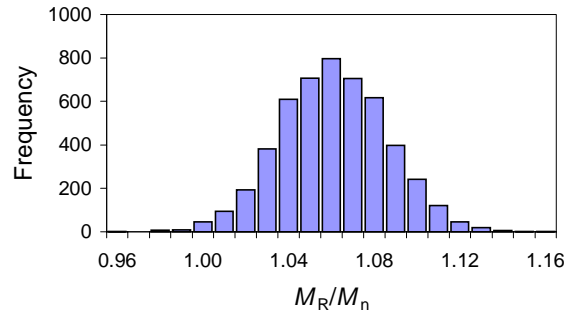
**Table 5.10:** Results of Monte Carlo simulation (moment units in kN.m)

Case	$M_L/M_D$	$M_n$	$M_R$			Reliability Index $\beta$
			Value	Bias	COV (%)	
<b>PS60</b>	1.40	4050	4232	1.045	2.84	3.93
<b>PS60-D1</b>		3683	3892	1.057	2.37	3.34
<b>PS60-D2</b>		3357	3559	1.060	2.26	2.70
<b>PS60-D3</b>		3358	3589	1.069	2.08	2.77
<b>PS80</b>	1.04	6756	7055	1.044	2.89	4.03
<b>PS80-D1</b>		6095	6436	1.056	2.36	3.35
<b>PS80-D2</b>		5606	5942	1.060	2.25	2.74
<b>PS80-D3</b>		5607	5988	1.068	2.12	2.81
<b>PS100</b>	0.80	10520	10980	1.044	2.87	4.24
<b>PS100-D1</b>		9495	10020	1.055	2.42	3.52
<b>PS100-D2</b>		8678	9180	1.058	2.28	2.81
<b>PS100-D3</b>		8677	9253	1.066	2.13	2.88

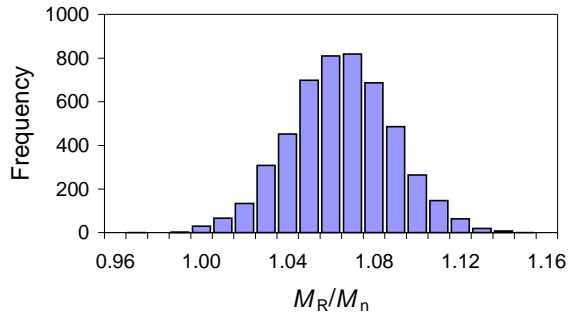
Analyzing each of the data sets results in a unique  $M - \theta$  relationship. Of interest in this study is the statistical variations in the ultimate moment strength ( $M_R$ ). Analysis of data for the 5000 values of moment capacity for each design yielded the resistance models shown in Table 5.10. The table lists the nominal moment,  $M_n$ , obtained from a calculation based on the nominal value of the variables involved. Also listed in the table are the flexural resistance models,  $M_R$ , for each cross section based on the Monte Carlo simulations. Each resistance model is represented by mean value, bias, and COV. Sample histograms of the resistance models are illustrated in Fig. 5.13 for Bridge PS80. As in the RC study, a Chi-squared goodness-of-fit study showed that all 12 distributions could be substituted with normal statistical distributions with good accuracy.



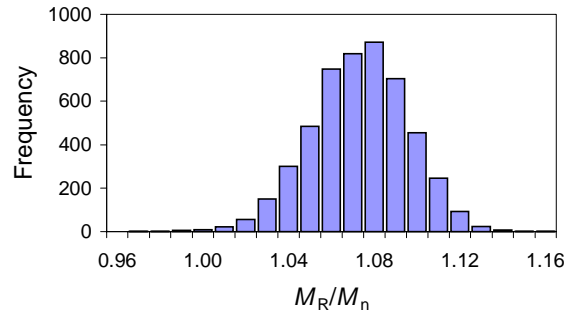
(a) PS80



(b) PS80-D1



(c) PS80-D2



(d) PS80-D3

**Figure 5.13:** Histograms of flexural resistance for Bridges PS80, PS80-D1, PS80-D2, and PS80-D3.

### 5.6.3 LRFD Calibration - $\beta$ based on current AASHTO provisions (LRFD - 1998)

The resistance models obtained are utilized to study the reliability of the designed cross sections. Equation 5.11 gives the limit state function used in this study.

$$Z = \alpha M_R - (M_{ws} + M_D + \eta M_L) \quad (5.11)$$

The uncertainties in the analysis model and live load moment are accounted for through the factors  $\alpha$  and  $\eta$  described in Section 5.4.5. The wearing surface moment ( $M_{ws}$ ) was separated from dead load moments ( $M_D$ ) to account for the different uncertainties associated with each variable (see Table 5.1).

The calculated twelve  $\beta$  values are given in Table 5.11 for the corresponding cross sections. The reliability index for the undamaged cross-sections is greater than 4.0, which significantly exceeds the AASHTO LRFD target. This is expected since the design for these undamaged cross sections was controlled by limit states other than strength (cracking, fatigue, ...etc.). The strengthened cross sections had lower  $\beta$  values because strength was the controlling factor in the design process, which assumed that  $\phi=1.0$  according to AASHTO-LRFD. The listed values show that the current AASHTO design procedure is deficient when used for designing the PSC girders strengthened with CFRP laminates, i.e. results in cross sections with a reliability index below what is normally accepted.

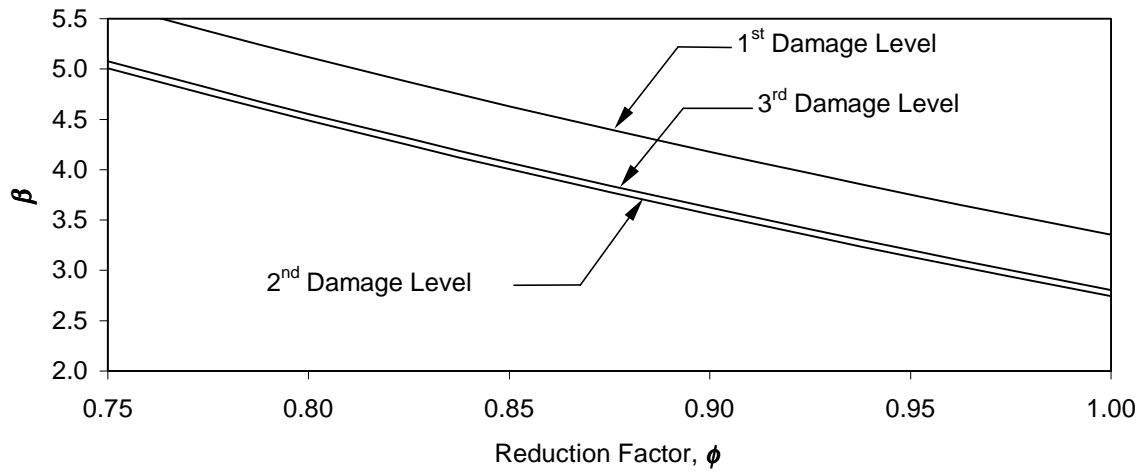
**Table 5.11:** Optimum  $\phi$  to achieve  $\beta_{PS-CFRP}^{target}$

Case		Optimum $\phi$
<b>PS60</b>	<b>D1</b>	0.936
	<b>D2</b>	0.875
	<b>D3</b>	0.884
<b>PS80</b>	<b>D1</b>	0.939
	<b>D2</b>	0.887
	<b>D3</b>	0.893
<b>PS100</b>	<b>D1</b>	0.954
	<b>D2</b>	0.899
	<b>D3</b>	0.905
<b>All D1 cases</b>		0.944
<b>All D2 cases</b>		0.888
<b>All D3 cases</b>		0.895
<b>All cases</b>		0.910

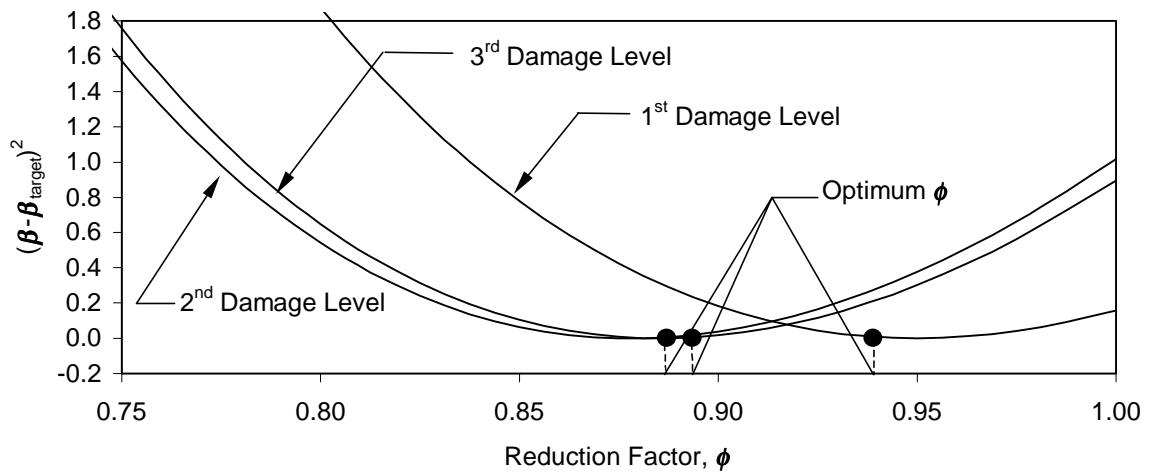
An examination of Table 5.11 shows that  $\beta$  decreases with the increase of damage level up to D2, but climbs slightly for D3. This can be explained as follows. For the D1 damage level, the cross-sections have greater strength than needed and hence the relatively high reliability index (compare Table 5.6 column 8 and Table 5.9 column 4). The reasons for this are: 1) the original sections are overstrength to start with because serviceability checks controlled; 2) the assumed amount of damage was mild so that the damaged sections still satisfied strength provisions; and 3) a minimum of one layer of CFRP was added anyway to protect the damaged girders since serviceability stresses could not be satisfied. For the D2 damage level which violates strength provisions, just enough CFRP is added to reach the target strength using an unconservative  $\phi=1.0$  value, and so the reliability drops compared to D1. As the damage level increases to D3, more CFRP is needed for repair than for D2. Since the CFRP has a relatively low *COV* as discussed earlier, the reliability of the cross-section improves slightly as more CFRP is used, thereby increasing  $\beta$ . This is a desirable property of CFRP because the added brittleness introduced by the CFRP is somewhat tempered by improved reliability. The previous discussion is valid for the failure mode observed in this study which was mostly controlled by CFRP rupture. Although other modes of failure may lead to other conclusions, it is unlikely for properly designed T-shaped bridge girders strengthened with CFRP laminates to fail by concrete crushing (due to the abundance of concrete in the deck) or steel rupture.

#### 5.6.4 LRFD Calibration of the design procedure

As discussed in Section 5.5.6, the target reliability index for PSC girders strengthened with CFRP is assumed to be  $\beta_{PS-CFRP}^{target} = 3.75$ , which is greater than the 3.5 targeted by AASHTO to account for the brittle nature of CFRP rupture. The impact of changing  $\phi$  on  $\beta$  is illustrated in Fig. 5.14-a for a wide range of  $\phi = 0.75 - 1.0$ . The plot shows that low  $\phi$  values result in overly conservative designs ( $\beta$  more than 4.5). A  $\phi$  value of 1.0 (current AASHTO provision for flexural design of PSC girders) is clearly unconservative, especially for the second and third damage levels. To reach a  $\phi$  value that results in cross-sections with  $\beta$  equal to 3.75 (target value), the plot in Fig. 5.14-b is used. The abscissa in this plot is the  $\phi$  value and the ordinate is the square of the difference between the resulting  $\beta$  and  $\beta_{PS-CFRP}^{target}$ ; i.e.  $(\beta - \beta_{PS-CFRP}^{target})^2$ . The lowest point on the curve corresponds to  $\phi$  that would result in  $\beta$  closest to  $\beta_{PS-CFRP}^{target}$  and is determined through nonlinear regression. The first nine values in Table 5.11 are the computed strength reduction factors obtained for the damaged cross sections. If the results for each damage level are considered together, a plot similar to the one in Fig. 5.14-b would be used, however, the ordinate would be the sum of  $(\beta - \beta_{PS-CFRP}^{target})^2$  from all cross sections. The resulting  $\phi$  in this may be called an optimum since it results in the least differences between  $\beta$  and  $\beta_{PS-CFRP}^{target}$  for a wider range of cross sections. A calibration of all the obtained data together shows a  $\phi$  value of 0.91 is needed to design cross sections with  $\beta$  values of 3.75.



(a)



(b)

**Figure 5.14:** (a) effect of changing  $\phi$  on the  $\beta$ , (b) determining the optimum reduction factor,  $\phi$ . (Bridges PS80-D1, PS80-D2, and PS80-D3)

### 5.6.5 Proposed Resistance Factor, $\phi$

A review of Table 5.11 shows that the choice of the lowest value of  $\phi$  (say 0.85) for design may result in overconservative cross sections, especially for low damage levels. It is therefore proposed that a transition relationship for  $\phi$  be used as shown in Fig. 5.15. The proposed reduction factor uses the ratio of cross-sectional capacity from CFRP laminates to the capacity

from prestressing strands ( $M_{CFRP}/M_{PS}$ ) as the controlling parameter. This ratio is believed to better represent the amount of CFRP laminates in the cross section than the actual area, which is to be determined in a design situation, thus eliminating the need for unnecessary design cycles. The calibrated  $\phi$  values for the 12 cross sections are plotted in Fig. 5.15 versus  $M_{CFRP}/M_{PS}$ . The undamaged cross sections are represented by the points on the ordinate axis; i.e.  $M_{CFRP}/M_{PS} = 0.0$ . The damaged cross sections are represented by the other nine points in the plot. The proposed reduction factor (dashed line) is a lower bound for the computed values, which is given by the following equation

$$\phi = 1.0 - \frac{M_{CFRP}}{M_{PS}} \geq 0.85 \quad (5.12)$$

The minimum limit of 0.85 is imposed on  $\phi$  to follow the trend observed in this plot.

The effect of using the proposed  $\phi$  for a wide range of dead load to live load ratios is given in Fig. 5.16 for Bridge PS60. It can be seen that using the proposed equation for  $\phi$  results in acceptable  $\beta$  values for a wide range of  $M_L/M_D$ . The difference between the four curves plotted in Fig. 5.16 is small since the  $\phi$  proposed in Eq. 6 is used in the calculations.

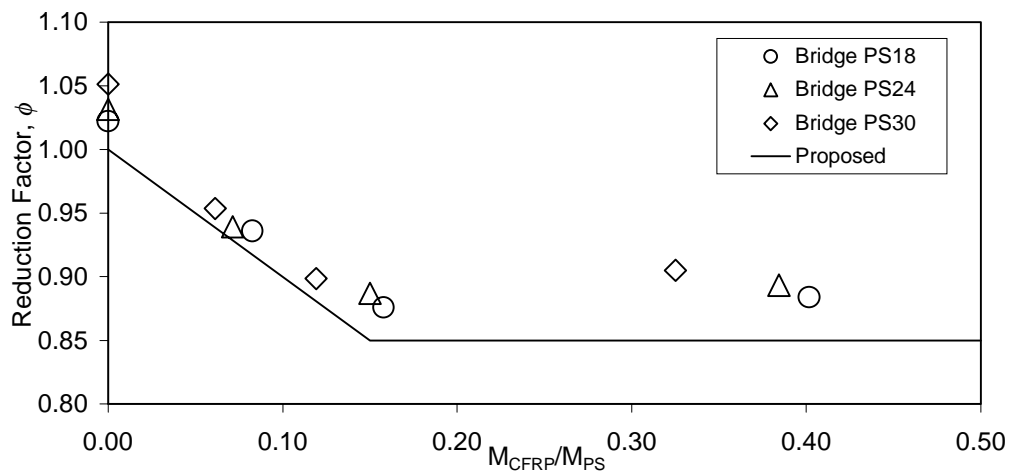


**Figure 5.15:** Proposed reduction factor,  $\phi$ .



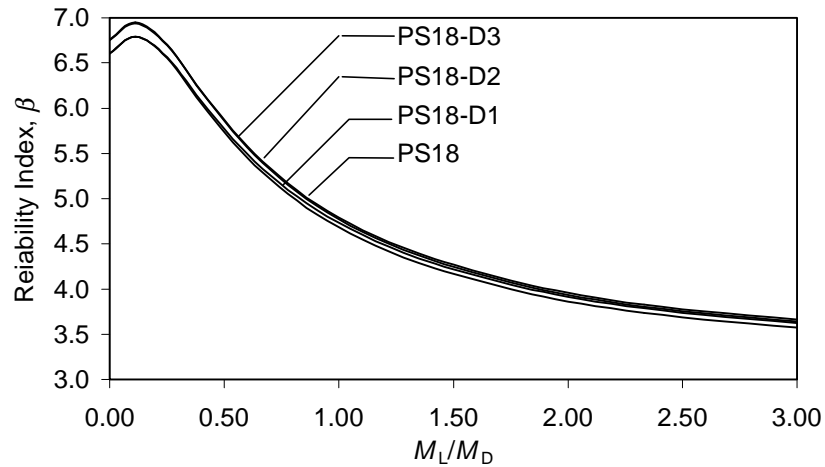


**Figure 5.16:** Effect of  $M_L/M_D$  on Reliability Index,  $\beta$ . (Bridge PS60, proposed  $\phi$ )

### 5.6.6 Design Implications for PSC Bridges

Monte Carlo simulations were performed using the developed model to determine resistance models for a limited number of PSC girder cross sections strengthened with CFRP. It is proposed that the strength reduction factor,  $\phi$ , follow Eq. 5.12, which is shown to result in acceptable reliability for a wide range of dead load to live load ratios. This study focused solely on flexural behavior of cross-sections strengthened with CFRP. Further research is needed to investigate the probabilistic nature of other modes of failure including shear resistance of PSC beams strengthened with CFRP laminates as well as peel-off and debonding of laminates.

## 6 SUMMARY AND CONCLUSIONS

### 6.1 Summary of Work

Externally bonded carbon fiber reinforced polymer (CFRP) laminates are a feasible and economical alternative to traditional methods for strengthening and stiffening deficient reinforced concrete and prestressed concrete girders. Concrete bridge girders become structurally deficient for many reasons including corrosion of reinforcing bars or prestressing strands, change in load requirements, vandalism, collision between vehicles and bridge components, etc. Carbon fiber reinforced plastic laminates are attached using epoxy adhesives to the bottom surface of beams or are wrapped around the girder stems to provide additional tensile reinforcement. Extensive testing has focused on the effect of CFRP rehabilitation on the stiffness, strength, fatigue, ductility, mode of failure, and reliability of reinforced concrete girders strengthened with CFRP laminates. Research in this field has matured to the extent that code committees are starting to crystallize available knowledge into code provisions.

The majority of research conducted to date for investigating both short term and long term behavior of CFRP strengthened bridge girders has been experimental in nature. Furthermore, while some studies have proposed design models and methodologies to identify the necessary number of laminates to achieve a target strength or stiffness, many important design issues still remain unresolved. The objective of the research reported herein is to use state-of-the-art numerical techniques to resolve some of these questions. The intent of this work is to provide information that will be useful for the development of comprehensive design guidelines for rehabilitation schemes employing CFRP technology.

To this end, models for simulating the static and accelerated fatigue behavior of reinforced and prestressed concrete beams strengthened with CFRP were developed. The models are based on the fiber section technique and account for the nonlinear time-dependent behavior of concrete, steel yielding, and rupture of CFRP laminates. The cyclic fatigue response of concrete is based upon test data in Holmen (1982) and Bennet and Raju (1971). The Weibull Theory is used to calculate the short-term tensile strength of CFRP laminates through a two step process, which accounts for the effects of size and stress-gradient.

The models were implemented in a MatLab computer program, T-DACS (Time-Dependent Analysis of Composite Sections), and were verified and exercised by comparing analytical results to data from several experimental investigations. A second computer program, MACS (Monotonic Analysis of Composite Sections), was developed to run only the static portion of the developed models. MACS is user-friendly and features an easy to use graphical user interface. Its user-friendly design allows repetitive calculations to be conducted in a convenient manner and the program is therefore ideal for design office use.

The developed computer programs were used to investigate the static and fatigue response of concrete girders strengthened with CFRP laminates. Both reinforced concrete and prestressed

concrete beams were considered in the investigation. An additional 120,000 Monte-Carlo simulations were conducted on MACS to develop resistance models for both reinforced and prestressed concrete bridge girders flexurally strengthened with externally bonded CFRP laminates. The resistance models were used to calculate the probability of failure and reliability index of CFRP strengthened cross-sections. The first order reliability method was employed to calibrate the proposed flexural resistance factors for a broad range of design variables.

## **6.2 Main Conclusions**

The following conclusions can be drawn from the research reported herein.

### **6.2.1 Tensile Strength of CFRP Laminates**

The short-term tensile strength of CFRP laminates can be calculated by applying the Weibull Theory. Two steps are needed to compute the short-term tensile strength. The first step accounts for the size effect and predicts the tensile strength of a uniformly stressed volume that shares the size of the CFRP used in the real structure. The second step accounts for the effect of stress gradients. Good agreement was found between theoretical calculations and test results.

The work described in this report suggests that coupon tests may lead to unconservative estimates of strength if the size effect is not properly considered.

### **6.2.2 Static Response of CFRP Strengthened Girders**

A series of monotonic analyses were carried out using MACS. The analyses were conducted for the control beam and beams with 1, 2, 3, and 4 CFRP laminates tested at FDOT. The following conclusions were drawn:

- The analytical results compare well to the experimental.
- The cracking moment for beams with CFRP laminates is almost the same irrespective of the number of CFRP laminates and is somewhat larger than the cracking moment of the control beam. On the other hand, moment capacity is significantly affected by the number of CRPF laminates and the strength increase per laminate is almost constant.
- Cross-sections with different number of CFRP layers reach their ultimate strength at approximately the same curvature.

### **6.2.3 Fatigue Response of CFRP Strengthened Girders**

A study of cross-section internal stresses obtained from T-DACS showed that cyclic fatigue leads to an internal redistribution of stresses similar to that obtained under static creep. The analyses show that the steel reinforcement stress in the specimens of Shahawy and Beitelman (1999, 2000) and Barnes and Mays (2000) increased by less than 5% during the fatigue life of the test beams. To account for the increase in steel stresses due to cyclic fatigue as well as

shrinkage, creep under dead loads and the variability in reinforcing steel strength, it is recommended that the service steel stress be limited such that

$$\sigma_s < 0.85f_y \quad (6.1)$$

Equation 6.1 should be applied when designing CFRP repair and/or strengthening schemes for reinforced concrete girders.

#### **6.2.4 Flexural Reliability of Prestressed Concrete Girders**

Monte Carlo simulations were performed using MACS to determine the resistance models for bridge girder cross sections strengthened with CFRP. A study using the developed resistance models showed that the reliability index of the strengthened cross sections is greater than that of the reinforced concrete sections and increases with increasing CFRP ratio. This is attributed to the low coefficient of variation for CFRP ultimate strength, which is lower than the coefficient of variation of the strength of steel or concrete. Although the reliability index improves with addition of CFRP, the flexural resistance factor is recommended as

$$\phi = 0.85 \quad (6.2)$$

which is lower than that recommended by AASHTO-LRFD for RC sections under flexure. The reduced  $\phi$  value is calibrated to result in a larger target reliability index than is normally specified in recognition of the brittle nature of CFRP behavior.

#### **6.2.5 Flexural Reliability of Prestressed Concrete Girders**

Monte Carlo simulations were performed using MACS to determine resistance models for a limited number of PSC girder cross sections strengthened with CFRP. The developed resistance models were then used to calibrate the AASHTO-LRFD strength provisions using the first order reliability method. It is proposed that the strength reduction factor,  $\phi$ , be calculated as follows

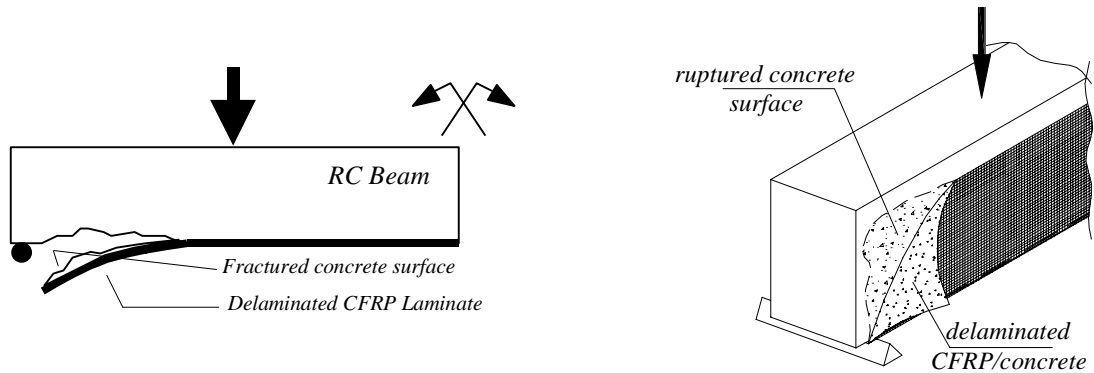
$$\phi = 1.0 - \frac{M_{\text{CFRP}}}{M_{\text{PS}}} \geq 0.85 \quad (6.3)$$

Equation 6.3 is shown to result in acceptable reliability for a wide range of dead load to live load ratios.

Since Eqs. 6.2 and 6.3 were calibrated using a limited design space, further studies are needed to confirm that they work well for a wider range of parameters. Furthermore, this study focused solely on flexural behavior of cross-sections strengthened with CFRP. Additional research is needed to investigate the probabilistic nature of other modes of failure including shear resistance of beams strengthened with CFRP laminates as well as peel-off and delamination of laminates.

### 6.3 Future Work

The delamination mode of failure in CFRP strengthened girders is among the least understood. Yet its effect is undesirable from the design point of view because it is a brittle failure mode that can have catastrophic consequences. Figure 6.1 illustrates two common delamination situations. It is recommended that future work focus on developing a good understanding of the mechanisms governing this mode of failure. Such an understanding is crucial for the development of comprehensive design provisions for CFRP strengthened beams.



(a) FRP delamination due to flexural action

(b) FRP delamination in shear region

**Figure 6.1:** Delamination due to shear and flexural actions.

## 7 REFERENCES

- AASHTO. (1998). *LRFD Bridge Design Specifications*, American Association of State Highway and Transportation Officials, Washington, D.C.
- ACI (1974), *Considerations for Design of Concrete Structures Subjected to Fatigue Loading*, ACI Report 215-74, American Concrete Institute, Detroit, Michigan 48219, USA.
- ACI (1996), *State-of-the-Art Report on Fiber Reinforced Plastic Reinforcement for Concrete Structures*, Report by ACI Committee 440, American Concrete Institute, Box 19150, Redford Station, Detroit, Michigan 48219, USA.
- ACI (1999), *Building Code Requirements for Structural Concrete*, ACI 318-99, American Concrete Institute, Detroit, Michigan 48219, USA.
- Allen, D.E. (1992). "Canadian Highway Bridge Evaluation: Reliability Index," *Canadian Journal of Civil Engineering*, 19, 593-602.
- Arduini, M. and Nanni, A. (1997). "Parametric Study of Beams with externally Bonded FRP Reinforcement," *Structural Journal*, ACI, 94(5), 493-501.
- Ayyub, B.M., and McCuen R. H. (1997). *Probability, Statistics, & Reliability for Engineers*, CRC Press, Boca Raton, Florida, USA.
- Bakht, B., Al-Bazi, G., Banthia, N., Cheung, M., Erki, M-A., Faoro, M., Machida, A., Mufti, A.A., Neale, K.W., and Tadros, G. (2000). "Canadian Bridge Design Code Provisions For Fiber-Reinforced Structures," *Journal of Composites for Construction*, ASCE, 4(1), 3-15.
- Barnes, R. A. and Mayes, G. C. (1999), "Fatigue Performance of Concrete Beams Strengthened with CFRP Plates," *Journal of Composites for Construction*, ASCE, 3(2), pp. 63-72.
- Barsom, J. M. and Rolfe. S. T. (1987), *Fracture and Fatigue Control in Structures*, Prentice-Hall, Englewood Cliffs, NJ.
- Batdorf, S. B. (1994). *Concise Encyclopedia of Composite Materials*, Revised Edition, Edited by A. Kelly, Pergamon, MIT, Cambridge, MA, USA.
- Batdorf, S.B. and R. Ghaffarian (1984), "Size Effect and Strength Variability of Unidirectional Composites," *International Journal of Fracture*, Martinus Nijhoff Publishers, Vol. 26, pp. 113-123.
- Bazant, Z. P. (1988), *Mathematical Modeling of Creep and Shrinkage of Concrete*, Wiley Series in Numerical Modeling in Engineering, John Wiley and Sons, New York.

- Bennet, E. W. and Raju, N. K. (1971), "Cumulative Fatigue Damage of Plain Concrete in Compression," *Structure, Solid Mechanics and Engineering Design*, pp. 1089-1102, Wiley-Interscience, London.
- Bullock, R.E. (1974). "Strength Ratios of Composite Materials in Flexure and in Tension," *Journal of Composite Materials*, 8, 200-206.
- Collins, M. P. and Mitchell, D. (1991), *Prestressed Concrete Structures*, Prentice Hall, Inc., New Jersey, USA.
- Corley, W. G., Hanson, J. M., and Helgason, T. (1978), "Design of Reinforced Concrete for Fatigue," *Journal of the Structural Division*, ASCE, 104(6), pp. 921- 932.
- Crespo-Minguillon, C. and Casas, J.R. (1999). "*Fatigue Reliability Analysis of Prestressed Concrete Bridges*," *J. of Structural Engineering*, ASCE, 124 (12), 1458-1466.
- Duva, J.M., Aboudi, J, and Herakovich, C.T. (1996) "A probabilistic Macromechanical Model for Damaged Composites," *Journal of Engineering Materials and Technology*, ASME, Vol. 118, No. 4, 1996, pp. 548-553.
- El-Tawil, S., Sanz-Picon, C. F., and Deierlein, G. G. (1995), "Evaluation of ACI-318 and AISC (LRFD) Strength Provisions for Composite Columns," *Journal for Constructional Steel Research*, Elsevier Applied Science, Essex, England, 34(1), pp. 103-126.
- Ellingwood, B. Galambos, T., MacGregor, J., and Cornell, A. (1980), *Development of a Probability Based Load Criterion for American National Standard A58: building code requirements for minimum design loads in buildings and other structures*, National Bureau of Standards, SP 577, Washington, USA.
- Estes, A. and Frangopol, D. (1998), "RELSYS: A computer program for Structural System Reliability," *Structural Engineering and Mechanics*, 6 (8), 901-919.
- Estes, A. and Frangopol, D. (1999), "*Repair Optimization of Highway Bridges using System Reliability Approach*," *J. of Structural Engineering*, ASCE, 125 (7), 766-775.
- Frangopol, D., Ghosn, M., Hearn, G., and Nowak, A. (1998), "*Structural Reliability in Bridge Engineering*," *Journal of Bridge Engineering*, Vol. 3, No. 4, Nov. 1998, pp151-154.
- Harlow, D.G. and Phoenix, S.L. (1981). "Probability Distributions for the Strength of Composite Materials II: A Convergent Sequence of Tight Bounds," *International Journal of Fracture*, Sijthoff & Noordhoff International Publishers, 17(6), 601-630.
- Holloway L.C. and Leeming M.B. (1999), *Strengthening of Reinforced Concrete Structures: Using Externally-bonded FRP Composites in Structural and Civil Engineering*, CRC Press, Boca Raton Boston New York, Washington, D.C.

- Holmen, J. O. (1982), "Fatigue of Concrete by Constant and Variable Amplitude Loading," *ACI Special Publication, Fatigue of Concrete Structures*, SP 75-4, pp. 71-110, American Concrete Institute, Detroit Michigan 48219, USA.
- Hull, D. (1981), *An Introduction to Composite Materials*, Cambridge Solid State Science Series, Cambridge University Press, London, England.
- Inoue, S., Nishibayashi, S., Kuroda, T., and Omata, F. (1995). "Fatigue Strength and Deformation Characteristics of Reinforced Concrete Beams Strengthened with Carbon Fiber-Reinforced Plastic Plate (in English)," *Transactions of the Japan Concrete Institute*, 17, 149-156.
- Jones, R., and Swamy, N. (1992), "Strengthening of Reinforced Concrete T-beams by Epoxy Bonded Plate Technique," *Proceedings of ACI Convention*, American Concrete Institute, Box 19150 Redford Station, Detroit, Michigan 48219, USA.
- Kaminski, B.E. (1973), "Effects of Specimen Geometry on the Strength of Composite Materials," *Analysis of the Test Methods for High Modulus Fibers and Composites*, ASTM, STP 521, 181-191.
- Kariyawasam, S.N., Rogowsky, D.M., and Macgregor, J.G. (1997). "Resistance Factors and Companion-action Load Factors for Reinforced Concrete Building Design in Canada," *Canadian Journal of Civil Engineering*, 19, 987-991.
- Kennedy, D.J.L., Gagnon, D.P., Allen, D.E., and MacGregor, J.G. (1992). "Canadian Highway Bridge Evaluation: Load and Resistance Factors," *Canadian Journal of Civil Engineering*, 19, 992-1006.
- Lavoie, J. A. (1997), *Scaling Effects on Damage Development, Strength, and Stress-rupture Life on Laminated Composites in Tension*, Ph.D. Dissertation, Virginia Tech, Blacksburg, VA, USA.
- Lu, R., Luo, Y. and Conte, J.P. (July 1994). "Reliability Evaluation of Reinforced Concrete Beams," *Structural Safety*, El Sevier, 14(4), 277-298.
- Mahadevan, S., Liu, X., and Xiao, Q. (1997), "A Probabilistic Failure Model of Composite Laminates," *Journal of Reinforced Plastics and Composites*, Technomic Publishing Co., Vol. 16, No. 11, pp. 1020-1038.
- McMahon, P.E. (1973), "Graphite Fiber Tensile Property Evaluation," *Analysis of the Test Methods for High Modulus Fibers and Composites*, ASTM, STP 521, 1973, pp. 367-389.
- Meier, U., Dearing, M., Meier, H., and Schwegler, G. (1992), "Strengthening of Structures with CFRP Laminates: Research and Applications in Switzerland," *Advanced Composite Materials in Bridges and Structures*, K. W. Neale and P. Labossiere, Editors, Canadian Society for Civil Engineers.



- Moustafa, S. E. (1986), "Nonlinear Analysis of Reinforced and Prestressed Concrete Members," *Prestressed Concrete Institute Journal*, 31(5), pp. 126-147.
- Neville, A. M. (1996), *Properties of Concrete*, 4<sup>th</sup> Edition, J. Wiley, NY, New York.
- Nowak, A.S., Yamani, A.S., and Tabsh, S.W. (1994). "Probabilistic Models for Resistance of Concrete Girders," *ACI Structural Engineering*, ACI, 91 (3), 269-276.
- Nowak, A.S. (1995). "Calibration of LRFD Bridge Code," *J. of Structural Engineering*, ASCE, 121 (8), 1245-1251.
- Nowak, A.S. and Collins, K.R. (2000), *Reliability of Structures*, McGraw Hill Higher Education Division, McGraw Hill, USA
- Plevris, N., Triantafillou, T. C. (1994), "Time-Dependent Behavior of RC Members Strengthened with FRP Laminates," *Journal of Structural Engineering*, ASCE, 120(3), pp. 1016-1042
- Plevris, N., Triantafillou, T.C., and Venesiano, D. (July 1995). "Reliability of RC Members Strengthened with CFRP Laminates," *J. of Structural Engineering*, ASCE, 121(7), 1037-1044.
- Popovics, S. (1970), "A Review of Stress-Strain Relationships for Concrete," *ACI Journal*, Vol. 67, No. 3, March 1970, pp. 243-248.
- Rao, A. S. P. and Jayaraman, R. (1989), " Creep and shrinkage analysis of partially prestressed concrete members," *Journal of Structural Engineering*, ASCE, 115(5), pp. 1169-1189
- Ritchie, P.A., Thomas, D.A., Lu, L., and Connelly, G.M. (1991). "External Reinforcement of Concrete Beams Using Fiber Reinforced Plastics," *ACI Structural Journal*, ACI, 88(4), 490-500.
- Saadatmanesh, M.A., and Ehsani, M.R. (1991). "R/C Beams Strengthened with GFRP plates I: Experimental Study," *Journal of Structural Engineering*, ASCE, 117(10), 3417-3433.
- Saadatmanesh, H. and Malek, A. M. (1998), "Design Guidelines for Flexural Strengthening of RC Beams with FRP Plates," *Journal of Composites for Construction*, Vol. 2, No. 4, 1998, pp. 158-164.
- Shahawy, M., and Beitelman T.E. (1995), "Structural Applications of Advanced Composite Materials in Bridge Construction and Repair," *Proceedings of the XIII ASCE Structures Congress*, ASCE, Reston, VA, 1995.
- Shahawy, M. A., Arockiasamy, M., Beitelman, T., and Sowrirajan, R. (1996), "Reinforced Concrete Rectangular Beams Strengthened with CFRP Laminates," *Composites, Part B*, 27B, pp. 225-233.

- Shahawy, M., and Beitelman T.E. (1999). "Static and Fatigue Performance of RC Beams Strengthened with CFRP Laminates," *Journal of Structural Engineering*, ASCE, 125(6), 613-621.
- Shahawy, M. and Beitelman, T. E. (2000), *Static and Fatigue Performance of RC Beams Strengthened with CFRP Laminates*, Report, Structural Research Center, Florida Department of Transportation, 2007 East Dirac Drive, Tallahassee, Florida, FL 32310.
- Stewart, M., and Val, D. (July 1999). "The Role of Load History in Reliability-Based Decision Analysis of Aging Bridges," *J. of Structural Engineering*, ASCE, 125(7), 776-783.
- Tabsh, S.W., and Nowak, A.S. (1991). "Reliability of Highway Girder Bridges," *J. of Structural Engineering*, ASCE, 117 (8), 2372-2389.
- Thoft-Christensen, P. (1998). "Assessment of the Reliability Profiles for Concrete," *Engineering Structures*, El Sevier, 20(11), 1004-1009.
- Thorenfeldt, E., Tomaszewicz, A., and Jensen, J.J. (1987). "Mechanical Properties of High Strength Concrete and Application in Design," *Proceedings of the Symposium "Utilization of High Strength Concrete"*, Stavanger, Norway, June 1987, Tapir, Trondheim, pp. 149-159.
- Triantafillou, T.C. and Pelvris, N. (1992). "Strengthening of RC Beams with Epoxy-bonded Fibre-Composite Materials," *Materials and Structures*, 25, 201-211.
- Val, D., Stewart M., and Melchers, R. (1998). "Bridges Effect of Reinforcement Corrosion on Reliability of Highway Bridges," *Engineering Structures*, El Sevier, 20(11), 1010-1019.
- Yushanov, S.P., and Bogdanovich, A.E. (1998), "Analytical Probabilistic Modeling of Initial Failure and Reliability of Laminated Composite Structures," *International Journal of Solids and Structures*, Pergamon, Vol. 35, No. 7-8, 1998, pp. 665-685.

## 8 APPENDIX A - IMPLEMENTATION OF FORM ALGORITHM IN MATLAB

### 8.1 First Order Reliability Method (FORM)

This research adopted the First Order Reliability Method (FORM) in determining the reliability index. From basic principles of the theory of reliability, the reliability index is defined as

$$\beta = \frac{\mu_Z}{\sigma_Z} \quad (\text{A.1})$$

where  $\mu_Z$  and  $\sigma_Z$  are respectively the mean value and the standard deviation of the Probability Density Function (PDF) of  $Z$ , which is a limit state function (performance function) that is equal to the difference between the random resistance of the member,  $R$ , and the random load effect acting on the member,  $Q$ .

$$Z = R - Q \quad (\text{A.2})$$

The previous equation gives the simplest form of  $Z$ , which is also illustrated in Fig. A.1. In the figure the shaded area represents  $Z < 0$ . In general,  $R$  and  $Q$  are not single random vectors. They are rather affected by many other random variables such as the case for the resistance which is a function of material properties, dimension, ...etc. This leads to a complex  $Z$  which instead of being a random variable, becomes a random vector  $g(\cdot)$  where

$$Z = g(X_1, X_2, \dots, X_n) \quad (\text{A.3})$$

where  $X_1, X_2, \dots, X_n$  are the random variables involved in determining  $Z$ .

Determining  $\mu_Z$  and  $\sigma_Z$  for use in estimating  $\beta$  according to Eq. A.1 is not straightforward. The First Order Reliability Method (FORM) assumes a first order Taylor series expansion of the limit state function, which approximates the failure surface by a tangent plane at the point of interest. According to FORM, the mean and variance of  $Z$  are evaluated and given as

$$\mu_Z \cong g(\mu_1, \mu_2, \dots, \mu_n) \quad (\text{A.4})$$

$$\sigma_Z^2 \cong \sum_{i=1}^n \sum_{j=1}^n \left( \frac{\partial Z}{\partial X_i} \right)_{\mu} \left( \frac{\partial Z}{\partial X_j} \right)_{\mu} \text{covariance}(X_i, X_j) \quad (\text{A.5})$$

where the partial derivatives  $\left(\frac{\partial Z}{\partial X_i}\right)_\mu$  and  $\left(\frac{\partial Z}{\partial X_j}\right)_\mu$  are evaluated at the mean of the basic random variables. In the case of uncorrelated variables, Eq. A.5 reduces to

$$\sigma_Z^2 \cong \sum_{i=1}^n \left(\frac{\partial Z}{\partial X_i}\right)_\mu^2 \sigma_{(X_i)}^2 \quad (\text{A.6})$$

The most probable failure point in the design space is located on the failure surface  $Z$  such that distance from the origin of the design space to the tangent plane to the failure surface is shortest (see Fig. A.2). To locate such a point, an iterative process is needed. The following section describes the details of this iterative algorithm.

### 8.1.1 FORM Algorithm

The iterations are executed on transformed standard normally distributed random vectors. A detailed description of the process can be found in Estes and Frangopol (1998). The procedure was implemented in a MATLAB script to utilize the symbolic manipulation capabilities in determining the partial derivatives in Eq. A.5 and A.6. A flowchart for the program can be seen in Fig. A.3.

The procedure is best explained through an example. The reliability of a reinforced concrete cross section in flexure is used for that purpose. The flexure strength of a properly-designed singly-reinforced rectangular RC cross section is

$$M_n = A_s f_y \left( d - \frac{A_s f_y}{1.7 b f'_c} \right) \quad (\text{A.7})$$

Thus the limit state function becomes

$$Z = A_s f_y \left( d - \frac{A_s f_y}{1.7 b f'_c} \right) - (M_D + M_L) \quad (\text{A.8})$$

where  $M_D$  and  $M_L$  are the applied moments due to dead and live loads, respectively.

Each of the variables in Eq. A.8 has its own statistical properties (bias and coefficient of variation) that can be found in the literature. The bias is the ratio between the mean and nominal value for a random variable. The coefficient of variation is the ratio of the standard deviation to the mean.

The nominal values for all variables (dimensions, material properties, ...etc. can be easily estimated by measurements. The magnitude of  $M_D$  and  $M_L$  can be estimated according to the following assumptions. If the cross section is perfectly designed, the factored moment,

$M_u = 1.4M_D + 1.7M_L$ , should be equal to the factored nominal moment,  $\phi M_n$ . By assuming that the ratio between  $M_L$  and  $M_D$  is 1.5, the resulting limit state function becomes

$$M_n = \frac{1}{\phi} (1.4M_D + 1.7M_L) = \frac{1}{0.9} (1.4M_D + 1.7(1.5M_D)) = 4.39M_D$$

or

$$M_D = 0.228M_L$$
(A.9)

and

$$M_n = 2.93M_L$$

or

$$M_L = 0.342M_n$$
(A.10)

The values for  $M_D$  and  $M_L$  from Eqs. A.9 and A.10 still need to be treated statistically to account for the uncertainty in the applied loads. Therefore, a bias factor and a COV are applied to both  $M_D$  and  $M_L$  like all other variables.

The FORM algorithm is executed to find the reliability index,  $\beta$ , for a T-shaped RC beam. Dimensions of the cross section can be found in Section 5.5.3. The partial derivatives of the limit state function are found after transforming the variables into the reduced standard normal space. The derivatives are:

$$\frac{\partial g}{\partial f'_c} = 466 \frac{(0.145A_s + 9.7)^2 (6450f_y + 66400)^2}{(2.52b + 84)(792f'_c + 4400)^2}$$
(A.11)

$$\frac{\partial g}{\partial f_y} = 6450(0.145A_s + 9.7) \left( (0.666d + 44.4) - 0.588 \frac{(0.145A_s + 9.7)(6450f_y + 66400)}{(2.52b + 84)(792f'_c + 4400)} \right) - 3800 \frac{(0.145A_s + 9.7)^2 (6450f_y + 66400)}{(2.52b + 84)(792f'_c + 4400)}$$
(A.12)

$$\frac{\partial g}{\partial b} = 1.48 \frac{(0.145A_s + 9.7)^2 (6450f_y + 66400)^2}{(2.52b + 84)^2 (792f'_c + 4400)}$$
(A.13)

$$\frac{\partial g}{\partial d} = 0.666 (0.145A_s + 9.7) (6450f_y + 66400)$$
(A.14)

$$\frac{\partial g}{\partial A_s} = 0.145(6450f_y + 66400) \left( (0.666d + 44.4) - 0.588 \frac{(0.145A_s + 9.7)(6450f_y + 66400)}{(2.52b + 84)(792f_c' + 4400)} \right) - 0.0856 \frac{(0.145A_s + 9.7)(6450f_y + 66400)^2}{(2.52b + 84)(792f_c' + 4400)}$$
(A.15)

$$\frac{\partial g}{\partial M_D} = -604000$$
(A.16)

$$\frac{\partial g}{\partial M_L} = -2.59 \times 10^6$$
(A.17)

The initial guess for the design point should be the mean values for each variable. However, the initial values are intentionally assumed away from the mean to show the convergence capability of the algorithm. Convergence in case of using the mean values as the initial guess is generally faster.

Table A.1 lists the results of the progress of the iterative procedure for the example. For each iteration, the coordinates of the design point in the original space and the reduced space are given. Also listed in the table are the direction cosines, which are determined at the end of each iteration and used for determining the design point values for the next iteration. It is said that convergence has been achieved if the change in the reliability index,  $\Delta\beta$ , is less than a user specified tolerance (taken as  $10^{-6}$  in this study). Eight iterations were needed to achieve convergence. Only the results for the first four iterations are given in Table A.1. The reliability index converged to a value of 3.09201. This value is expected as it falls within the range targeted by most design codes.  $\beta = 3.0 - 3.5$ .

**Table A.1:** Progress of FORM algorithm

Variable	1 <sup>st</sup> iteration			2 <sup>nd</sup> iteration			3 <sup>rd</sup> iteration			4 <sup>th</sup> iteration		
	$x_i^*$	$u_i^*$	$\alpha_{g,U_i}^*$	$x_i^*$	$u_i^*$	$\alpha_{g,U_i}^*$	$x_i^*$	$u_i^*$	$\alpha_{g,U_i}^*$	$x_i^*$	$u_i^*$	$\alpha_{g,U_i}^*$
$f'$	3000	-1.7677	0.0472	4355	-0.0564	0.0271	4333	-0.0851	0.0198	4351	-0.0614	0.0198
$f''$	65000	-0.3704	0.6540	62218	-0.7826	0.6984	52713	-2.1906	0.7007	52876	-2.1665	0.7012
$b$	80.00	-1.5873	0.0056	83.98	-0.0067	0.0045	83.96	-0.0140	0.0033	83.97	-0.0101	0.0033
$d$	48.00	5.4252	0.0949	44.31	-0.1135	0.1041	44.17	-0.3267	0.0887	44.21	-0.2743	0.0890
$A$	8.000	-11.6612	0.1178	9.675	-0.1410	0.0997	9.651	-0.3128	0.0854	9.658	-0.2641	0.0857
$M_{\sigma} (\times 10^6)$	5.000	-1.7166	-0.1681	6.158	0.2011	-0.1592	6.338	0.4993	-0.1596	6.334	0.4935	-0.1595
$M_{\mu} (\times 10^7)$	1.500	1.7984	-0.7203	1.258	0.8619	-0.6822	1.588	2.1401	-0.6841	1.582	2.1151	-0.6835
$\Delta\beta$	1.19653			1.94036			-0.04497			0.00009		
$\beta$	1.19653			3.13689			3.09192			3.09201		

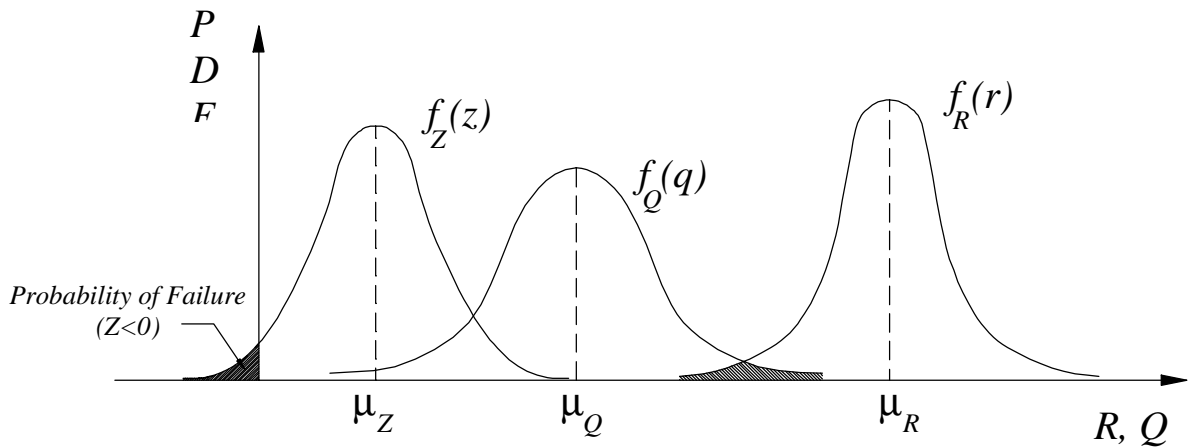


**Figure A.1:** Statistical distribution (PDF) of resistance ( $R$ ), loads ( $Q$ ), and performance function ( $Z$ ).

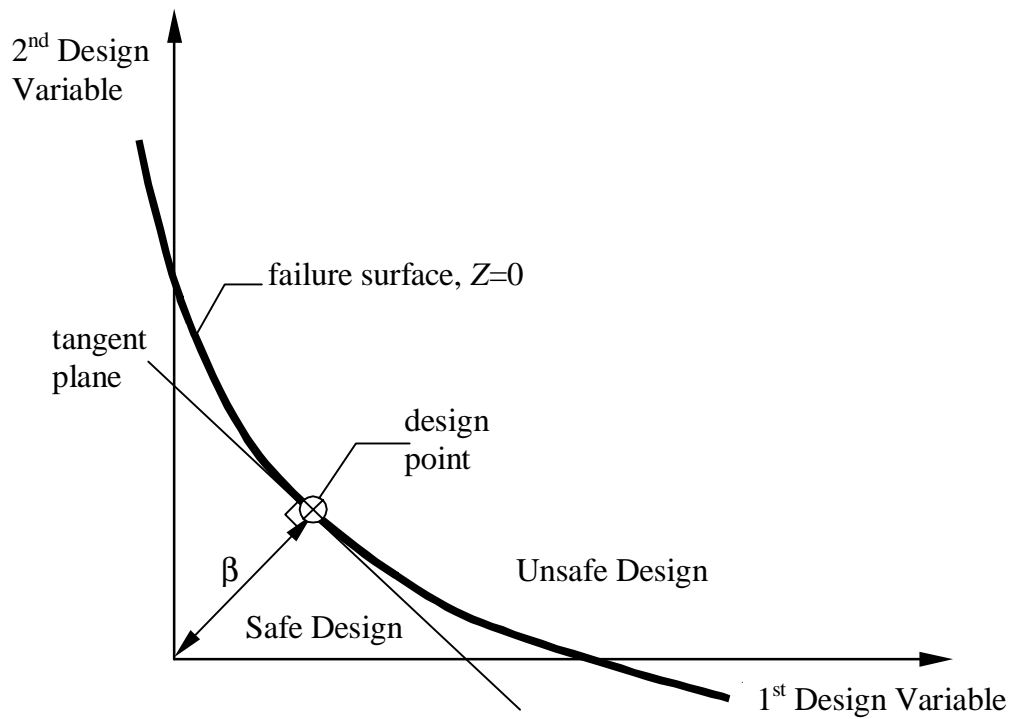


**Figure A.2:** A simple reduced design space showing the design point, reliability index



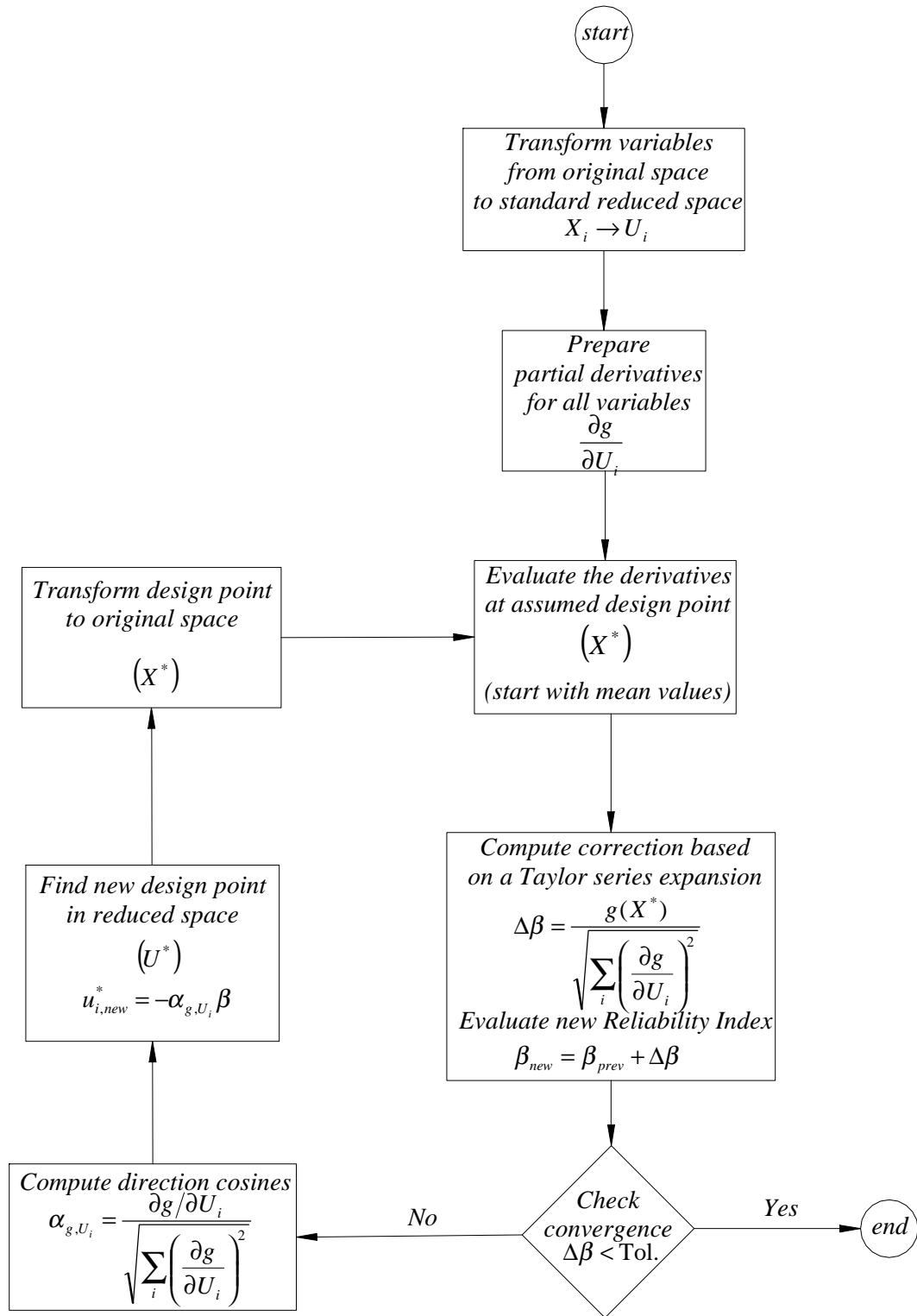


**Figure A.3:** Flow chart for MATLAB implementation of FORM

## 9 APPENDIX B - USER'S MANUAL FOR MACS<sup>®</sup>

This section is a manual to accompany the MACS<sup>®</sup> (Monotonic Analysis for Composite Strengthening) computer program. The manual helps the user in installing the program on personal computers running MS-Windows operating system. The manual also describes the basic features of the program with few illustrations.

### 9.1 Program Installation

MACS<sup>®</sup> may be downloaded from its home page hosted by UCF at <http://pegasus.cc.ucf.edu/~el-tawil>. The following steps should be followed to install MACS<sup>®</sup> on a PC:

1. Download the Zip archive (MACS.zip - 1970 kB) from the web site and save the file in a temp directory. The archive includes 4 files
  - **Readme file (MACSReadme.txt)** (1 kB)
  - **Cabinet file (MACS.cab)** (1500 kB)
  - **Setup control (Setup.lst)** (4 kB)
  - **Setup program (Setup.exe)** (138 kB)
2. Extract all four files from the Zip file in the temp directory using **Winzip** or any other archiving program.
3. Exit all running programs that may interfere with the installation, especially virus scanners.
4. Execute the program **Setup.exe** in one of the following two ways:
  - Visit the temp directory where the files were extracted using **Windows Explorer** and double click on **Setup.exe**.
  - Click on **Start->Run...** from the Start menu. Browse to the temp directory and pick **Setup.exe**. Click OK.
5. Follow the installation instructions from the setup program. During the procedure, the user will be asked for an installation directory, which by default will be installed in "**C:\Program Files\MACS**". If another folder is desired, the user is allowed to feed the path to this folder.

A successful installation creates the appropriate icons and groups. It will also add a link to MACS<sup>®</sup> in **Start->Programs->MACS** the menu. After a successful installation, it is possible to start using MACS<sup>®</sup>.

## 9.2 Using MACS<sup>®</sup>

MACS<sup>®</sup> can be invoked using any of the following methods:

- Click on **Start->Programs->MACS** from the Start menu.
- Click on **Start->Run...** from the Start menu. Browse to the folder where **MACS<sup>®</sup>** is installed and pick **MACS.exe**. Click OK.
- Open the **MACS<sup>®</sup>** group and double click on **MACS.exe**.

The **MACS<sup>®</sup>** main window will appear on the upper left corner of the screen. The main window has several options and menus. Each performs a specific task depending on the type of problem being analyzed. The possible scenarios are:

- Inputting data for the analysis a new beam.
- Retrieving the input data of a previously analyzed beam.

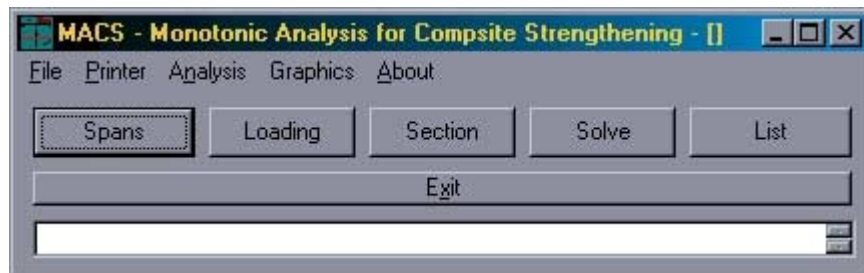


**Figure B.1:** Main window of the MACS<sup>®</sup> program.


## 9.3 Starting a New Analysis

The analysis is performed in three major steps:

- Data Input.
- Solving Problem.
- Retrieving Results.

Data of a new beam is entered in following order:

### 9.3.1 Span Length

The first step in a new analysis is to enter the span length of the girder. By clicking on the  button, the span data window will appear in the upper right corner. Of the many fields

in the span window, the user is required to fill the Span Length field only. Other fields (BEAM NAME, Span Name, and Span No.) are optional for clarity of results. After typing the span length, click OK. The first span length is stored and the **NEW** icon disappears. Adding, Deleting, and Browsing spans is possible using the provided buttons. Note that the current version of **MACS**<sup>®</sup> is capable of analyzing single span structures only.

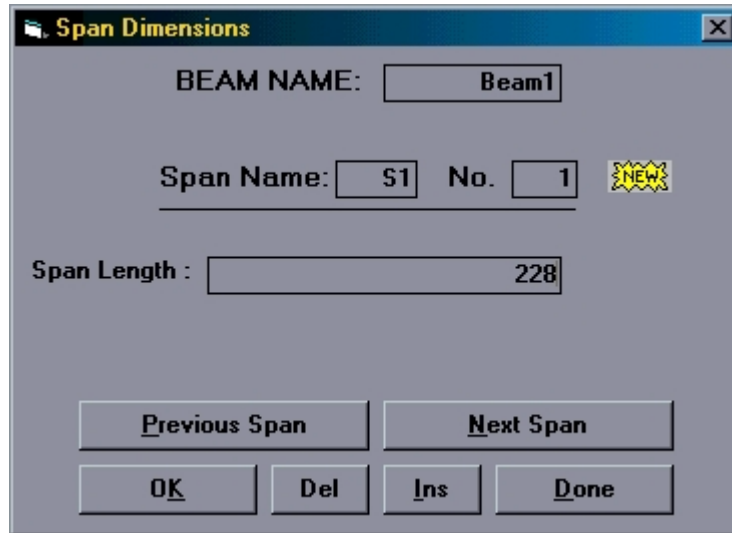


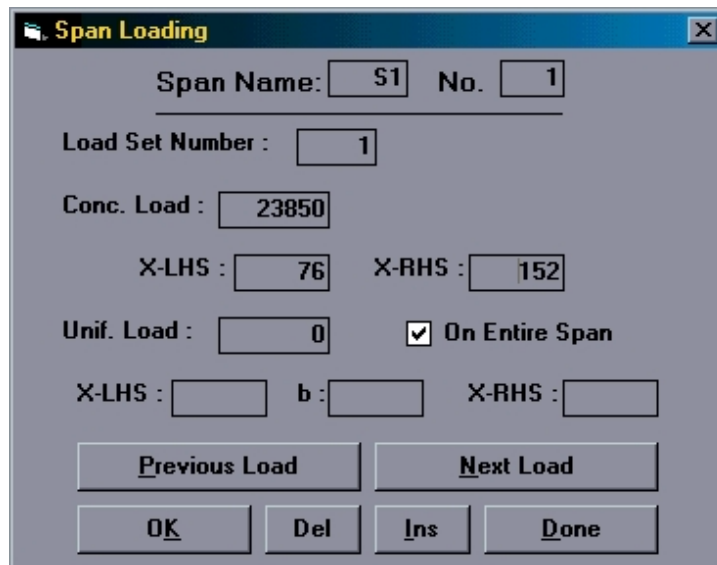
**Figure B.2:** **MACS**<sup>®</sup> Span data window.

### 9.3.2 Span Loads

Loads are grouped in load sets. Each load set consists of a concentrated load and a uniformly distributed load. As many as 20 load sets are allowed. By clicking the **Loading** button, the span loading window will appear below the span data window. The fields should be filled with loads representing the analyzed case. Figure B.3 shows one of the concentrated loads for the T-shaped beams tested by Florida DOT.

### 9.3.3 Section Details

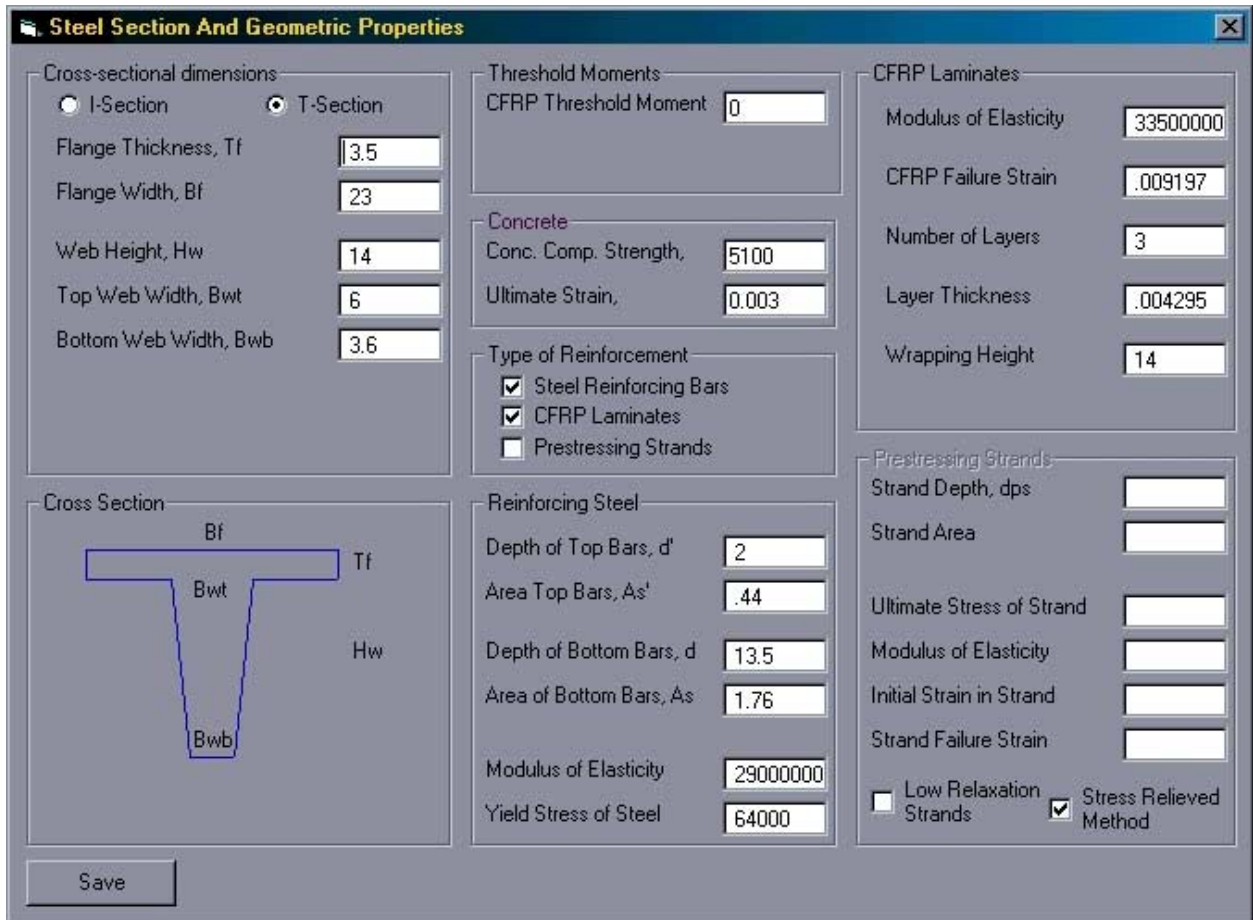
The details of the cross section are entered in the Section Details window, which is invoked by clicking the **Section** button. The current version of **MACS**<sup>®</sup> is capable of analyzing two geometries; I-girders and T-girders. Three possible reinforcement type may be entered; namely steel reinforcement, prestressing strands, and CFRP sheets. Any combination of these reinforcements is allowed including adding all types. At least one type should be provided, since the program prohibits analyzing plain concrete cross sections. Clicking Save after filling the appropriate fields stores the cross sectional data.



The image shows a software dialog box titled "Span Loading". It contains several input fields and buttons. The fields are: "Span Name:" with value "S1", "No." with value "1", "Load Set Number:" with value "1", "Conc. Load:" with value "23850", "X-LHS:" with value "76", "X-RHS:" with value "152", "Unif. Load:" with value "0", and a checked checkbox labeled "On Entire Span". Below these fields are two buttons: "Previous Load" and "Next Load". At the bottom are four buttons: "OK", "Del", "Ins", and "Done".

Span Name:	S1	No.	1
Load Set Number :	1		
Conc. Load :	23850		
X-LHS :	76	X-RHS :	152
Unif. Load :	0	<input checked="" type="checkbox"/> On Entire Span	
X-LHS :		b :	
		X-RHS :	
Previous Load		Next Load	
OK	Del	Ins	Done

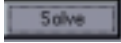
Figure B.3: MACS<sup>®</sup> Span Loading window.



**Figure B.4:** MACS<sup>®</sup> cross section interface for Florida DOT tested T-girders. [All fields in US customary units (i.e. inch and pound)]

In the Section Details window, the Threshold Moment field is the moment value at the time of CFRP application, which in real life scenarios is equal to the dead load moment acting on the girder. For the example of FDOT T-girders, this field is empty (zero) since CFRP sheets are attached from at beginning of loading.

### 9.3.4 Problem Execution

Completion of the previous steps ends the data input phase of the analysis. The second phase is solving the problem which first requires specifying the type of the analysis. From the analysis menu, the user should chose **Elastic** or **Nonlinear Analysis**. Clicking the  button started solution algorithms. During a nonlinear analysis, a Status window appears in the upper right corner to show the analysis progress.

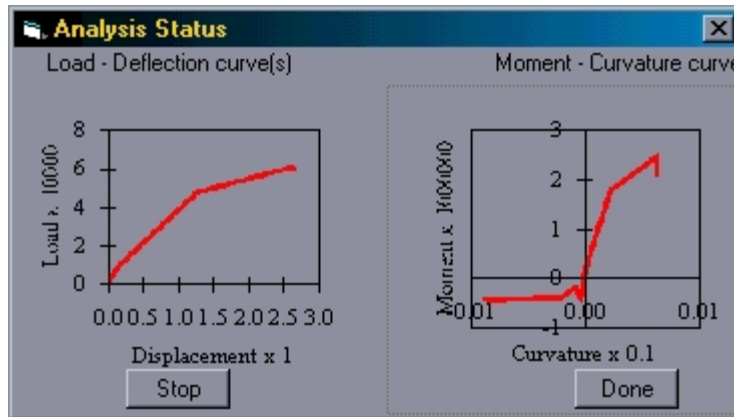


**Figure B.5:** Status window of the MACS<sup>®</sup>.

The analysis proceeds as follows:

- Prepare positive Moment-Curvature relationship for cross section.
- Prepare negative Moment-Curvature relationship for cross section.
- Analyze beam based on the obtained Moment-Curvature relationships.

During the solution phase, the status bar in the main windows shows message to help the user understand the solution progress. The following message appears at the end of an analysis **"Analysis of beam (done) at hh:mm:ss on mm-dd-yyy - Elapsed Time = ss.s seconds"**

### 9.3.5 Viewing Results

Results can be viewed using the Graphics menu. Choosing any of the options expands MACS<sup>®</sup> main window and shows the type of result chosen by the user. The program is capable allows the user to view the Moment-Curvature relationship of the cross section. It also allows the user to view the Load-Deformation relationship for the midspan point. Figures B.6 and B.7 show the show these curves for FDOT T-beam strengthened with 3 layers of CFRP sheets.

In addition to the plots, MACS<sup>®</sup> writes the following two files:

- **Mphi.dat** holds the moment curvature data for the analyzed cross section.
- **Pd.dat** holds the load deflection results for the analyzed beam.

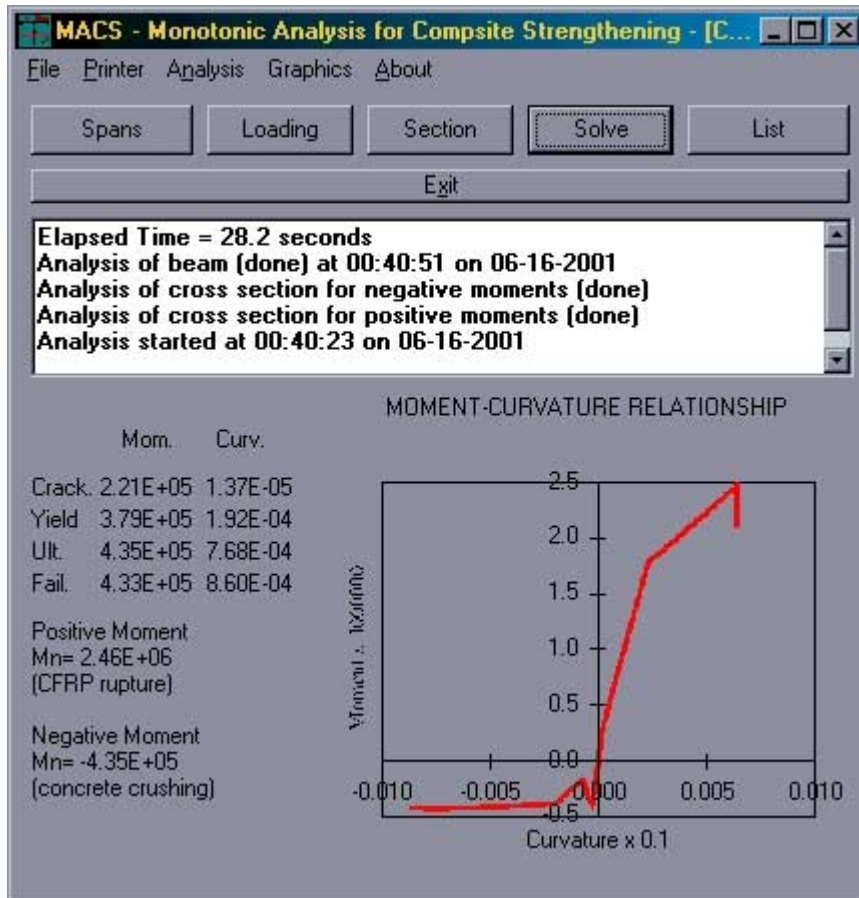


**Figure B.6:** Main Interface of MACS<sup>®</sup> showing Moment-Curvature for Specimen W-3L5.



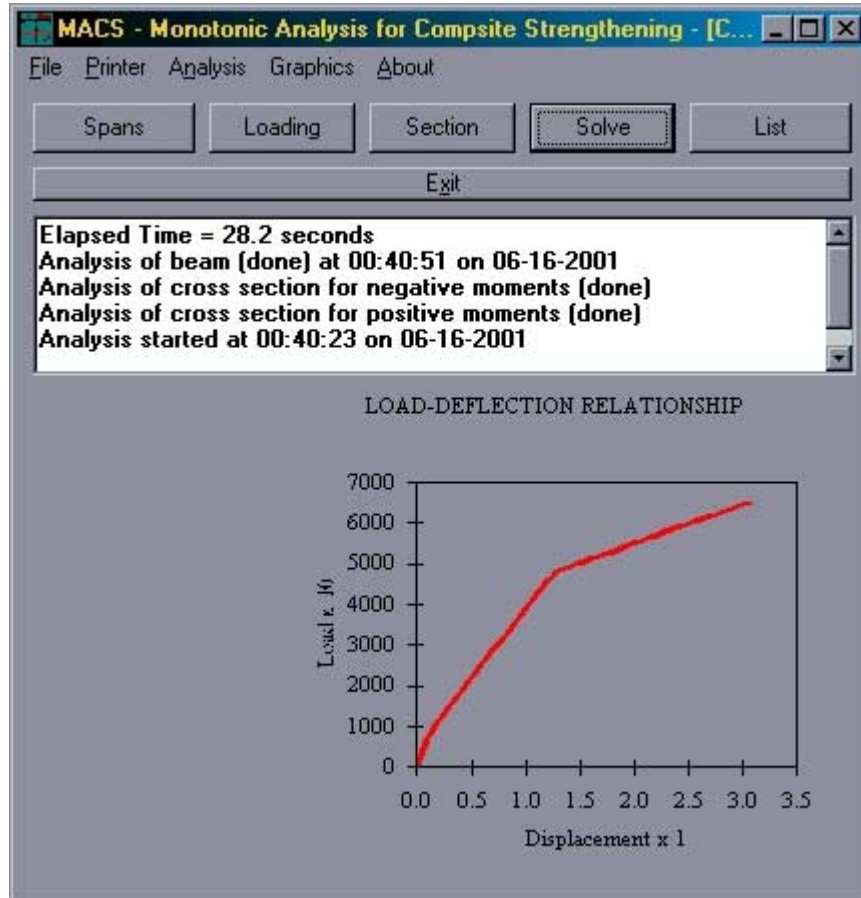


**Figure B.7:** Main Interface of MACS<sup>®</sup> showing Load-Deflection relationship for Specimen W-3L5.

## 10 APPENDIX C - REHABILITATION EXAMPLE

In this section a complete example is illustrated for the strengthening design of a deficient RC beam using MACS.

### 10.1 Cross Section Geometry

The beam is originally designed for the simply supported slab/girder bridge. The span length is 18 meters and the cross section is given in Fig. C.1. An analysis of the bridge showed that interior girders are subjected to a dead load moment,  $M_{DL}=1005\text{kN.m}$ . [741k.ft.], and a live load moment including the dynamic allowance factor,  $M_{LL+IM}=1290\text{kN.m}$ . [951k.ft.]. The cross section was designed using a reduction factor,  $\phi=0.9$ , which leads to a required nominal flexural capacity:

$$M_n = \frac{1.25M_{DL} + 1.75M_{LL+IM}}{\phi} = 3904\text{kN.m. [2879k.ft.]}$$

From basic RC principles, it can be shown that the cross section in Fig. C.1-b has a flexural capacity equal to 3917kN.m. [2888k.ft.] for the given dimensions and reinforcement,  $A_s=8900\text{mm}^2$  [13.795in<sup>2</sup>]. Analyzing this cross section using MACS results in a capacity of 3883kN.m. [2863k.ft.], which is a difference of less than 1% than the value obtained from basic principles. It should be noted that not only is this difference small, it is also on the conservative side.

### 10.2 Design of Damaged Cross Section

The case of 15% damage to main steel (e.g. due to corrosion) will now be considered to illustrate how MACS can be used for that purpose. The nominal capacity of the damaged cross section ( $A_s=0.85 \times 8900=7565\text{mm}^2$  [11.726in<sup>2</sup>]) is calculated to be  $M_n=3347\text{kN.m}$ . [2468k.ft.] (3312kN.m. [2442k.ft.] from MACS), which is less than the required  $M_u/\phi=3904\text{kN.m}$ . [2879k.ft.]. This violation of strength requirement will be compensated for by bonding FRP sheets to the stem of the cross section. The following steps are to be followed:

1. The required nominal capacity for a RC bridge girder strengthened with CFRP sheets is first calculated based on a reduction factor,  $\phi=0.85$  to account for the brittle nature of the behavior of the strengthened cross section

$$M_n = \frac{M_u}{\phi} = \frac{M_u}{0.85} = 4133\text{kN.m. [3047k.ft.]}$$

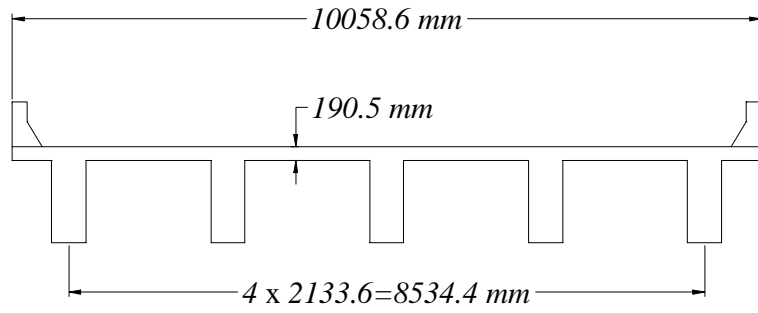
2. The data for the damaged cross section is used to perform the analysis. The strengthening of the cross section is achieved via CFRP sheets that are wrapped about the stem; i.e.  $h_{\text{CFRP}} = 1104.9\text{mm}[43.5\text{in}]$ . The sheets used in this example are of the same properties as tested in the Structural Research Center of Florida DOT. The longitudinal direction of the sheets has a yarn density of 0.23/mm [6/inch]. Each of the yarns consists of 12000 fibers. The diameters of each fiber is 7  $\mu\text{m}$ . This arrangement results in a pure carbon thickness of 0.109mm[0.004295in]. At the time of application of CFRP, the girder is probably subjected to dead loads. This is taken into account by inputting a threshold moment equal to the design dead load moment,  $M_{\text{DL}}=1005\text{kN.m.}[741\text{k.ft.}][8893\text{k.in.}]$ .
3. Several design trials are executed. It is first assumed that one layer of CFRP sheets is glued to the sides and soffit of the girder. The analysis of this first trial shows that the capacity of the girder is  $M_n=3695\text{kN.m.}[2725\text{k.ft.}]$ . It is obvious that this arrangement is not sufficient for the required capacity. Therefore, the number of layers is increased until the required capacity is achieved. Table 1 lists the nominal flexural capacity for each attempt (1 layer through 3 layers).

It is clear from the Table C.1 that 3 layers of CFRP are sufficient. Figures C.2 and C.3 are provided to show the how main windows the designer deals with. The data in Fig. C.3 are for the 3<sup>rd</sup> design trial. It should be noted that the program in its current version requires that all data be in US customary units (i.e. inch and pound). Fig. C.3 shows the data for the cross section after converting them into these units.

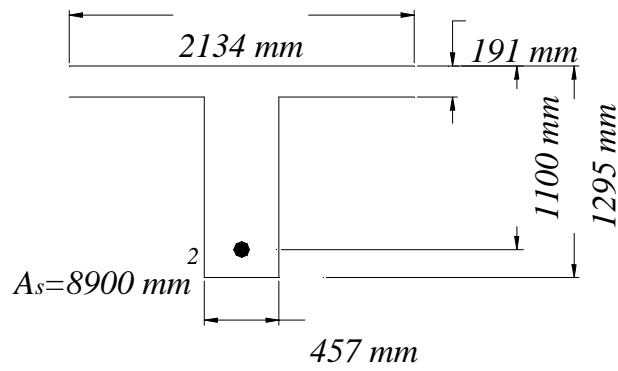
**Table C.1:** Design trials for damaged cross section

Trial	Number of Layers $N_L$	Pure CFRP thickness $t_{\text{CFRP}}$ mm [in]	Nominal Flexural Capacity $M_n$ * kN.m. [k.ft.]	Acceptable Design?
--	--	--	3883 [2863]	undamaged
0	0	0	3312 [2442]	damaged
1	1	0.109 [0.004295]	3695 [2725]	Not O.K., deficient
2	2	0.218 [0.008590]	4038 [2977]	Not O.K., deficient
3	3	0.327 [0.012885]	4381 [3230]	O.K.

\* Target  $M_n = \frac{M_u}{\phi} = \frac{M_u}{0.85} = 4133\text{kN.m.}[3047\text{k.ft}]$



(a)



(b)

**Figure C.1:** Cross sections of undamaged interior bridge girders.

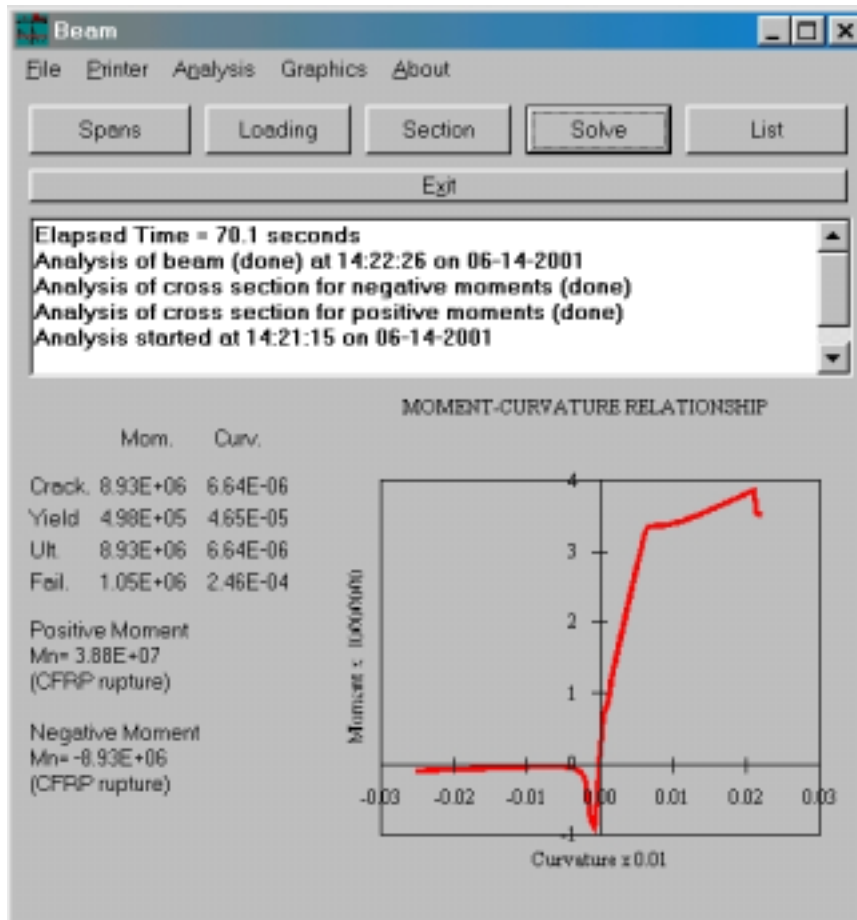


**Figure C.2:** Main Interface of the MACS program.

**Steel Section And Geometric Properties**

Cross-sectional dimensions

I-Section     T-Section

Flange Thickness, T1: 7.5

Flange Width, Bf: 84

Web Height, Hw: 43.5

Top Web Width, Bwt: 18

Bottom Web Width, Bwb: 18

Threshold Moments

CFRP Threshold Moment: 8892677

Concrete

Conc. Comp. Strength: 4000

Ultimate Strain: 0.003

Type of Reinforcement

Steel Reinforcing Bars

CFRP Laminates

Prestressing Strands

CFRP Laminates

Modulus of Elasticity: 33500000

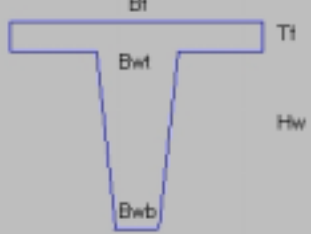
CFRP Failure Strain: .009146

Number of Layers: 3

Layer Thickness: .004295

Wrapping Height: 43.5

Cross Section



Reinforcing Steel

Depth of Top Bars, d': 1

Area Top Bars, As': .0001

Depth of Bottom Bars, d: 43.307

Area of Bottom Bars, As: 11.726

Modulus of Elasticity: 29000000

Yield Stress of Steel: 60000

Prestressing Strands

Strand Depth, dps: [ ]

Strand Area: [ ]

Ultimate Stress of Strand: [ ]

Modulus of Elasticity: [ ]

Initial Strain in Strand: [ ]

Strand Failure Strain: [ ]

Low Relaxation Strands     Stress Relieved Method

Save

**Figure C.3:** MACS cross section interface for 3<sup>rd</sup> design trial. [All fields in US customary units (i.e. inch and pound)]

## 11 APPENDIX D - RESEARCH DISSEMINATION

### 11.1 Papers Accepted for Publication

Okeil, A. M., El-Tawil, S., and Shahawy, M. (2001), "Canadian Bridge Design Provisions for Fiber Reinforced Structures - Discussion," *Journal of Composites for Construction, ASCE*, Vol. 5, No. 2, April 2001.

El-Tawil, S., Okeil, A. M., and Shahawy, M. (2001), "Static and Fatigue Analyses of RC Beams Strengthened with CFRP Laminates," *in press, Journal of Composites for Construction, ASCE*.

Okeil, A. M., El-Tawil, S., and Shahawy, M. (2001), "Short-Term Tensile Strength of CFRP Laminates for Flexural Strengthening of Concrete Girders," *in press, ACI Structures Journal*, will appear June 2001.

### 11.2 Papers Submitted for Publication

Okeil, A. M., El-Tawil, S., and Shahawy, M. (2001), "Reliability of RC Girders Strengthened with CFRP laminates," *Submitted for publication in the Journal of Bridge Engineering, ASCE*.

Okeil, A. M., El-Tawil, S. (2001), "Reliability of PSC Concrete Girders Strengthened with CFRP laminates," *Submitted for publication in ACI Structural Engineering, ACI*.

### 11.3 Theses

Cahit Ogunc (2001), *Static and Fatigue Behavior of RC Beams Strengthened with CFRP*, MS Thesis, Department of Civil and Environmental Engineering, University of Central Florida, Orlando, FL 32816-2450, May 2001.